Signal Enhancement by the SABRE Method in High Magnetic Fields

Magbool Ali A Al-Elyani

PhD in Cognitive Neuroscience and Neuroimaging

University of York

Psychology

July 2017

Abstract

In this thesis, I investigate the Signal Amplification by Reversible Exchange (SABRE) technique as a hyperpolarisation method to solve the MRI sensitivity problem and use it to study the interaction of hyperpolarised molecules with biological tissues. The fundamental issue in MRI and NMR is the very low sensitivity produced as a result of small population differences between nuclear spin states in a magnetic field. The main aim of my project is to develop imaging procedures for use in a human 3T MRI scanner with hyperpolarised samples and to investigate the use of spin hyperpolarisation in the study of biological processes in vitro. The objective is to understand, develop and optimise the use of the SABRE method of spin hyperpolarisation with a variety of biologically relevant molecules.

This thesis shows how the fringe field of the 3T magnet can be used for polarisation and how the time dependency of the decay of signals in the scanner can be investigated. In particular I investigated the non-exponential decay of the signals and have attempted to explain the origin of this decay. The observations show strong evidence that the signal from hyperpolarised Pyrazine decays with a non-exponential time course. The major evidence against this being turbulence is that the deviation from an exponential decay is field dependent. This has also been shown with Nicotinamide and with Pyridine. Further investigations show that exposing the sample to heart tissue shows faster decay (shorter T1) than the sample without tissue. It is postulated that this effect is due to binding to specific ion channels that leads to the change in T1. It is postulated that this could be exploited to develop a specific imaging method for tissue bound hyperpolarised molecules. Moreover, with longer imaging times, it was shown that a signal returned in the presence of tissue and that this was evidence of possible long-lived states.

The observations in the final chapter demonstrate progress in developing the exploitation of long-lived states. The SABRE method was used to create magnetisation in Pyridazine. This large signal was then converted into a singlet state and it is shown that this signal can be read out some time later. The long-lived state was used to store the signal for over three minutes. This was repeated with and without heart tissue in the NMR sample. The presence of biological tissue, added after the formation of the singlet state, resulted in an increased signal and it is argued that this is evidence of an interaction between the tissue and the hyperpolarised molecule, It is suggested that the singlet state evolves into observable magnetisation on interaction with the tissue and that this could form the basis of a unique imaging contrast storage and readout method for specific molecular-tissue interactions.

Contents

List of Tables

List of Figures

List of Symbols

B_0	Magnetic field strength
$\hbar$	Planck's constant
I	Nuclear quantum number or intensity
J	J-coupling or Joules
γ	Gyromagnetic ratio
T_1	Longitudinal relaxation time
T_2	Transverse relaxation time
T_2^*	Transverse relaxation time due to spin-spin interaction and inhomogeneity
μ	Net magnetic moment
ρ	Angular momentum
ψ	Wave function
δ	Relative chemical shift
σ	Chemical shift
ω	Larmor frequency
V_{RFF}	The reference line frequency in a NMR spectrum
V	The NMR frequency
N	The number of nuclei in a sample
T	The temperature in Kelvin
K	Boltzmann's constant

Acknowledgements

Declaration

I hereby declare that I wrote this thesis work under the supervision of Professor Gary Green and Professor Simon Duckett. I confirm that these original works have not submitted to any other universities and all sources including diagrams and figures which have been copied from books, academic articles and Internet mentioned are cited as references.

The data in **chapter 1** were accepted and presented as a poster in the 9th Saudi Students Conferences in Birmingham, UK – 2016 as "Signal Enhancement by using the SABRE method in MRI", Magbool Alelyani, Gary Green, Simon Duckett. York Neuroimaging Centre, Dept. of Psychology, University of York, York YO105DD, UK

The practical work in the thesis was carried out by myself expect for the following

- Throughout the thesis the operation of the 3T scanner was performed by Ross Devlin.
- In chapter 6 the NMR machine was kindly operated by Dr. Soumya Roy.
- In chapter 6 Prof. Simon Duckett programmed the NMR machine to perform the M2S and S2M experiment and he also kindly run the NMR machine.
- Dr Stephen Hall prepared the heart sample

I am very gratefully for their assistance.

Chapter 1   Introduction

Nuclear magnetic resonance (NMR) and conventional magnetic resonance imaging (MRI) play a vital role in physical, biological and medical imaging. Some 40 million MRI scans were carried out in clinical practice around the world in 2011.

Most of these scans were of the water and fat distribution in the body and very few were related to the detection of other biologically relevant molecules. This is due to the insensitive nature of MRI and to the low concentration of these other molecules.

The very low sensitivity of Magnetic Resonance Imaging (MRI) and Magnetic Resonance Spectroscopy (MRS) is a result of the small population differences between nuclear spin states in the magnetic field of the scanner. In normal MRI machines, there are almost equal amounts of the two spin states of Hydrogen and most of the signal is cancelled as a result leaving only relative few nuclei to contribute to a resultant net magnetic vector.

There are many ways of increasing MRI signals such as by exploiting hyperpolarisation techniques. In this thesis Parahydrogen is used with the Signal Amplification by Reversible Exchange (SABRE) method to overcome the sensitivity problem. These so-called hyperpolarisation methods work by creating much larger spin population differences than those seen in the normal thermal equilibrium. In SABRE highly ordered spin states in Parahydrogen (which are non-observable magnetic signals) are transferred from that source into a molecule of interest (R. W. Adams et al., 2009).

Once the MRI signal is increased, dramatically, then molecular imaging becomes possible and allows the characterization and measurement of biological, living, processes and makes it possible to consider its use in diagnostic, biochemical, imaging. Molecular imaging is a method that will extend conventional diagnostic imaging and will lead to the investigation of molecular markers at different locations of the body and in different diseases such as in neurological diseases and cancer (Chen & Chen, 2010).

To appreciate the importance of hyperpolarisation, it is necessary to place it in the context of the development of NMR and MRI as core technologies. Although Rabi demonstrated the ability to flip the magnetic orientation of nuclei in a vacuum chamber using an oscillating magnetic field, and that this was highly dependent upon field (or frequency), it was in 1945, that Bloch and Purcell conducted the first experiments in NMR using solid materials and water samples respectively (Bloch F., 1946; Purcell, 1946). Bloch and Purcell were awarded the Nobel Prize in NMR physics in 1952 for that work. They showed that the absorption or transmission of energy at 8MHz or 30MHz in different magnetic fields for their respective samples, was a manifestation of Rabi's nuclear magnetic resonance in liquid or solid samples. Crucially, their approach, using continuous wave excitation, and the observation of both absorption and transmitted effects led to the modern methods of NMR and MRI.

Using a pulse based method, rather than continuous waves in magnetic resonance spectroscopy (MRS) is one of the main techniques that Ernst developed. It involves sending short RF pulses to the sample to be examined and observing the response as a Fourier transform of the signal. Changing a continuous wave to normal pulse based excitation could have led to a weak signal-to-noise ratio (SNR) due to the inherently lower amount of energy at each frequency in a pulse, but Ernst showed that intense brief pulses could be used to advantage. The major benefit of using Fourier analysis, compared to the conventional spectral sweep technique, is that it can acquire the spectrum in seconds and actually increased the sensitivity by over 100-fold. Ernst's experiment in 1965 showed that the sensitivity of high proton magnetic resonance spectroscopy could be increased in a fixed, short, time (R. Ernst & Anderson, 1966). The result was that NMR has become a useful, practical, method of analysing microscopic materials and isotopes such as 13C. Two dimensional (Aue, Bartholdi, & Ernst, 1976; R. Ernst, R, 1990) and three dimensional (Oschkinat et al., 1988) NMR techniques were originally by Ernst's group for use in NMR. In the last few decades, NMR has become an essential technique in biology and chemistry.

NMR and MRI depend on a fundamental property of atoms. That a signal can be detected and measured is due to the magnetic property of nuclear spin. NMR is based on the ability to interact with the nuclear spin property of atoms. All atoms have spin but the most useful elements for NMR and MRI have spin ½.

A nucleus is composed of protons and neutrons each made of subatomic particles called quarks. These quarks fundamentally have spin and charge amongst other properties. The spin

properties of quarks produce the signals that are observed in NMR and MRI (E. A. Davis, 1997).

The nuclei of all atoms can be described by a nuclear quantum number 'I'. This I value may be greater than or equal to zero and has multiples of ½. All nuclei with I=0 have no spin and hence these are not used in NMR; this spin value is known as being 'NMR silent'. This means any atom with an even number in both atomic number and atomic mass will produce zero spin, such as Carbon 12. Fortunately, there are many common isotope atoms, found in metabolites and drug molecules such as 1H, 13C and 15N, that do not have both an even atomic number and atomic mass. Crucially those that have spin ½ give rise to observable signals and are not NMR silent.

NMR works when the sample is placed in a magnetic field and the each nuclear ½ spin will align either in the magnetic field direction or align against that direction This population difference provides a net magnetic moment (Claridge, 2008).

The net nuclear magnetic moment can be described as

$$\boldsymbol{\mu} = \boldsymbol{\gamma\rho} \qquad 1$$

Where γ is a constant measuring how magnetic a particular nuclide is, known as the gyromagnetic ratio. The net magnetic moment $\boldsymbol{\mu}$ and angular moment $\boldsymbol{\rho}$ are vector quantities and have both direction and magnitude.

The proton 1H can easily be detected by NMR because it has a high natural abundance of 99.98% and a high gyromagnetic ratio, while others, e.g. 13C and 15N, have a low natural abundance, of 1.11% and 0.37% respectively and lower gyromagnetic ratios.

Importantly the distribution of the spin population into those nuclei that are aligned with the field and those that are opposite, is determined by temperature and magnetic field. If the external magnetic field is zero, then the distribution of the individual nuclear magnetic moments is random and hence the net magnetic moment is also zero. As the external magnetic field, B0, is increased, then the spin of the nuclei will be distributed into two populations (for spin ½) with net alignment in two vectors, parallel and anti-parallel. The difference, as stated above, gives rise to the net magnetic moment or vector (NMV).

From the number of nuclei in both the two population states, the NMV can be calculated from the Boltzmann distribution of the two states:

$$\mathbf{N} -/ \mathbf{N} += e^{\Delta E/kT} \qquad\qquad 2$$

$$\triangle E = \hbar\gamma Bo \qquad\qquad 3$$

where N is the number of nuclei in a sample, $\hbar$ is the Planck constant $(6.626070040){\times}10{-}^{34}m^2$ kg/s, T is the temperature in Kelvin and K is the Boltzmann constant $= 1.38 \times 10^{-23}$ J/K. ω is determined by the magnetic field B_0.

$$\omega = \mathbf{B}o \times\gamma \qquad\qquad 4$$

where ω is the Larmor frequency which is also known as the precessional frequency, γ is the gyromagnetic ratio and B_0 is the magnetic field.

In clinical MRI, the temperature cannot be changed so the main determinant of the net magnetic vector is the static magnetic field, B_0.

Once a sample is placed in a magnetic field and a net magnetic moment is established then that moment can be manipulated to produce useful signals that allow the characterization of the sample and the spatial distribution of the molecules within it. This is carried out by transmitting a RF pulse to the sample such that it has the same frequency as the precessional frequency of the sample nuclei to be probed. The RF pulse is normally applied perpendicular to B_0. Thus, the nuclei are absorbing energy from the RF and will start to resonate. This process is called excitation. In a situation of high field strength, high energy (high frequency) it is necessary to generate the resonance because the difference between the energy states is increased.

There are two results of this resonance. The first result is that after an RF of 90º, the NMV flips to the transverse plane and keeps precessing in that plane at the Larmor frequency. The second result is that the contributions to the net magnetic moment will start in phase. These two consequences cause a voltage that is induced as a sinusoidal current in a receiver coil, according to Faraday's law, which states that alterations in a magnetic field cause an electric current in the coil. This voltage is the MR signal that relies on the magnitude of the NMV in the X and Y planes. This means if there is more magnetization in the transverse plane, we will find a greater signal.

Water is a simple example of the use of NMR for its characterization. The human body is mainly water which contains Hydrogen nuclei. The NMR or MRI of water depends upon the Hydrogen protons (Jerrold T. Bushberg, 2011). In terms of NMR, these two Hydrogen atoms

behave in a similar manner in a magnetic field in that they have the same precessional frequency.

A crucial concept in NMR and MRI concerns the time course of how the net magnetic moment behaves in a static magnetic field and in response to RF excitation. T1 and T2 time constants are the relevant key concepts here. It is essential to understand the T1 and T2 of hyperpolarised substances to be able to optimise NMR and imaging protocols. It is also essential to understand the time courses in order that the correct interpretation can be made about spectra and images.

The time course of the formation of a net magnetic moment in the Z direction, the direction of the B_0 field depends upon T1. After application of a RF pulse around X or Y, the lifetime of the signal in the horizontal plane depends upon T2 (and T2*). The signal from water, in the horizontal plane, can be viewed as a spectrum and can be seen in figure 1.
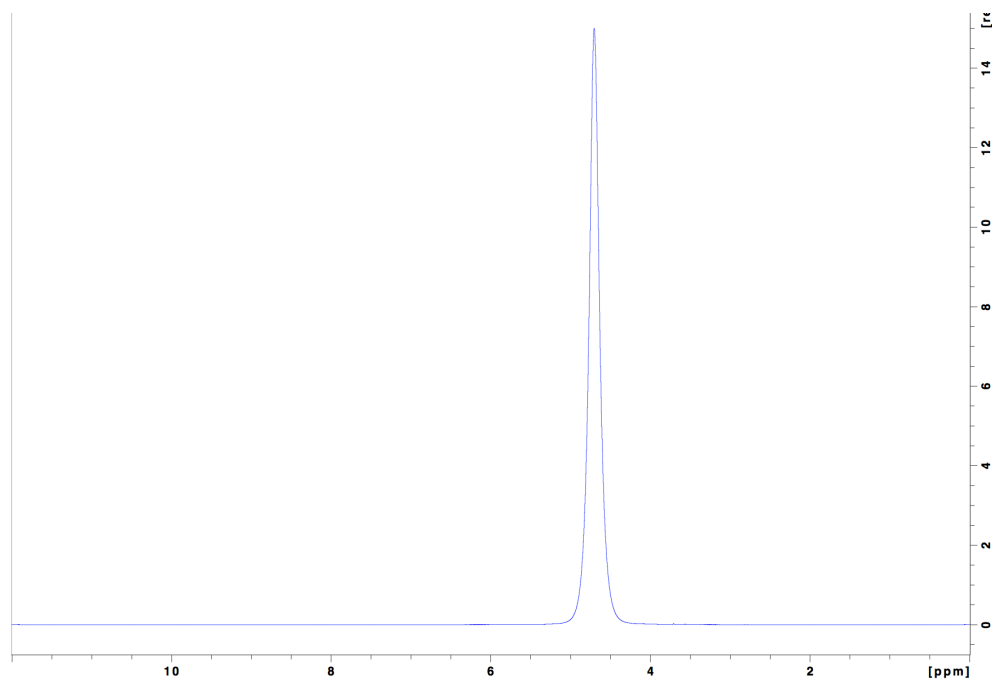
Figure 1 The water signal at 4.76 ppm

The frequency of the signal, the Larmor frequency, is not given in absolute terms but is measured relative to a standard defined as being the frequency of Hydrogen protons in Tetramethylsilane (TMS).

If a magnetic field is applied to a molecule, the electrons will interact with that magnetic field (Bock & Thøgersen, 1983). The interaction effectively changes the apparent static field (B_0) by a tiny fraction, σ. Sigma may be positive or negative depending on the interaction

Based on the kind and the bonds of a molecule, the density of electrons in every nucleus is different. This means each chemical molecule has special chemical characteristics that affect on the interactions between molecule and magnetic field. Therefore, the magnetic field and the interacting field at every nucleus is molecule dependent. Sigma, the size of this effect, gives rise to a change in the apparent Larmor frequency of the nuclear spin (Levitt, 2008).

The variance is described in terms of a defined standard frequency from which the degree of the frequency shift can be measured. This quantity is described in parts per million (ppm) and given the symbol delta, δ (Levitt, 2008). This is because the degree of shift is then independent of the B_0 field and is described as a relative shift in frequency. As gyromagnetic ratio is in terms of MegaHertz per Tesla and the B_0 field is often several Tesla, the relative shift is easily described in terms of shift per MegaHertz and it is why 10^6 (million) is multiplied by the δ definition (Keeler, 2013).

$$\delta \text{ (ppm)} = (\nu - \nu_{REF}) \times 10^6 / \nu_{REF} \qquad\qquad 5$$

Where ν is the NMR frequency and ν_{REF} is the line frequency from the reference compound. By definition, the line from the reference compound emerges at $\delta = 0$.

Tetramethylsilane (TMS) is a standard in NMR spectroscopy which is not in the body (Levitt, 2008) and is the reference compound for 1H and 13C (Keeler, 2013) . The signal from water with its identical Hydrogen atoms included is at 4.76 ppm (Levitt, 2008).

The use of a relative measure means that the same spectrum describes the NMR signal of a sample irrespective of the B_0 field in which the measurement is made. The time decay of the NMR signal (T2 and T2*) is seen in the Free Induction Decay of the signal in the receiver coils and is reflected in the width of the spectral peak.

A B
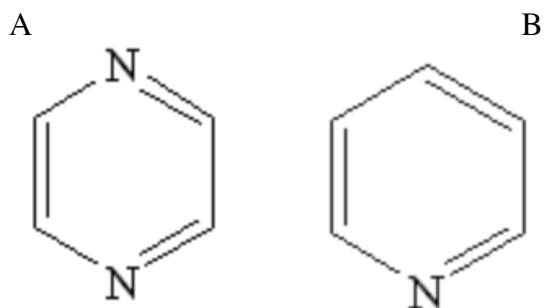
Figure 2: A shows Pyrazine chemical structure and B shows the Pyridine chemical structure

Similar investigations can be made of other substrates. Pyrazine ($C_4H_4N_2$) is a common component of many pharmaceutical drugs and in this thesis it is used to test the hypothesis that is also biologically relevant in itself as an NMR/MRI probe (Daniel Bellus, 2014), ie that it binds to Pyrazine binding protein in tissues. The Pyrazine molecule is shown in figure 2.

The Hydrogen, Carbon and Nitrogen atoms in Pyrazine are each located within the molecule in a very symmetric manner. The result is that each are in a neighbourhood that is identical to atoms of the same type (assuming that they are of the same isotopic form). The symmetry is such that they will experience the same chemical and magnetic influences from the neighbouring, and distant, components of the molecule. The result of this property is that, like in water, the spin of Hydrogen nuclei behave in the same manner in a B_0 field and in response to a RF pulse.

In figure 3A, we can see the Pyrazine NMR spectrum; it is also a single peak. The position of the peak, in ppm from the standard, is at 8.7. The other two peaks are from the solvent.

A   B
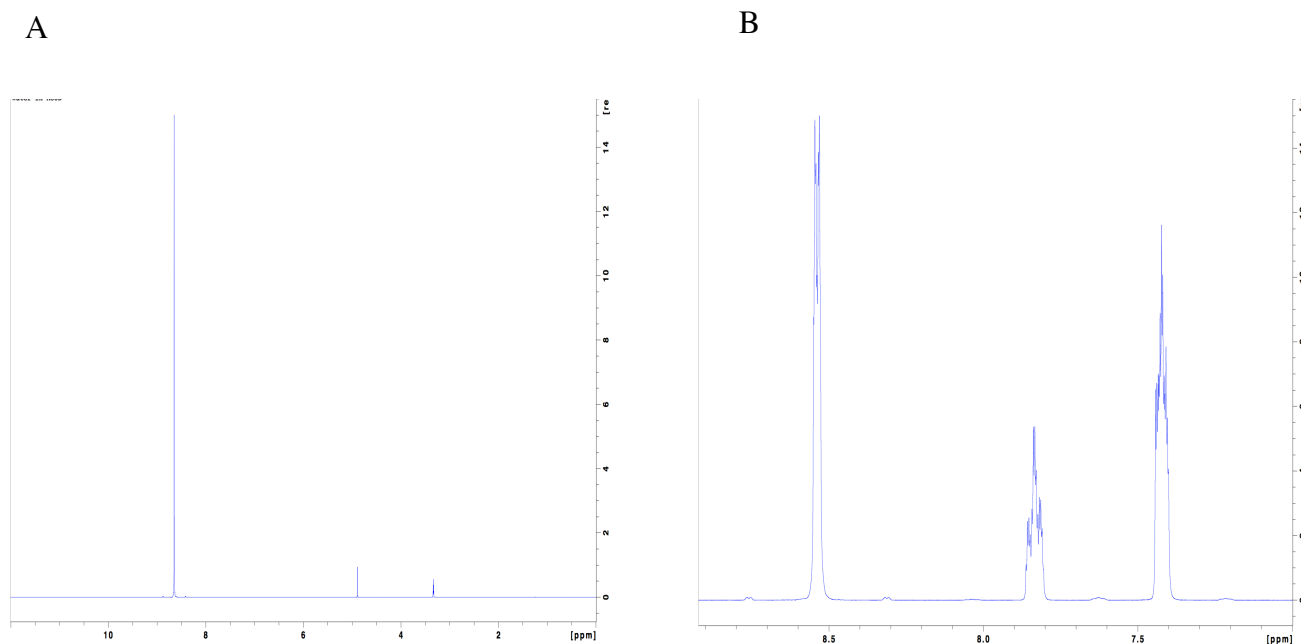
Figure 3 Image A shows NMR spectrum of Pyrazine at 400MHz and the ppm is 8.7. Image B shows the three peaks of the spectrum for Pyridine

The same approach can be used with other molecules. In figure 3B, the NMR Hydrogen spectrum of Pyridine is shown. In this case the Hydrogen atoms that contribute to the net magnetic vector are not in the same chemical or magnetic environment within the molecule and a spectrum is observed that directly reflects that. The three peaks appear in pyridine spectrum because it is not symmetric and does not have the same chemical environment as pyrazine molecule.

a) Thermal equilibrium   b) Hyperpolarised spin distribution
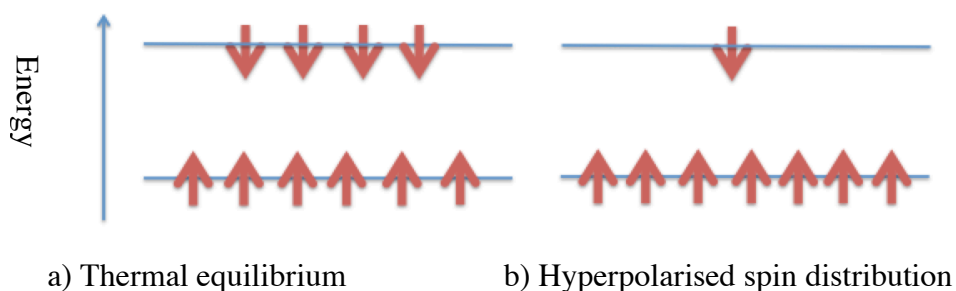
Figure 4 Image A shows the Boltzmann distribution, known as the thermal equilibrium, image B indicates the non-Boltzmann distribution, known as the hyperpolarised spin distribution

As mentioned above, spin up and spin down are referred to as the spin state. The proportion in every state is determined by static magnetic field and temperature. This is known as the thermal equilibrium distribution. The fundamental problem is an inherent low sensitivity with the spin up and spins down in almost the same population percentage. The population difference of molecules depends on the magnetic field. For example, when a 7 Tesla magnet is used instead of a standard Human 3 Tesla machine, the signal will increase 7/3 times. The financial cost of increasing the field therefore, to overcome the low sensitivity, may be considerable. Alternatively this insensitivity may be overcome by exploiting a hyperpolarisation technique. In figure 4, the difference between the state distributions at thermal equilibrium and in the hyperpolarisation state can be seen.

Hyperpolarisation techniques can increase the NMR signal by dramatically changing the spin state distribution. This method can allow the investigation of the molecules that have low concentration and can be used to almost routinely acquire images based on different nuclei other than protons. Hyperpolarisation methods have been used to investigate the molecular imaging in biological tissues to see the distribution and metabolism of hyperpolarised substrates(Kurhanewicz et al., 2011b). In vivo human studies have been done using the hyperpolarised method. The first spectrum images of an *in vivo* human organ using hyperpolarised Xe-129 were documented in 1997 (Swanson et al., 1997).

There are many different approaches to achieving hyperpolarisation of the spin states. These include Brute Force methods, Optical pumping, Dynamic Nuclear Polarization (DNP), Parahydrogen Induced Polarization (PHIP) and Signal Amplification by Reversible Exchange (SABRE)(Kurhanewicz et al., 2011b). In this thesis, I will focus and use the SABRE method for all my experiments.

The main purpose of signal enhancement is to increase the signal by exploiting a non-Boltzmann distribution. As an introduction I now review the main methods and their advantages and disadvantages:

1.1   The brute force method

This method was proposed in 1961 (Roberts & Dabbs, 1961). This method of producing nuclear polarisation, requires a high magnetic field and low temperature. It just exploits the Boltzmann distribution equation and the dependence on magnetic field and temperature. For

example, using this method, the polarisation of Hydrogen and Carbon 13 can be increased in a high magnetic field of 11.75 T and reducing the temperature of the sample from 310K to 1K. The polarisation is increased 75 times using this approach. Although spin polarisation is significantly increased, it is challenging to go to much higher fields or to further reduce the temperature in high field and as such these are the disadvantages of the brute force method (De Graaf, 2008).

Even though the brute force method is theoretically straightforward, it is not utilized in practice examinations. This is because there may be long T1 relaxation times at low temperature and this determines the time to achieve the new equilibrium. Furthermore, this technique is only used with specific molecules and as yet no report has been made of translation of the polarized substance to room temperature, which would be essential for *in vivo* applications (De Graaf, 2008).

In a recent study, very high nuclear polarisation was created at extremely low temperature by using nanoparticle-mediated relaxation. This will increase the enhancement and reduce the time scale (T1 relaxation) (Kelvin, 2013).

1.2   Dynamic Nuclear Polarisation (DNP)

This first DNP experiment was performed in 1950 (T. Carver & Slichter, 1953; T. R. Carver & Slichter, 1956).

DNP depends on the solid effect discovered by Proctor and Abraham (De Graaf, 2008). DNP is used to transfer the almost 100% polarisation of electron spins to nuclear spin via irradiation at high frequency. Then the nuclei become polarised and this significantly increases the NMR signal by up to 20,000 times. The polarization of the electrons is achieved at a low temperatures of about 1K (Kemsley, 2008). There are four mechanisms of transfer: The Overhauser effect (OE), the solid effect (SE), thermal effect (TM) and the cross effect (CE). These mechanisms have been used effectively in both liquids and solids (Maly et al., 2008). The OE mechanism is widely used in liquids. However, the TM, SE and CE mechanisms are used widely for polarisation transfer in the solid state (Bajaj et al., 2007).

The DNP method has up until recently been restricted to applications in high field NMR spectroscopy. This was due to the shortage of microwave sources at suitable frequencies.

Currently, however, sources are now accessible which could lead DNP to become a crucial technique.

DNP is an important technique that enhances the NMR signal of both liquids and solids and hence is an essential tool in molecular biology studies (Maly et al., 2008). The solid-state method is limited to use *in vitro*. However, in liquid state polarisation, the sample is dissolved with a source of free electrons using a radical in a high magnetic field of 3T and at then cooled to low temperature. After radiation with microwaves for often many hours the sample can be rapidly thawed (this is termed the dissolution step) and the NMR or MRI signal can be interrogated. The spectrum of naturally abundant Carbon-13 has been achieved and compared with the spectrum of thermal equilibrium as seen in Figure 5. The polarisation of Carbon-13 was 37% whereas the polarisation from the same spectrum of Nitrogen-15 was 7.8%. DNP-NMR based on a liquid sample provides a variety of ways of using this method *in vivo* and *in vitro* due to the strong enhancement of nuclear polarisation, (Ardenkjær-Larsen et al., 2003).
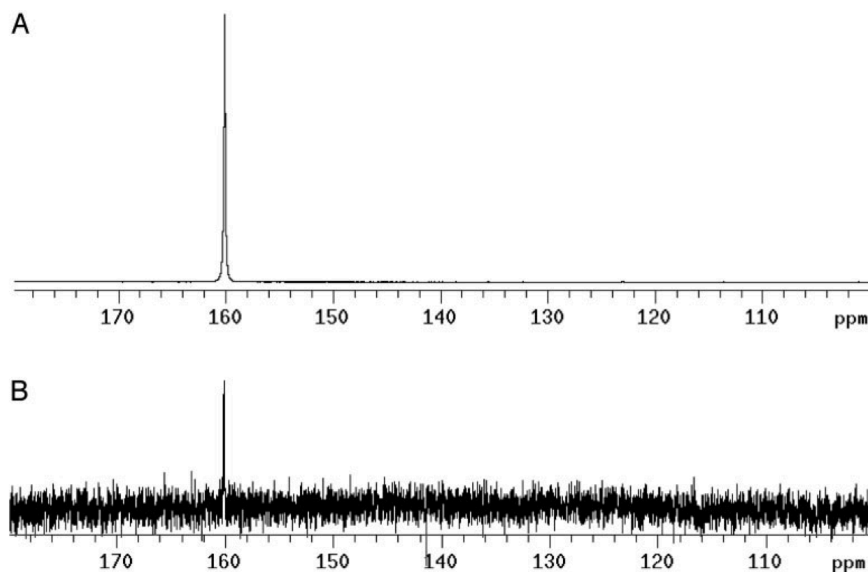
Figure 5 Image A shows the hyperpolarised spectrum of Carbon-13 with SNR of 4592. Image B shows the Carbon-13 spectrum of thermal equilibrium with SNR of 7. Both are at 9.4T and are the same temperature, taken from (Ardenkjær-Larsen et al., 2003).

Hyperpolarised water images have a high SNR compared to images from injected non hyperpolarised water. The image quality was enhanced in post-processing and the movement of the water bolus should be monitored. In Figure 6 this enhancement can be seen in the images of a rat which were created using DNP (Lingwood et al., 2012).
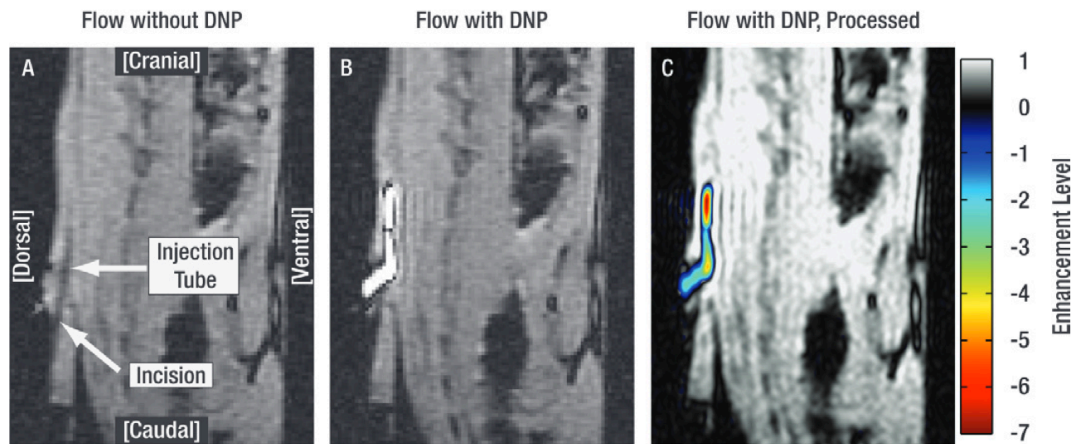
Figure 6 Image A shows the spin density of the non-injected water hyperpolarised with no contrast see. Image B indicates the spin density throughout the injection of hyperpolarised water, showing a high signal. Image C shows the enhancement after injection of the hyperpolarised water. The colour bar provides the level of signal intensity and enhancement, taken from (Lingwood et al., 2012).

In addition, 13C -1 pyruvate has been hyperpolarised by the DNP technique. The spectrum of hyperpolarised Pyruvate and its metabolic products, such as Lactate, bicarbonate and alanine (Kohler et al., 2007) have been demonstrated. There are several reasons for using pyruvate; the relaxation time is long and it is quickly transported through the cell membrane. In addition, the solubility of pyruvate in water is high and this means that after dissolution the concentration of the hyperpolarised sample is still high. The hyperpolarisation of 13C -1 pyruvate and its metabolites have been measured both in an isolated heart and in an *in vivo* rat heart (Kurhanewicz et al., 2011a).

These rat studies were carried out at 1.5T and 3T. After injecting pyruvate, bicarbonate was noticed in the skeletal muscle, vasculature and kidney. However, at 3T, alanine was noticed in the liver and skeletal muscle, whereas lactate, bicarbonate and pyruvate were observed in the kidneys and vasculature. The use of pyruvate as polarized using the DNP method as observed in several organs in a rat are shown below in Figure 7 (Kohler et al., 2007).
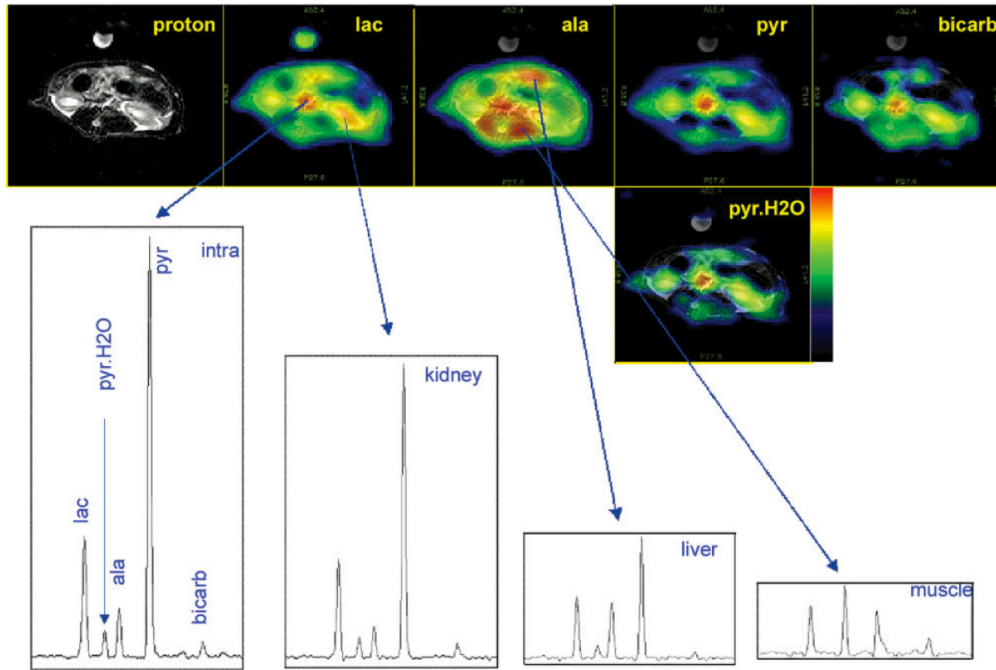
Figure 7 These Images show the spectra of different organs created with 13C-1 Pyruvate DNP. In addition, the show different metabolites and single spectra of different tissues, taken from (Kohler et al., 2007).

Recently, hyperpolarised DNP has been developed further and is used in biological tissue. In *in vivo* studies, the relaxation time should be long in order to be able to inject the contrast agent until the area of interest inside the subject is reached; this can be done using 13C. This method provides more specific information not afforded by current conventional imaging. However, even though hyperpolarised DNP is well established enough to be used in biological cancer imaging, it is limited in that it requires a long relaxation time, hyperpolarised molecule labelling, new technical instrumentation (which incorporates sterile methods and quality control and new contrast agents which may need to pass regulatory controls (Kurhanewicz et al., 2011a).

1.3   Optical Pumping (Hyperpolarised gases)

This method was developed by Albert and his group. The two nuclear spins He_3 and Xe-129 with spin ½ were hyperpolarised by optical pumping (M. S. Albert et al., 1996).   The polarisation of He-3 and Xe-129 can be increased to 100,000 times the equilibrium levels and this leads to the detection of hyperpolarisation without background signals (Couch et al., 2014).

This technique has been mainly used in studies of the lung. There are challenges associated with scanning lungs, such as low signal as a result of low numbers of protons inside the lung, and because of cardiac and respiratory movement. Therefore, using optical pumping to hyperpolarise noble gases such as He-3 and Xe-129 can solve a number of these problems. Both gases have been used effectively. However, Xenon is preferable for many reasons; for example, it allows MR investigation to obtain accurate information of the lipid membrane and may be able to provide better imaging of the lipid rich areas inside the brain. This could lead to using the hyperpolarised Xe-129 technique in fMRI examinations (M. Albert & Balamore, 1998).

Optical pumping uses two different techniques, spin exchange and metastability exchange, both of which were discovered in 1960 (Kauczor, Surkau, & Roberts, 1998). Both methods move the angular momentum from the circular polarised laser light into the noble gases' nuclear spin (Couch et al., 2014).

Both of the noble gases He-3 and Xe-129 solve the limitations of conventional H MRI and provide high quality lung images that are more sensitive to gas exchange (Altes & Salerno, 2004). In 1994, Albert performed the first imaging of this using hyperpolarised Xe-129 to investigate the lung of a mouse; the images of mouse lung and heart were obtained as shown below in Figure 8 (M. Albert et al., 1994).
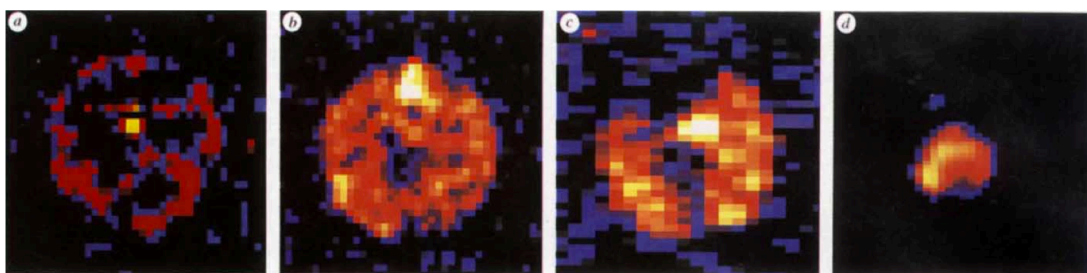
Figure 8: The Xe-129 hyperpolarised images of mouse heart and lung. Images were taken by Albert in 1994 and are of poor quality with unclear structural borders, taken from (M. Albert et al., 1994).

The hyperpolarisation noble gases method has been further developed to investigate and give more functional details of the lung and brain (Cleveland et al., 2010; Goodson, 2002). Hyperpolarised Xe-129 was used to investigate alveolar gas uptake by imaging the Xe-129

dissolved within the pulmonary capillaries and the gas exchange in human lung tissues. Therefore, the result of Xe-129 dissolving in the body is that the image is displayed more clearly; the signal intensity is increased, with greater directional heterogeneity and quicker uptake of hyperpolarised Xe-129 as seen in Figure 9 (Cleveland et al., 2010).

Recently, polarising technology has improved the hyperpolarisation of Xe-129 to greatly improve the SNR in the lung during MRI scanning (Kirby et al., 2012)). This concentrates on validating lung imaging to compare images of hyperpolarised Xe-129 and He-3 in the same subjects. In Figure 9, the lungs of healthy and non-healthy chronic obstructive pulmonary disease (COPD) subjects are shown using this approach. The MR images of hyperpolarised Xe-129 and He-3 show the difference between the two noble gases. Generally, the images look similar; however, the measurements of the ventilation defect volume (VDV) in COPD patients are higher in the Xe-129 MR images.
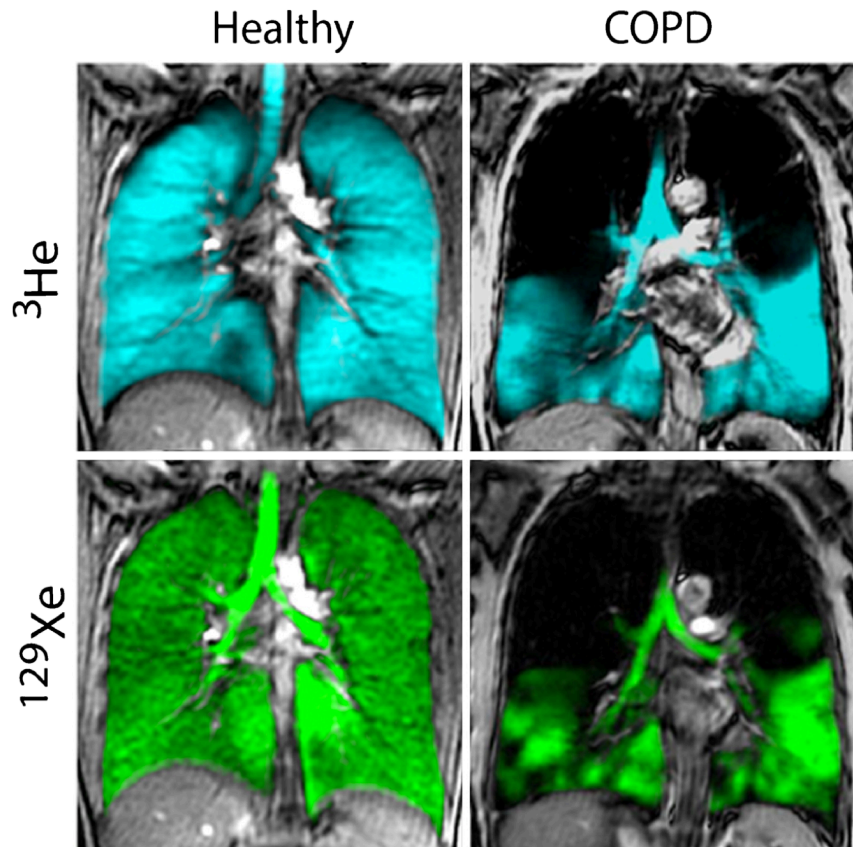
Figure 9: These MR images show the hyperpolarised He-3 and Xe-129, which were taken in the same healthy and non healthy COPD patients, taken from (Kirby et al., 2012).

Hyperpolarised Xe-129 is possibly a helpful MR tracer for providing functional information of the brain. This is because the high solubility of Xe-129 means that it easily crosses the blood-brain barrier and the chemical shift is high. The first spectrum images of an *in vivo* human brain using hyperpolarised Xe-129 were documented in 1997 (Mugler et al., 1997), as were the first animal images using hyperpolarised Xe-129 (Swanson et al., 1997). The initial image results using hyperpolarised Xe-129 in rat brain were shown to measure damage due to a stroke (Zhou et al., 2011) and cortical brain function (Mazzanti et al., 2011). In Figure 10, the hyperpolarised Xe-129 MRI imaging shows the area of damage due to a stroke in the rat model and the hyperpolarised Xe-129 signal voids were noticed in areas of the ischemic core; this was demonstrated by H-1 diffusion weighted imaging (DWI) and histology (Zhou et al., 2011).
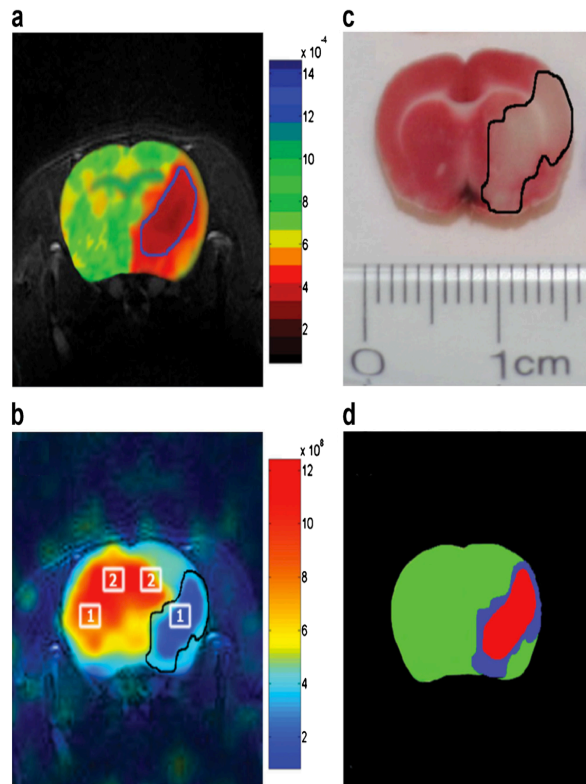
Figure 10: Images of brain stroke in a rat model using H-1 and hyperpolarised Xe-129 MR scanning. Image (a) shows the area of weak perfusion. Image (b) matching Xe-129 shows the signal void in the ischemic core area. Image (c) shows the histological verification of the stroke model associated with ischemia. Image (d) shows the colour map of normal tissue (green), penumbra (blue) and ischemic core (red), taken from (Zhou et al., 2011).

In a recent study (Rogers et al., 2016), the use of the hyperpolarised noble gas Krypton has been developed for the investigation of the lung in health and disease. Hyperpolarised ^{83}Kr in MRI imaging has many advantages for the diagnosis of pulmonary diseases. However, it had been thought to be difficult to produce hyperpolarised ^{83}Kr as a result of its physical characteristics. Molecular nitrogen had been used in spin exchange optical pumping (SEOP) as a buffer gas, however, in this study this has been changed to molecular hydrogen such that highly spin-polarised ^{83}Kr could be produced on demand. The nuclear spin polarisations of ^{83}Kr and ^{129}Xe were 29% and 63% respectively. The key advantage of using Hydrogen as a buffer gas is that it can be removed quickly. Hyperpolarised Krypton has been used successfully to demonstrate surface to volume changes in emphysema(Lilburn et al., 2015). In future, there are many possibilities for using hyperpolarised gases in the diagnosis of human diseases, and these new methods may lead to novel developments in understanding disease pathophysiology.

1.4　What is Parahydrogen?

Parahydrogen is a source of spin polarisation and can be exploited to create a non-Boltzmann distribution method. Parahydrogen can be used in two techniques: one is Parahydrogen induced polarization or PHIP (Hydrogenatively) and the other is signal amplification by reversible exchange or SABRE (non-Hydrogenatively).

Molecular Hydrogen has two Hydrogen atoms that are joined by a single bond. The effect of a magnetic field on the nuclear spin of each atom is determined by a simple set of principles that was first described by Pauli. Once the magnetic field is applied, the spin, based on its energy, will spin up with the magnetic field (α, + ½) or spin down (β, - ½) against the magnetic field. There are four nuclear spin configurations of diHydrogen (spin isomers). These four spin configurations of $\alpha\alpha$, $\beta\beta$, $\alpha\beta+\beta\alpha$, and $\alpha\beta-\beta\alpha$ can be described by quantum mechanics. The whole angular momentum quantum number (S) is 1 or 0. The values of S and Z direction (M_z) for diHydrogen are seen in Table 1 (Duckett & Mewis, 2012).

Table 1 The four spin states of Hydrogen (Ψs), the total spin in the Z-axis (Mz) and the quantum number of spin angular momentum (S)

S	M_z	Ψ_s
1	+1	$\alpha\alpha$
1	0	$(\alpha\beta+\beta\alpha)$
1	-1	$\beta\beta$
0	0	$(\alpha\beta-\beta\alpha)$

Two isomers of molecular Hydrogen exist, para and ortho-Hydrogen, which have different nuclear spin configurations. According to the Pauli principle, these isomers need the overall wave function (Ψ) of protons to follow specific rules. The total Hydrogen wave function contains elements of translational, vibrational, rotational, electronic and nuclear contributions. The symmetric components are vibrational, electronic and translational, whereas the rotational and nuclear contributions are antisymmetric. The wave function can be calculated mathematically as

$$\Psi = \psi_{\text{(translational)}} \psi_{\text{(electron)}} \psi_{\text{(nuclear)}} \psi_{\text{(rotational)}} \psi_{\text{(vibration)}} \text{ (Blazina et al., 2005).} \qquad 6$$

There are a limited number of antisymmetric and symmetric nuclear configurations to rotational states, with J = 1, 3, 5 and J = 0, 2, 4 respectively (Duckett & Wood, 2008).

The first three ($\alpha\alpha$, $\beta\beta$, $\alpha\beta$+$\beta\alpha$) are symmetric with nuclei exchange and are orthoHydrogen, whereas the singlet state ($\alpha\beta$-$\beta\alpha$) is antisymmetric and known as Parahydrogen, as shown in Figure 11.
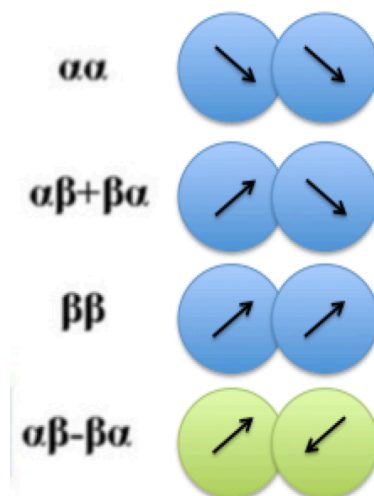
Figure 11: The triply degenerate and symmetric orthoHydrogen (blue circles) and the singlet antisymmetric Parahydrogen (green circle).

The variance in rotational states leads to different energies in the two isomers. As a result of low energy of rotational state, Parahydrogen is more stable than orthoHydrogen. Therefore, Parahydrogen is favoured at low temperature and this is exploited to provide high

concentrations of Parahydrogen. The four spins states at room temperature give 25% Parahydrogen and 75% orthoHydrogen. There is an inverse relationship between temperature and Parahydrogen. If the temperature is decreased towards 0 K, the Parahydrogen is increased to 100% as shown in Table 2 (Duckett & Wood, 2008).

Table 2 The different temperatures with different percentages of para and ortho-Hydrogen (Duckett & Sleigh, 1999).

Temperature (K)	Parahydrogen (%)	OrthoHydrogen %
0	100	0
20	99.82	0.18
75	51.86	48.14
150	28.54	71.46
273	25.13	74.87

1.5   Parahydrogen generation

Interconversion between isomers (para and ortho) is prohibited; however, it can be facilitated by the presence of a paramagnetic surface material such as iron oxide. Cooling the Hydrogen gas can generate Parahydrogen with the appropriate catalyst.

The first method of producing Parahydrogen is to cool the gas contained with liquid Nitrogen to a temperature of 77 K to obtain 50% Parahydrogen. This method has been utilized for several years and produces a high concentration of Parahydrogen. The second method has been improved in order to increase the quantity of Parahydrogen. A vacuum is created over the coolant of liquid Nitrogen, leading to a decrease in the temperature to 65 K and Nitrogen freezing. In addition, much more liquid Nitrogen is consumed in the process of increasing the Parahydrogen by 1.5 and this is followed by increased enhancement. The best temperature for Parahydrogen production is about 22 K, which leads to a high concentration of Parahydrogen (99%) without requiring an expensive machine.

Figure 12: The Parahydrogen generator used at the University of York Hyperpolarisation Centre.

At the Hyperpolarisation Centre at the University of York, generating Parahydrogen has been achieved with a device manufactured to a design by Duckett. The generator model is cooled to about 30 K and creates approximately 90% Parahydrogen (see Figure 12).

1.6   Parahydrogen induced polarisation (PHIP)

Bowers and Weitekamp (1986) reported that large nuclear polarisation can be produced by chemically adding Parahydrogen to a molecule (Bowers & Weitekamp, 1986). A study in 1987 demonstrated the results of a Parahydrogen reaction. In the study, the Hydrogenation of acrylonitrile (CH_2CHCN) was converted to Propionitrile (CH_3CH_2CN), catalyzed by tris (tripheny1- phosphine) rohodium(I) chloride at ambient pressure and temperature. The first spectra were acquired in high NMR fields (200 MHz) and can be seen in Figure 13 (Bowers & Weitekamp, 1987).
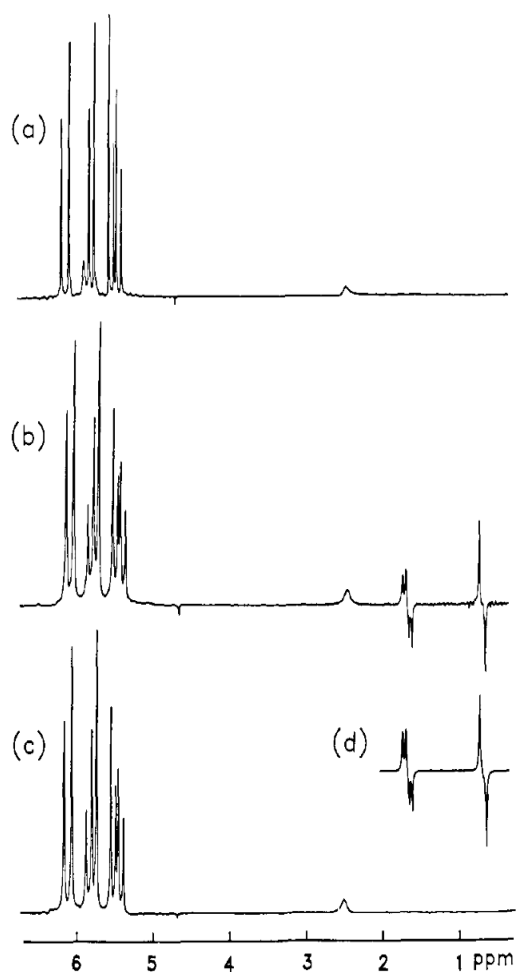
Figure 13: Image A indicates the Hydrogenation of acrylonitrile (CH$_2$CHCN) spectrum before Parahydrogen. Image (B) shows the spectrum after Hydrogenation. Image (C) shows the spectrum of the equilibrated sample. Image (D shows the line shape simulation displaying the predicted theory published in 1986, taken from (Bowers & Weitekamp, 1987).

PHIP enhancement led to signal increases of 8,100 - fold and the population difference is about 1 in 10 (Michael J. Cowley et al., 2011). Parahydrogen has no angular momentum and so cannot be detected by NMR spectrometers. To produce signals the Parahydrogen symmetry is essentially broken and then is moved into a substrate to place the Hydrogen in two magnetically inequal environments (Eisenschmid et al., 1987). If normal Hydrogen is used, the Boltzmann distribution will give different spin and a low NMR signal and this gives four splitting patterns in the H-1 NMR spectrum, as seen in Figure 14a (Natterer & Bargon, 1997).
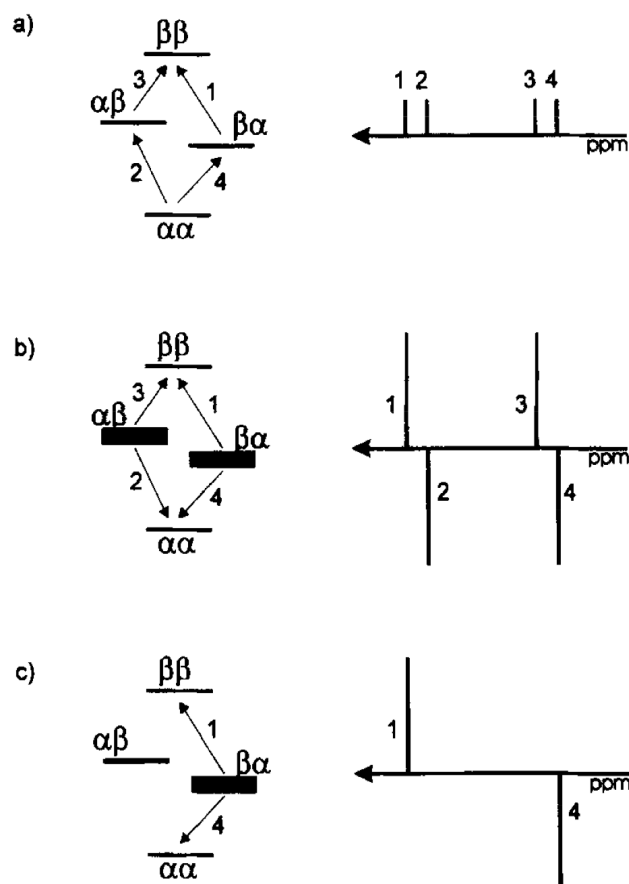
Figure 14: (A) shows the normal NMR spectrum, (b) PASADENA, (c) ALTADENA, taken from (Swanson et al., 1997).

Two methods of PHIP have been discovered. Firstly, the Parahydrogen And Synthesis Allow Dramatically Enhanced Nuclear Alignment (PASADENA). When the NMR intensity is based on the variance in population, the Parahydrogen will give much more signal compared to normal Boltzmann distribution. This is noticed once the Parahydrogen is added to the sample and is used in a high magnetic field. In the PASADENA method (figure 15b), the $\alpha\beta$ and $\beta\alpha$ levels are converted to be overpopulated. The NMR signals are provided from two pairs of signals with similar intensity. Each pair has two lines, one is up and another is down; this known as anti-phase and produces high signals.

The second method is the Adiabatic Longitudinal Transport After Dissociation Engenders Net Alignment (ALTADENA) as shown in Figure 15c. This appears in a low magnetic field and then the substrate sample is transported to the high magnetic field of the NMR. Under the ALTADENA conditions, only the $\beta\alpha$ spin state is overpopulated and gives antiphase

doublets in the Hydrogen spectrum. The NMR signals are produced from two lines that have different phases.

Compared to DNP, these techniques are quick and cheap; polarisation can be done in a few seconds and gives high signals (Glöggler, Colell, & Appelt, 2013). However, there is an essential need for a chemical hydrogenation of a precursor molecule. This means that the technique may not apply to all molecules and that, for use in humans, the chemical process has to be amenable to being performed in sterile conditions and that catalysts are removed before injection.

1.7   PHIP applications

PHIP has been used in animal models and the image was produced by applying the rapid acquisition single-shot turbo spin-echo (RARE) pulse sequence. In Figure 15, the three images were acquired by spin echo (SE), gradient echo (GE) for proton images and PHIP technique. The first image (a) was acquired by using the spin echo (SE) sequence, leading to the production of high resolution but a long scan time. The second image (b) was acquired using fast gradient echo (GE), leading to a short scan time but low SNR and resolution. The third image (c) was a 13C image acquired by RARE sequence after one second of injecting 3 ml of contrast into the tail vein of the animal. In Figure 15, some venous branches and the vena cava can be seen clearly against the black background (Golman et al., 2001).
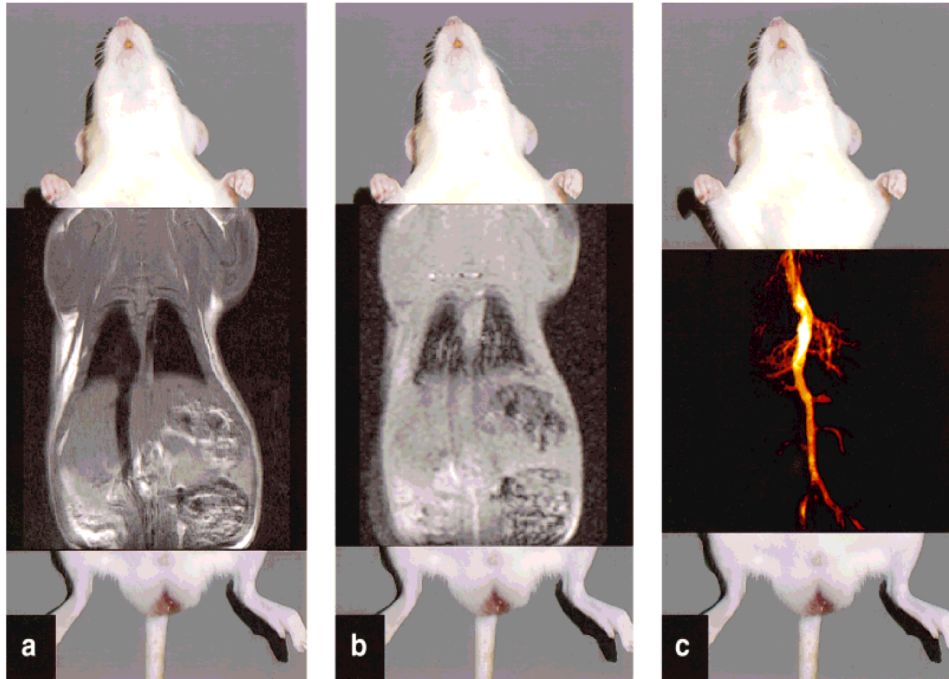
Figure 15: Rat images produced at 2.4T. Image (a) shows the proton image acquired by SE in 5.9 minutes. Image (b) indicates the proton image acquired by GE in 0.9 seconds. Image (c) shows the 13C image acquired by RARE sequence in 0.9 seconds, taken from (Golman et al., 2001).

The hyperpolarised 1H image is interesting and could lead to clinical medical applications. However, the need for Hydrogenation and the decay of the image, in high-resolution angiography, diffusion and perfusion imaging, leads to difficulties in using this technique currently in clinical settings (Golman et al., 2001).

The 13C angiogram has been investigated in animals *in vivo*. The head and neck of a guinea pig were scanned using a fast imaging spin echo sequence and the image was acquired in 230 ms. The PHIP method can provide a molecular solution with high polarisation that can be used in MRI. This leads to fast angiographic scanning and high contrasts. However, the main requirements of this method are that the longitudinal relaxation time of hyperpolarisation spins should be longer than or similar to the time period between imaging and field cycling (Jóhannesson, Axelsson, & Karlsson, 2004)

1.8   Single amplification by reversible exchange (SABRE)

The first paper outlining this method was published in 2009 (R. W. Adams et al., 2009). The SABRE technique used Parahydrogen as a source of polarisation in a low magnetic field with

the substrate Pyridine and an Iridium based catalyst. In the SABRE process, two Pyridine molecules and Parahydrogen reversibly associate with the catalyst At this point, J coupling transfers the characteristics spin state of the Parahydrogen to Pyridine in approximately one second. Thus when the Parahydrogen is added, the polarisation is transferred across the formed Parahydrogen-catalyst-substrate complex. The complex then disassociates and the polarisation remains in the substrate. This leads to hyperpolarisation of free Pyridine and no hydrogenation was required.

The effectiveness of SABRE hyperpolarisation relies on magnetic field strength and the lifetime of Parahydrogen and the substrate binding with the metal catalyst.. The polarisation transfer from Parahydrogen can be done in seconds compared to that of DNP, in which several hours are needed to transfer polarisation from unpaired electrons. Recently, SABRE has been developed as an alternative method to PHIP and shows that polarisation can occur without the reaction of Hydrogen and chemical hydrogenative change of the substrate. In Figure 16, Parahydrogen is added to a substrate with a catalyst and this produces a free hyperpolarised substrate. The early publications showed enhancements of 550 to 8,200 -fold.
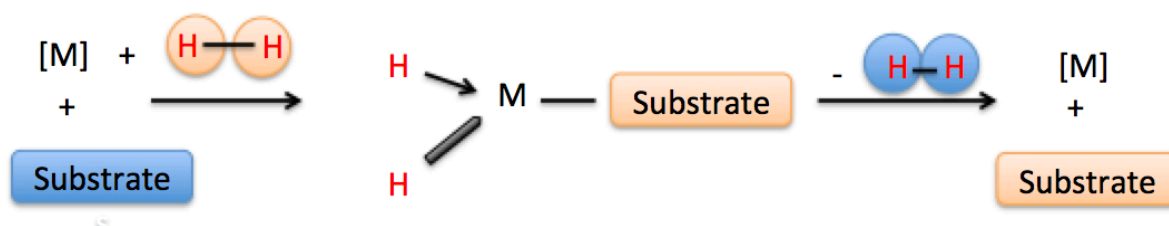
Figure 16: The SABRE method, showing the process of magnetisation that leads to a free substrate. [M] is the metal catalyst, the pink diHydrogen is Parahydrogen and the blue diHydrogen is OrthoHydrogen. The pink substrate is hyperpolarised.

Recently the SABRE method has been further developed by other groups and can now be used with low power deposition and a simple pulse sequence known as LIGHT- SABRE (Low Irradiation Generation of High Tesla). The most important point is that the low power pulses can lead to huge polarisation in any magnetic field by moving magnetic signal in the Parahydrogen to a substrate in the presence of a metal based catalyst. In addition, the *in situ* hyperpolarisation can be used in MR clinically without the need for strong RF irradiation,

microwaves, cooling of cryogenics and without reprocessing times between experiments. However, there is one requirement, which is that the apparatus should be able to produce a simple pulse sequence able to conduct any new NMR spectrometer. It is expected that the SABRE will be used to produce hyperpolarisation both *in situ* and *ex situ* with no expensive instrumentation (Theis, Truong, Coffey, Chekmenev, & Warren, 2014).

The SABRE mechanism has been further developed in York. SABRE hyperpolarisation can be used as a tool in biologically active tissue, using Pyridine or Nicotine, for example, which have similar structures. The Nicotine is hyperpolarised quickly using Crabtree's catalyst in a Methanol-d4 solvent. The Iridium in such a metal complex allows temporary binding to many molecules and therefore is a flexible way of using SABRE to polarise a large number of substrates. In addition, Carbon13 and Nitrogen15 polarisation have been investigated and successful hyperpolarisation was achieved with SABRE. Iridium can be used to provide many different catalyst complexes that are available for use with SABRE and suitable for a range of different ligands. In low-field studies, peptides and alkaloids such as Harmine have also been hyperpolarised (R. W. Adams et al., 2009). It has also been suggested that amino acids can be hyperpolarised in Methanol-d4 solvent by SABRE (Glöggler et al., 2011). The catalyst has been further developed and even allows biological active molecules to be polarised in water, which could lead to the development of a novel contrast agent for MRI applications (Glöggler et al., 2013). The Parahydrogen polarisation of samples makes the chemical shift accessible in low fields and a high signal is observed. This may lead to a novel application of NMR research (Glöggler et al., 2013). The Pyridine polarised spectra with 15N using SABRE method can be obtained even after transfer at zero-field (Theis et al., 2012).

The team in York's Centre for Hyperpolarisation in Magnetic Resonance (CHyM) have documented these developments in SABRE (Duckett & Mewis, 2012). The first template to be investigated using SABRE was $[Ir(H)_2 (PCy_3) (substrate)_3][BF_4]$, where the two Hydrogen atoms were located in a Parahydrogen molecule with an appropriate substrate (Nitrogen) donor such as Pyridine. The substrates appeared in the magnetic field in which the transfer of polarisation occurred at 5.0×10^{-3} T. The hyperpolarisation signals resulting from 1H, 13C and 15N of Pyridine were compared with these atoms at thermal equilibrium. Other substrates such as Nicotine, Quinoline and Pyridizine were also hyperpolarised. The enhancement of NMR spectra of 19F and 31P in a metal complex were verified and this

illustrates that the hyperpolarisation substrate of these molecules can be achieved in protio solvent (having a proton (H) atom, for example CH_3OH, Methanol) (Aguilar, Elliott, Lopez-Serrano, Adams, & Duckett, 2007).

The theory of SABRE experiments is based on utilizing numerical models and mathematical software. The analysis was completed on a simplified model with two 1H nuclei in one substrate coupled to two Hydrogen nuclei from Parahydrogen bound to a metal centre. Hence, there is a two-spin system in the free substrate and four-spin in the bound complex (Green et al., 2012).

Several substrates such as Pyridine and Nicotinamide have been used in the model and practical experiments, which include five and six 1H nuclei in every substrate and two substrate molecules joined to the centre of the metal within the equatorial of the complex (R. W. Adams et al., 2009). Therefore, in the bound complex there are seven and eight spin systems. On the other hand, the ligands of equatorial substrate do not need to be the same. Figure 17 below shows an octahedral complex with the two ligands of substrate, indicated L_c and L_d.
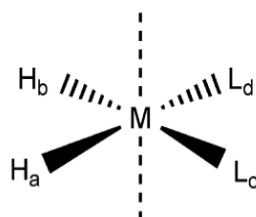
Figure 17: The diHydride octahedral complex, taken from (Green et al., 2012).

The SABRE experiments can be analyzed at three time points, see E1, E2 and E3 in Figure 18. The initial point is for time evaluation (t_0) which is known as an instant the complex forms. The E1 interval lasts between t_0 and t_d. This is the time when the substrate is assumed to be separate from the complex. Secondly, the E2 interval is that from t_d to the time, t_f, when the sample is placed in the stray field of the magnet. The last interval is E3, known as the dynamic field time. This is observed from when the sample enters the magnet until it is held at t_m (the static measurement field). Throughout the last interval, the sample experiences a quick increase in magnetic field till the field measurement is achieved (Green et al., 2012). To appreciate the events that happen at each time point, the concept of scalar coupling has to be described.
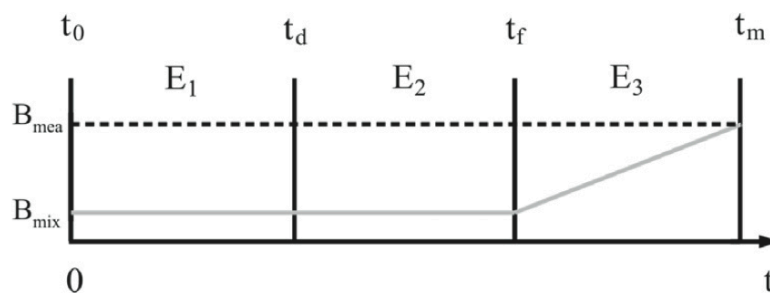
Figure 18: The different strengths of magnetic field (Bmea and Bmix) in the SABRE technique as a time function. The gray line shows the spin at each interval, taken from (Green et al., 2012).

1.9   Scalar coupling

Also known as J coupling, scalar coupling occurs from spin-spin interactions that appear through bonding electrons (Rule & Hitchens, 2006). Scalar coupling between nuclei is independent of chemical shift and can show the relationships between the nuclei, which are close one to another in the bonding framework. The coupling causes multiples in the spectrum such as in Figure 19. If two spin half nuclei are coupled, the resonance will split from each spin into two lines, known as a doublet. Hence, every doublet is split into the same amount, a quantity indicated as a coupling constant, J. The coupling constant values are found independent of magnetic field strength and are quoted in Hertz (Keeler, 2013).
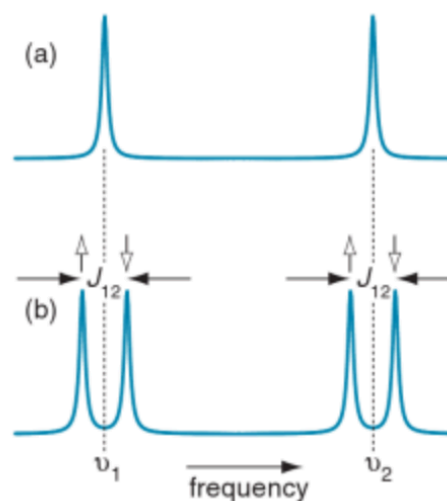
Figure 19: Spectrum indicates two peaks at frequencies v1 and v2 from diverse spins; the j coupling will split the spin into two doublets, each doublet is the coupling constant, J12, as shown in (b), taken from (Keeler, 2013).

The example of the ethanol spectrum (CH_3CH_2OH) shows three different parts of information (Figure 20). Firstly, the chemical shift of individual resonance appears as a result of the surrounding atoms that create a small magnetic field and change of frequencies. Secondly, the signal intensity is proportional to the Hydrogen atoms in the molecule. In the ethanol spectrum, the integral ratios for Hydrogen A, B and C are 3:2:1. The last part of information is the splitting in the signal. The splitting rule (n+1) is based on the closest resonance used (Levitt, 2008). For instance, proton A shows a triplet splitting pattern because the closest Carbon (B) has two protons. However, proton C shows a single peak with no splitting from the oxygen atom. These three parts can help to analyse and characterise complicated molecules.
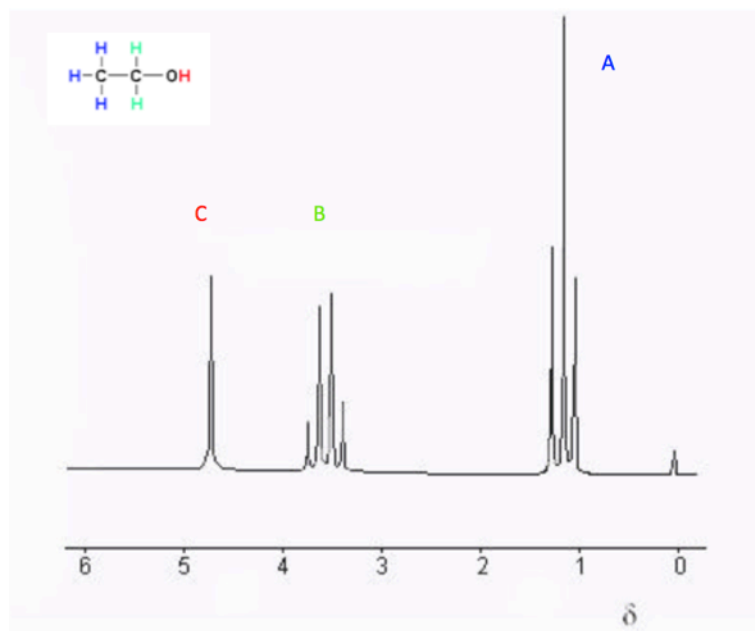
Figure 20: Image shows the 1H NMR ethanol spectrum and the three chemical environments of a proton, as seen in A, B and C

1.10 Magnetic Resonance Imaging

Magnetic resonance imaging (MRI) is common in both animal and human applications. Raymond Damadian discovered the signal from Hydrogen in cancer tissue and found there was a difference between healthy and non-healthy tissue images due to more water being present in tumours (Damadian, 1971).

Lauterbur took the first NMR images by using a gradient field and the main field (Figure21) (Lauterbur, 1973).

Lauterbur used two different samples with different relaxation times in his experiments. The first sample was pure water while other was $MnSO_4$, which has a shorter relaxation time. Damadian noticed the different relaxation rates of biological tissue in 1971. The measurements of T1 and T2 were used to show the difference between control and non-control tissue (Damadian, 1971; Weisman, Bennett, Maxwell, Woods, & Burk, 1972).

Mansfield and Maudsley achieved the first NMR image of human tissue in 1977 (Mansfield, Pykett, Morris, & Coupland, 1978).

Figure 21: The first proton magnetic resonance image (zeugmatographic image) of two objects in a glass tube containing water and surrounded by C_2O973, taken from (Lauterbur, 1973).

1.11 The importance of MRI

MRI depends on NMR fundamentals and plays a vital role in research and diagnostic work in clinical trials (Clark, Hockings, Joyce, & Mazucco, 1997). MRI uses gradients in three dimensions (3D) to generate signals and then produce the image (Morris, 1986). MRI can be used to scan the internal organs and soft tissue without surgery since it is a non-invasive technique. This is the great value of using MRI in clinical applications. Recently, MRI has been used to investigate brain function by different methods such as functional MRI (fMRI) (Ogawa, Lee, Kay, & Tank, 1990), MR spectroscopy, perfusion, diffusion and chemical shift imaging (Faro, Mohamed, Law, & Ulmer, 2011).

Conventional MRI depends on magnetic resonance from protons in the body and the magnetic field strength. MR signal is proportional to concentration and nuclear spin polarization. There is a clear advantage of using high magnetic field but the MR signal is still modest and costly. However, there are alternative methods can be used to gain high MR signal such as SABRE, DNP and PHIP. These methods not only detect protons but also can polarise many nuclei such as 13C, 129XE, 3He and 15N. The decay of these hyperpolarised nuclei can be long and the chemical compounds long relaxation make them valuable as hyperpolarised contrast agents (Gateway, 2013).

1.12 Aims and Objectives

PHIP is a well-researched hyperpolarisation technique because the signal enhancement is bigger compared to thermal equilibrium. However, this method is limited because of the need of a suitable bond for hydrogenation. Thus, the SABRE method is possibly a better technique to overcome these limitations

This study focuses on hyperpolarisation techniques, and especially on the different aspects of the SABRE method. The thesis aims 1) to develop a method that can overcome the sensitivity problems of NMR and MRI by exploring a method which changes the spin distribution in nuclei in biological molecules; 2) to investigate, develop and determine the best substrate to use in biological tissue; and 3) to develop imaging methods suitable for hyperpolarised samples produced using SABRE, leading to the use of SABRE.

In this thesis, the second chapter describes the general methods that were applied throughout the thesis. The third chapter demonstrates that the SABRE method can be used in a standard clinical MRI scanner. This was done by means of a shake and drop experiment using 3-Tesla scanners and using the fringe field for spin polarisation. Different substrates were investigated with different conditions. One aspect that was explored in detail was that Pyrazine, which is a highly symmetric molecule, should have a simple signal that would decay exponentially as only one spectral peak contributed to the longitudinal magnetisation. However, it is shown that a non-exponential decay is observed and that this is magnet polarisation field dependent. It is argued that this is evidence for the existence of other magnetic states that are evolving with time. In Chapter 4, the optimisation of SABRE was explored to improve its use in imaging by varying flip angle and the delay between volume acquisition. The effect of deuterisation is also explored with the result that imaging over long durations is shown to be possible such that good image contrasts can be maintained for dynamic imaging. In chapter 5, Pyrazine samples were investigated at 3 T with *ex vivo* tissue to investigate whether SABRE could be used to produce novel contrast methods for use in a clinical scanner. It is shown that tissue can affect the relaxation time of the hyperpolarised molecule and that this could be used as an image contrast mechanism such that the presence of a particular tissue would result in less signal. Chapter 6 explores whether the theoretically predicted long-lived states explored in earlier chapters are revealed when biological tissue is present. The theory being that breaking the symmetry of Pyrazine, by putative binding to

naturally occurring Pyrazine binding proteins would allow long-lived states to evolve into observable magnetisation. Chapter 7 is the conclusion of the thesis and also describes possible future work.

Chapter 2   Methodology

This chapter provides a summary of the main methodologies that were used during this PhD. In chapter 3 and 4 all the experiments have been performed on a 3Tesla HDX Excite General Electric (GE) device whereas the experiments of chapter 5 was performed on a 3T Siemen's magneto prisma machine. Chapter 6, the exploration of long-lived states was performed on a vertical Bruker NMR scanner. SABRE as mentioned in chapter 1 is used in all experiments in this thesis. More details of this technique are given here.

2.1   MRI hardware

MRI Scanner Cutaway
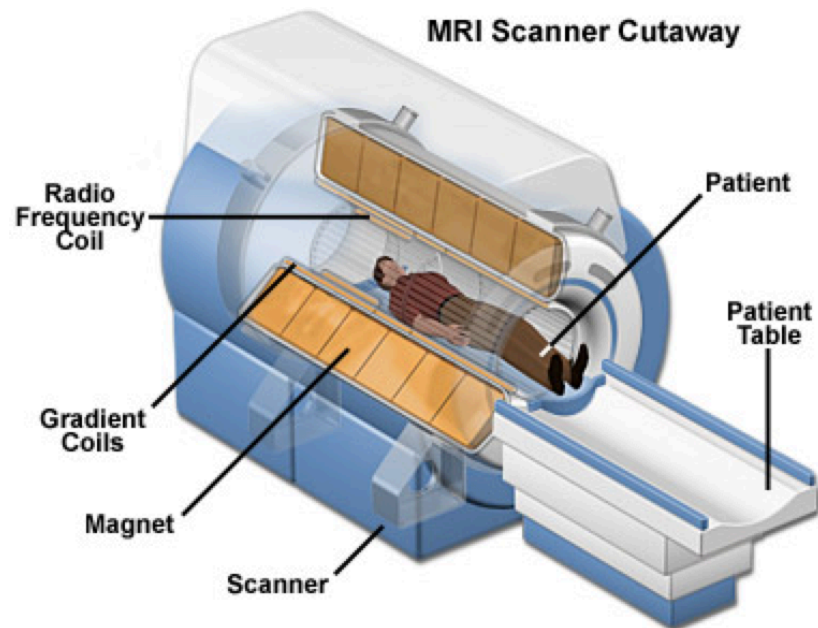
Figure 22: MRI scanner components, taken from (https://snc2dmri.weebly.com/components--functions.html)

A MRI scanner has four main components: the magnet, gradient coils, radiofrequency coil and console as seen in figure 22.

2.2   Main magnet

The main magnet is an expensive, an important and the biggest component of the whole scanner. The magnet system used has a unit of measure called the Telsa or Gauss (1 Tesla = 10000 Gauss). A superconducting magnet is an electromagnet built form several coils of superconducting wire. The coils are cooled to a very low temperature throughout scanning. The superconducting magnet can produce large magnetic fields which are not possible if a simple resistive wire magnet is used. (E. Adams & Goodkind, 1963).

2.3   Shim coil

The shim coils are utilized to regulate the homogeneity of the main magnetic field. To interpret the signals from nuclei placed in the magnetic field, the homeogeneity has to be high

so that frequency is directly proportional to the location of the nuclei. There are two kinds of shimming: active shim and passive shim. Passive shimming is applied by imaging a phantom and adjusting the shim plates location until the ideal field homogeneity is obtained. Passive shimming is run at installation time and reduces inhomogeneity without the subject being positioned in the magnet. Active shimming is run for every sequence in the protocol or every patient. It is achieved by driving shimming coils by passing current through them appropriate to the particular conditions throughout the magnet volume. This leads to a field as homogenous as possible depending on subject or sample size or composition.

2.4   Radiofrequency (RF) Coils

There are two coils; one for sending RF signal to the sample and is known as the transmit coil or coils and another is to receive signal from specific part of a subject or sample and is known as the receive coil or coils. Sometimes the same coil can be used for both transmit and receive and in this case switches are used to couple the coil to either the transmit circuitry or the receive amplifiers. The signal that is transmitted is known as the excitation pulse and is often highly filtered to contain a particular bandwidth of transmit RF to the subject or sample. If this is carried out when a field gradient has been established along the main magnet field, then this can be used to excite a specific slice of nuclei distributed along that gradient.

2.5   Gradient coils

These provide the opportunity to obtain an image by varying the field around that of the main magnet field. The concept of a gradient coil is quite straightforward. For example, in a simple electromagnetic coil consisting of many equally spaced windings, and which is attached to an electrical terminal at each end, the current passes one way through the coil (the right hand rule). On the other hand, if this is changed by adding a third terminal in the middle of the coil, the polarisation of the terminals can change. Thus, the current moves in the reverse direction to both ends of the coil. Significantly, this provides the same magnetic field but in an opposite way (Maximilian F Reiser, 2007; Westbrook & Roth, 2013). By combining these, a gradient in the field can be established. The result is that the Larmor frequency of any nucleus within the field will vary systematically across the gradient field. This can be

exploited to create a 2D image by recording the signal and using the Fourier information to be a measure of distance in one direction, for example across a slice if only the nuclei in a particular bandwidth are excited. Gradient coils are used to establish two forms of encoding, phase and frequency encoding, which when combined with slice selected excitation, provides 3D imaging.

2.5.1 Phase Encoding

A second stage after the slice selection in spatial encoding, can be used to give us a two dimensional image. The relationship between phase and frequency is the time.

A gradient in the Y direction is turned on after the spins are excited and a resonance in the XY plane is established. The processional frequency of the spin is changed by phase encoding gradient because of the location of the Larmor frequency spin along the field gradient. The phase shift can be known as it is proportional to the magnetic field in the direction that it needs to encode. The signal from protons is also dependent upon the sample phase change, so if we apply a (phase) gradient to rephase the protons to a different phase we can exploit this to provide 2D image information. Usually, the phase encoding is turned on just before sending a 180degree rephasing pulse, See figure 23.
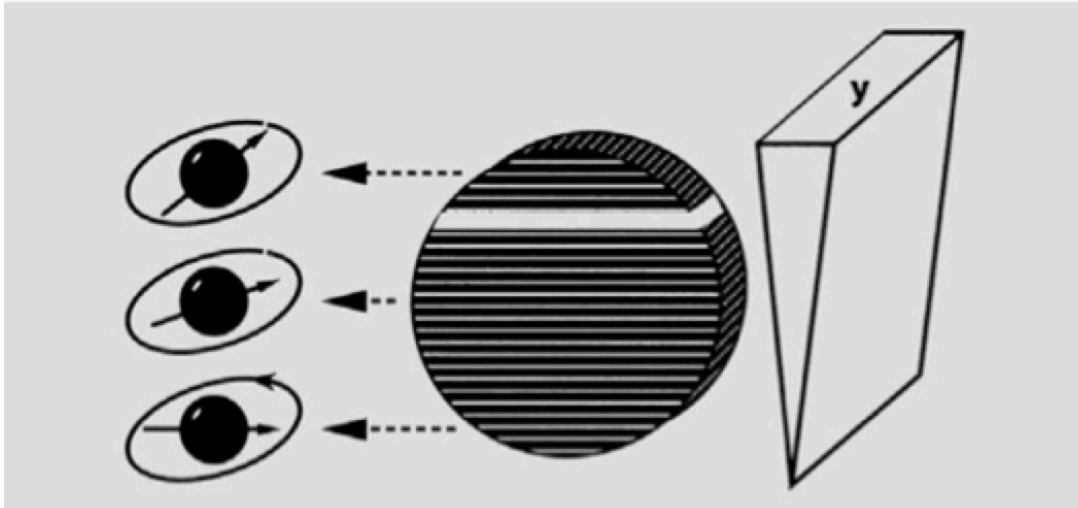
Figure 23: Phase encoding is the y gradient. Every horizontal line (white line) is known by a special amount of phase shift, taken from (Weishaupt et al., 2008).

2.5.2 Frequency encoding or readout gradient:

Frequency encoding is the last step for spatial encoding. If a readout gradient is switched on, the strength of the magnetic field and, thus the nucleus resonance frequency is a linear function along an axis in the magnet and nuclei will precess according to the frequency. The readout gradient switches on during signal acquisition (at the same time of free induction decay or echo signal). The receiver coil measures the echo signal and Fourier transformation digitizes it. The sampling time is the time when the frequency gradient encoding is switched on and the value in general is between 5-30 ms. It is worthwhile noting that it is determined by the magnitude of the readout gradient, by the desired field of view and by the Nyquist frequency. The relationship is given by this formula

$$\Delta\omega_{RO} = 2\omega_{NQ} = \gamma(G_{RO} \times FOV_{RO}) \qquad 7$$

Where $\Delta\omega_{RO}$ is the total range of frequency in the image, where ω_{NQ} is the Nyquist frequency, where G_{RO} is the proton located in the edge of field of view.

There are two ways to characterise an image: in terms of spatial resolution and frequency resolution. The spatial resolution gives us the voxel size (mm/pixel) which comes from FOV_{Ro} and N_{Ro} (Brown, 1999), see figure24.
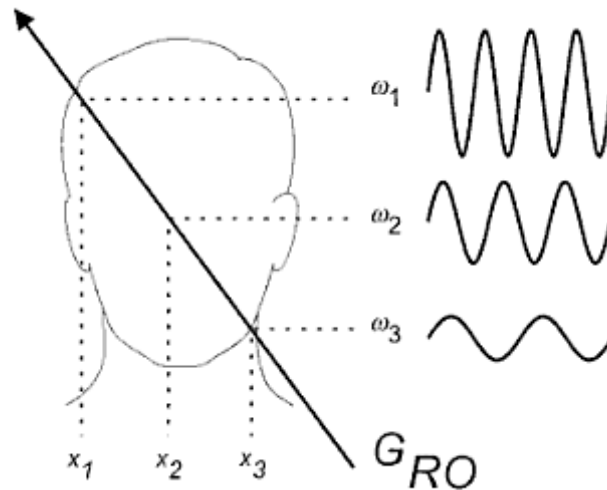
Figure 24: The Readout process, taken from (Brown, 1999).

2.6   Console

The console is an integral section of an MRI system located outside the magnet room. The console is the control system that determines the magnitude of the gradients, the timing of RF transmit pulses and when the transmit/receive coils are switched into their respective circuits. It is the console that was used throughout this thesis to modify the transmit pulse sequences, the details of the features such as the flip angle of the excitation pulse, the time to echo, the acquisition time, the slice thickness, the number of volumes, and the time delay between volumes. The console was also used to create specific pulse sequences to convert longitudinal magnetisation into singlet states and also from stored magnetisation in singlet states back into observable magnetisation in chapter 6.

2.7   The free induction decay (FID) signal

When the excitation RF is turned off, the net magnetisation vector (NMV) will rotate around the magnetic field and produce a signal (by induction in a receiver coil). The energy of the Parahydrogen induced magnetisation will be lost and this is called relaxation. When relaxation occurs, the NMV will realign with the main magnetic field and return to the

thermal equilibrium with a time constant termed T1. However, at the same time, magnetisation is decreased in the transverse plane (T2 decay). Therefore, magnetisation in the transverse plane is decreased and the voltage magnitude induced into the receiver coil reduces with time. The induction of this decreased signal is known as the free induction decay (FID) signal (Westbrook & Roth, 2013). To create images from hyperpolarised substrates, it is crucial to understand the mechanisms involved in determining the duration of the free induction decay

2.8   Relaxation

After the RF pulse is switched off, the B_0 causes the realignment of the NMV to the field. Hence, the NMV will lose the energy received from the RF pulse. This process is called relaxation. If relaxation occurs, an increase in the magnitude of the longitudinal magnetisation will happen (longitudinal recovery) and the magnitude of the transverse magnetisation is reduced (transverse decay). A reduction in the transverse magnetisation leads to a decrease in the current that was induced in the receiver coil. The recovery of the longitudinal magnetisation is carried by T1 recovery, which is caused by the Hydrogen nuclei losing energy to the surrounding tissues; this is called spin lattice relaxation. The decay of the transverse magnetisation is mediated by a T2 decay caused by the mutual exchange of energy with other nuclei; this is called spin-spin relaxation(Westbrook & Roth, 2013).

2.8.1   Spin lattice T1

After the 90º RF has ended, the net magnetisation vector will have flipped to the transverse plane and continues to precess in that plane and initially in phase. This is termed coherence. When the RF is switched off, the NMV will begin to decay in the transverse plane and will recover back to the B_0. This decay is because the contributions from individual nuclei dephase with respect to each other and the overall vector in the plane decrease as the signal returns to the longitudinal plane. As an example, fat can appear to have more longitudinal magnetisation because it has a longitudinal recovery time faster than that of water. After the next RF pulse is sent, we find more magnetisation in the X and Y plane in the fat and this will appear as a bright area in the image. As the repetition time controls how much we see of the T1 recovery, with fat having a faster longitudinal recovery time than water; hence using a

short TR provides better contrast between the fat and the water. If a long TR is used, the full recovery of water and fat will take place and after the next RF pulse is sent, there will be no difference between the fat and the water, as shown below in figure 25. The effect of a long TR is that it provides high signal images but with poor contrast(Westbrook & Roth, 2013).
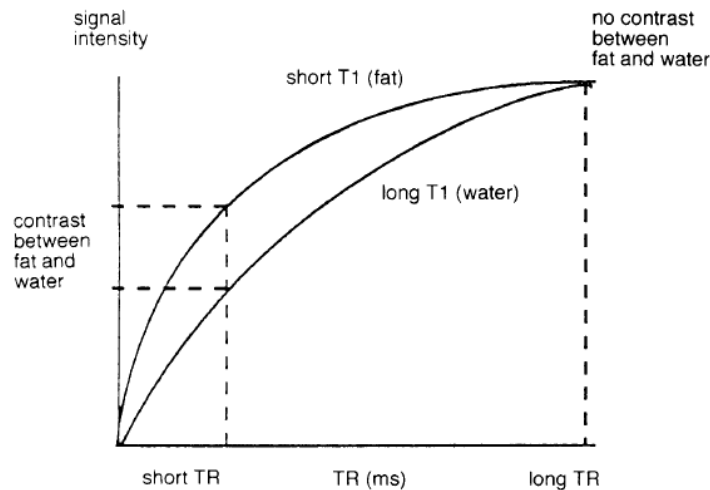
Figure 25: The longitudinal curve (T1 recovery), taken from (Westbrook & Roth, 2013).

2.8.2   Spin - Spin T2

Fat has a short T2, because it has a very fast decay rate in the transverse plane, whereas water has a long T2, because it maintains transverse magnetisation for longer. This is because the signal in fat dephases faster. Thus, water shows as a bright area of the image and fat shows as dark area. As the echo time parameter creates a control for the magnetisation in the transverse plane, a long TE is used to obtain the T2 weighted images. When using a short TE, the fat and water do not have enough time to decay and hence they have an equal amount of magnetisation in the X and Y planes, see figure 26 (Westbrook & Roth, 2013). Whereas if a long TE is used, then a high contrast can be seen between fat and water.
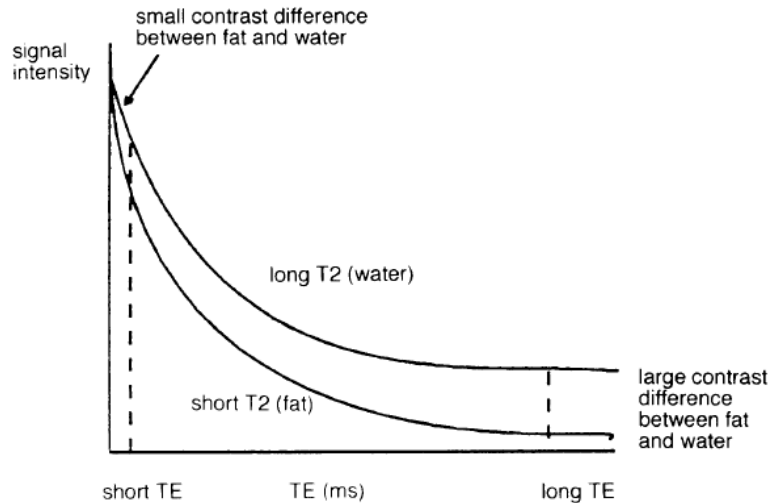
Figure 26: Transverse decay (T2 decay), taken from (Westbrook & Roth, 2013).

2.8.3 Decay of T2*

Losing phase coherence in the X and Y planes shows the decay of the T2*, which is a combination of the inherent T2 mechanisms within and between molecules and the inhomogeneity in the magnetic field. This inhomeogeneity can also be brought about by the presence of molecules in the sample which have either diamagnetic or paramagnetic properties. Thus T2*, appears faster than the T2 decay. We can compensate for the loss of X- and Y-plane phase coherence and hence the loss of signal by applying an 180º RF pulse, which refocuses the time independent loss of phase coherence (magnetic susceptibility and magnetic field inhomeogenities). The T2* decay is the main loss of phase coherence

2.9 MRI machine

3T MRI scanners have been used to investigate different substrates. In this thesis, the reason for using a high magnetic field is to increase spatial resolution and achieve high image quality, which is affected by many factors. It is not to create the actual spin distribution (see chapter 3)

2.10 Signal-to-noise ratio (SNR)

There are a number of factors influencing the SNR.

2.10.1 Proton density

Areas of low proton density, such as the lungs, have a low signal and thus a low SNR. However, areas with a high proton density, such as the pelvis, have a high signal and hence a high SNR (McRobbie, Moore, Graves, & Prince, 2006). In hyperpolarisation, the apparent proton density is increased as the number of protons contributing to the net magnetisation vector (NMV) increase.

2.10.2 Voxel volume

This is determined by slice thickness and pixel area. If the voxel size increases, the SNR will increase, but this does not mean that the quality of the image will be higher. The signal intensity will be averaged between the tissues, because a large voxel can have more than one tissue. This leads to a low spatial resolution(Ray Hashman Hashemi, 2012). In this thesis, the slice thickness has been limited by the size of sample tubes and the need to be aware that edge susceptibility effects and partial volume effects could lead to poor image quality. The slice thickness used was, in general, 3mm.

2.10.3 TR, TE and flip angle

These parameters influence the image contrast and the SNR and therefore affect the image quality. The T1 relaxation process is controlled by the TR. Thus, if a long TR is used, the magnetisation has enough time for a full recovery and thus has more transverse magnetisation from the following RF pulse. Therefore, a high SNR occurs as a result of a long TR. The T2 relaxation process is controlled by the TE. Here, the magnetisation decay in the X and Y planes but because the TR is short, and thus a repeated high current is induced in the receiver coil. Therefore, a short TE provides a high SNR rather than TR. There is also the influence of the flip angle on the SNR in both the SE and GE sequences. In the spin echo pulse, we would normally use a 90º RF pulse angle to transfer all net magnetisation vectors to the X and Y planes and hence this provides a high SNR. On the other hand, the flip angle that is used in

the gradient pulse sequence is often less than the 90º RF pulse, so little magnetisation will be transferred to the X and Y planes, providing a low SNR (Westbrook & Roth, 2013) but a low flip angle does allow repeated measurement of a hyperpolarised signal. A 90º flip angle pulse uses up all available hyperpolarisation. In this thesis the optimisation of flip angle and TR are investigated.

2.10.4 Number of Excitations (NEX)

The NEX is not the best method to raise the SNR as the increase in signal is limited because of the random motion of noise, which has a significant influence on the scan time. In general SNR is increased in proportional to the square root of the number of excitations (averages). However, reducing NEX can also assist in decreasing the artefact due to motion, leading to an increase in image quality (Dominik Weishaupt, 2013). Using multiple excitations for averaging is not used in this thesis as each excitation uses up available hyperpolarisation and thus simple averaging is not available.

2.10.5 Receive bandwidth

While the readout gradient is applied, a range of frequencies is sampled and this is the receive bandwidth. Decreasing the bandwidth leads to decrease in noise and thus an increase in SNR will result. Note that if we reduce the bandwidth, the artefact due to chemical shift will potentially increase (Westbrook and Roth, 2013). In the studies in this thesis the receive bandwidth was set at 30kHz.

2.10.6 Contrast

Contrast is known as the variance in the SNR between adjacent areas. We control the contrast by using the same factors that influence the SNR. Note that contrast and signal need to be compromised for good image quality.

Because of T1 and T2 relaxation characteristics in MRI, discrimination between different tissues inside the body is possible. Contrast in tissue is influenced by T1 and T2 values of different tissues and also by variations in the magnetic field, alterations in temperature and other factors. A perfect contrast in the image depends on the best selection of suitable pulse

sequences. Inversion recovery, SE, turbo sequence, slice profile, saturation and GE. TE, TR, TI (inversion time) and flip angle are essential pulse sequence parameters. They are combined with PD, T1 and T2 relaxation times. The values of these parameters are affected dissimilarly by various tissues. Saturation is acquired if we use a TR of less than (5*T1). If the first RF pulse is sent, the whole longitudinal magnetisation will transfer to the X and Y plane. If the next RF at less than 5*T1 is applied, less magnetisation will recover and thus there will be less transverse magnetisation. Regarding inversion recovery, the benefit of this is to gain the best contrast among water and fat by exploiting the T1 of the tissues. This is an intense T1 weighted image (Westbrook and Roth, 2013). In this thesis, the TR is systematically investigated.

2.10.7 Spatial resolution

This is determined by the voxel size. Small voxels give us a perfect resolution, whereas large voxels lead to a low resolution. The voxel size is influenced by the thickness of slice, FOV and number of pixels or matrix. If the thickness of the slice is reduced, the spatial resolution will increase. Moreover, if the number of pixels is increased by increasing the matrix size, the spatial resolution will also increase. The size of the pixels is also controlled by the FOV. Thus, if the FOV is increased, the pixel size will increase and hence decrease the spatial resolution. The pixel in the field of view is either rectangular or square. If the pixel is square, the number of the frequencies and the number of the phases are the same. However, if they are different, a rectangular pixel will appear. Rectangular pixels don not always provide less spatial resolution than the square(Westbrook & Roth, 2011). Here we used a FOV of 18cm by 18cm and a matrix size of 192 by 128. Thus, the pixel size was 0.937mm by 1.4mm. On a few occasions when a 5mm sample tube was used, the FOV was also 18 by 18 cm but the matrix size was 64 by 64, thus the pixel size was 2.81 by 2.81mm.

2.10.8 Scan time

If the scan time is increased, the chance of the patient moving will increase and therefore the quality of the image will reduce. To decrease the scan time, the number of acquisitions, TR and number of phase encodings has to be as low as possible. In this thesis, the issue was not

one of the subject moving but one of fluid sample movement after shaking the tube as part of the preparation, tissue movement through gravity or thermal convection within the sample.

2.10.9 K-space in MRI

This is normally rectangular and is the result of using series of echoes where there is a systematic variation of the pulse sequence for each echo or echo train. It has two axes, the first axis is the read axis or frequency axis, which is normally considered horizontal in K-space. The second is the phase axis, which is normally vertical. The space is a two-dimensional spatial frequency domain. In the middle of K-space we can normally find the maximum signal intensity of the lowest spatial frequency components. The unit of K-space is radian per cm(Westbrook & Roth, 2013).

Along the read axis we can apply a frequency gradient during acquisition of the echo to fill one horizontal line of K-space. Along the other axis, the phase encoding gives us the second direction by applying the phase gradient during the pulse sequence for a short time to fill the vertical line in the K- space.

It is very important to remember that there is no relationship between positions of the data in K-space and positions in the image. Thus, a two-dimensional Fourier transforms is required because there are two directions in K-space and from this the spatial image can be obtained. (Westbrook and Roth, 2013; Ray Hashman Hashemi, 2012). One of the key issues when K-space is considered is where one starts during image acquisition. This is particularly important when considering the use of hyperpolarised samples as each acquisition and excitation pulse uses up some of the prepared signal that is not returned after each pulse, and at the same time, the hyperpolarised signal is relaxing back to the thermal equilibrium. Thus the path used through K-space is important. One can use different trajectories through the space to maximise the use of the hyperpolarised signal whilst focussing on say the low spatial frequency content or, if applicable, the high spatial frequency content. In this thesis the K-space was acquired by starting in the centre of K-space and only one half of K-space was acquired - filled (the lower half being redundant).

2.10.9.1 MRI Parameters

In general, the excitation pulse had a 5° flip angle although this was systematically varied for some observations. Again, in general, gradient echo pulse sequence was used with k space-centre acquisition of a matrix with 192 lines and 128 samples,. A TR = 6.3 ms, TE = 3 ms, FOV = 18*18 cm, with a slice thickness = 3 mm was used to create an image that was reconstructed to 256*256. When multiple volumes were acquired, normally 70 volumes were collected with 0.8 seconds between volumes, thus the total scan time was 56 seconds. For some specific experiments, more volumes were collected and the delay between volumes was systematically varied.

2.10.9.2 Head coil

The head coil was supplied by General Electric (GE) and was used in all of the experiments. It contains 8 channels used as a phased array coil, with each individual coil having a pre-amplifier. These 8 channels work separately and the data is collected to create the image. Figure 27A shows the head coil. The 12 channels head coil was used in the 3T Seimen's scanner as seen in figure 17B

Figure 27: Image A shows the 8 channel head coil used in GE scanner and image B shows the 12 channels head coil in Siemen's scanner

2.10.9.3 Phantom

A phantom was placed inside the bore of the magnet within the head coil. It was designed to have two inserts; one for the 10 mm reference tube containing pure water and other for the sample tube. This phantom was used for all of the experiments inside the 3T scanner, see Figure 28.

Figure 28: The phantom was used while scanning the tubes

2.10.10   Hyperpolarised Signal Acquisition

After the preparation of a fresh sample, it was activated by the addition of Parahydrogen 24 hours before scanning. This was performed to activate the catalyst as Parahydrogen would bind to the catalyst and remove any other molecules from the hydride binding site. The Parahydrogen was also freshly added immediately before each scan for each experiment. The samples were shaken for 10 seconds horizontally and for 45 seconds in different fringe fields of the 3T MRI. This was performed for two reasons, first to dissolve Parahydrogen in the solvent and second to allow the ligand binding of the substrate onto the catalyst whilst the Parahydrogen had also formed hydride groups on the catalyst *in a magnetic field*. It is in this situation, when the catalyst-substrate-Parahydrogen complex is formed in a magnetic field that the spin transfer through J-coupling occurs from the hydrides to the substrate. In each scan the Parahydrogen was added to the sample and the samples were dropped in the phantom at physical angles of 90°, 45° and 30°. For most experiments, a physical angle of 45° was used.

A radiofrequency (RF) pulse was applied to excite the sample. A series of FLASH sequences was used in imaging across the samples to obtain specific information from specific parts of K-space. The K-space data was then converted to images by Fourier transformation. Gradient

echo imaging was used as it is known that further RF pulses would decrease the hyperpolarised signal.

2.10.10.1 The Fast Low Angle shot Magnetic Resonance Imaging (FLASH) sequence

In MRI examinations, the FLASH sequence or spoiled gradient echo (SPGR) is used because it is a fast technique and uses the spoiler gradient to dephase the magnetisation on the transverse axes. Then, the artifacts of images can be decreased. The efficiency of spoiler gradients to remove artifacts was done experimentally on two-dimensional (2D) MR images on the phantom. This led to comparison of the magnetisation before every RF excitation in every phase encoding (Wood, Silver, & Runge, 1987). The FLASH sequence was developed in 2010 to create the T1 weighted image within a short period of time (Leupold, Hennig, & Scheffler, 2008), making it possible to acquire an image in 20 ms with a high SNR ratio, high spatial resolution and no artifacts (Uecker et al., 2010).

The sequence used in our experiments consists of a series of pulse excitations each with a 5º flip angle. Where the flip angle was changed this is stated in the specific sections. This pulse sequence was used when the 3T scanners were used (see Figure 29).
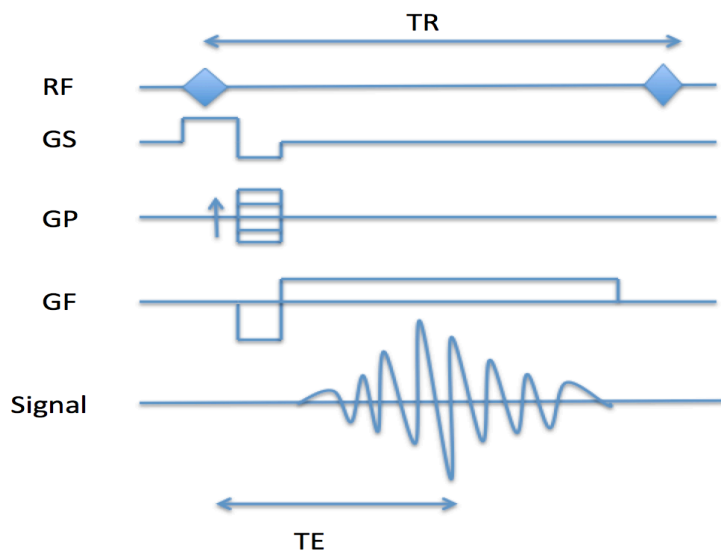
Figure 29: FLASH sequence.

2.11 Chemical Substrates

In this thesis, three main substrates have been investigated by the SABRE method, namely Pyrazine, Nicotinamide and Pyridine. The reason for using these substrates that they either have interesting symmetry that is of importance when considering hyperpolarisation, they have biological relevance because they bind to tissue receptors or they are the basis of a large range of pharmaceutical agents. A few variations on these basic compounds are used and these specific compounds are introduced as appropriate in later chapters.

2.11.1 Pyrazine ($C_4H_4N_2$)
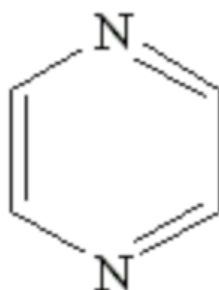
Figure 30: The molecular structure of Pyrazine

Pyrazine is a common component of many pharmaceutical drugs but in this thesis, it is used to test a different hypothesis, which is that when it binds to Pyrazine-binding protein in tissues, the magnetic and chemical symmetry of the molecules is broken and new observable magnetic signals are released. The chemical structure is shown in Figure 30.

2.11.2 Nicotinamide ($C_6H_6N_2O$)

It is also a biological substrate and is a water-soluble vitamin from the vitamin B group. Nicotinamide is a potentially safe agent for injection as the lethal dose (LD_{50}) for this agent is very high. Nicotinamide is converted into many metabolically active compounds including routes to Nicotinic acid, Nicotinate and eventually Maleamate and then Fumerate. It is therefore a route to test many metabolic pathways. The chemical structure is shown in Figure 31 below.
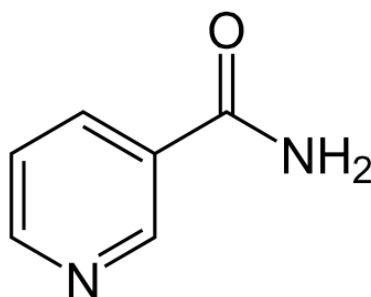
Figure 31: The molecular structure of Nicotinamide

It should be noted that the carbonyl group, if labelled with 13C is predicted to have a long T1 and therefore of some interest for imaging.

2.11.3 Pyridine (C$_5$H$_5$N)

Pyridine is a heterocyclic organic compound, which is related to benzene, but with one methine group that is replaced by a Nitrogen atom. The Pyridine ring can be found in vitamins, azines and pyridoxal. The chemical structure is shown in Figure 32.
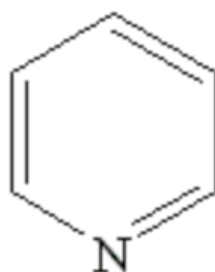
Figure 32: The Molecular structure of Pyridine

Pyridine was one of the first compounds to be hyperpolarised using SABRE and therefore remains a good reference compound for comparing methodologies. Pyridine is the basis of the creation of many pharmaceutical agents and Pyridyl groups are common in such agents.

2.12 Catalyst

The Catalyst plays a vital role in the signal enhancement that occurs in the process of signal amplification by reversible exchange (SABRE). A metal catalyst is used to bring the Parahydrogen and a molecule into close contact (Mewis et al., 2014). This means SABRE catalyst moves the spin polarisation form Parahydrogen ligands to the substrate. Therefore, the ligand architecture around the metal centre is an essential in enabling a facile analyte to join the metal centre. During the catalytic cycle, it is very important to have enough vacant sites to permit analyte and Parahydrogen derived hydride joins to bind. Moreover, the analyte

molecules and Parahydrogen ligands should be exchanged easily at the metal centre(Mewis, 2015). Throughout this thesis the catalyst was Ir (IMES)(COD)Cl (Michael J Cowley et al., 2011).

2.13   The solvent

Deuterated Methanol-d4 (Methanol-d4) was used as the solvent for all experiments in this thesis. This was used so that no NMR/MRI signals came from the solvent and the only signals would originate from the substrate. In most of the imaging experiments a second tube sample was placed in the field of view so that the degree of hyperpolarisation could be quantified. Water was used as the reference.

2.14   Parahydrogen Generation

A purpose-built Parahydrogen generator was used for all the experiments in this thesis. This generator model cools pure Hydrogen, in the presence of charcoal, to about 30º K and creates approximately 90% pure Parahydrogen‹ see figure below (33).

Figure 33: The Parahydrogen Generator at York

Chapter 3   Establishing and measuring hyperpolarisation using a standard clinical imaging machine

3.1   Introduction

The signal amplification by reversible exchange technique (SABRE) is one of the best methods for producing polarisation; as it can achieve high polarisation levels in seconds, in low magnetic fields and no chemical change occurs. The effectiveness of SABRE hyperpolarisation relies on the magnetic field strength that samples are exposed to (the polarisation field) and the lifetime of the ligand and parahydrogen on the metal catalyst complex. Polarisation transfer from Parahydrogen can be done in seconds compared to that in DNP, which takes several hours to transfer from unpaired electrons. The SABRE technique provides hyperpolarised molecules that can be investigated utilizing MRI and NMR.

The aims of this chapter are:

1. to establish the background to polarisation and produce polarised images as most previous work has concentrated on using non-image based NMR measurement procedures;

2. to investigate the parameters that optimise the spin hyperpolarisation signal;

3. to investigate different samples in different fringe fields of the MRI scanner (the polarisation field) to observe the decay in the different fields.

.

3.2   Specific methods

3.2.1   Chemical Substrates

In this chapter, three substrates have been investigated by the SABRE method, namely Pyrazine, Nicotinamide and Pyridine.

3.2.1.1 First sample: Pyrazine

The following were placed in a 10mm tube: 25 mg Pyrazine (see figure 34), 10 mg Iridium-IMES-COD (the catalyst) and 3 ml Methanol-d4. A separate sample was also prepared using 1mg of the catalyst.
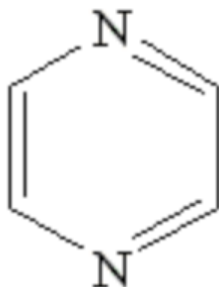
Figure 34: The molecular structure of Pyrazine

3.2.1.2 Second sample: Nicotinamide

The following quantities were used: 37.8 mg Nicotinamide (see figure 35), 10 mg catalyst and 3 ml Methanol-d4. This was prepared as for the previous sample.
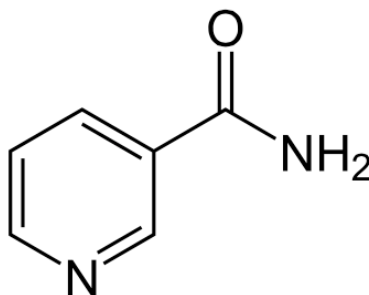
Figure 35: the molecular structure of Nicotinamide

3.2.1.3   Third sample: Pyridine
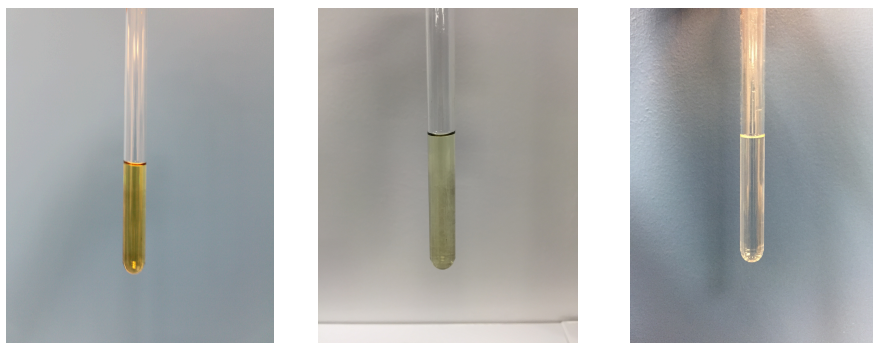
Figure 36: Tubes showing three of the samples. From left to right: Pyrazine, Nicotinamide and Pyridine.

The quantities used were: 27.7 mg Pyridine, 10 mg catalyst and 3 ml Methanol-d4, prepared as previously described. The first three sample tubes are shown in Figure 34. The molecular structure of pyridine can be seen in figure 32.

3.2.1.4   Fourth sample: Deuterated methylNicotinate

The main aim of this experiment that has fewer Hydrogens in the molecule and might lead to increase the relaxation time. A tube of deuterated methylNicotinate was prepared as for the previous samples. The quantities used were 37.8 mg deuterated methylNicotinate, 10mg of catalyst and 3 ml of Methanol-d4. The molecule has Hydrogen replaced by Deuterium in the heterocylic ring. This molecule was provide courtesy of Dr P. Rayner and was synthesised such that one Hydrogen next to the Nitrogen was retained and all others, bar one at the furthest distance from the Nitrogen, except those in the methyl group, are Deuterium. This means that the hyperpolarised signal; should be concentrated in just two Hydrogens rather than the usual four in Nicotinamide.

3.2.1.5   Fifth sample: Pyrazine with biPyridine

The main aim of this experiment is to see the effect on the Pyrazine after adding bipyridine to remove the catalyst. It was shown that this did increase the lifetime of the signal and therefore the removal of the catalyst is important to preserve the signalThe quantities used in this sample were 25 mg Pyrazine, 10 mg catalyst and 3 ml Methanol-d4. The biPyridine quantity used was 487.4 mg and the tube is shown in Figure 37. In this experiment, two steps

were carried out. Firstly, the Pyrazine sample was scanned after polarisation at 5mT, after adding the Parahydrogen. Secondly, the Parahydrogen was added to the Pyrazine sample and the biPyridine was mixed with the Pyrazine sample after polarisation but before scanning to remove the effect of the catalyst.

BiPyridine sample
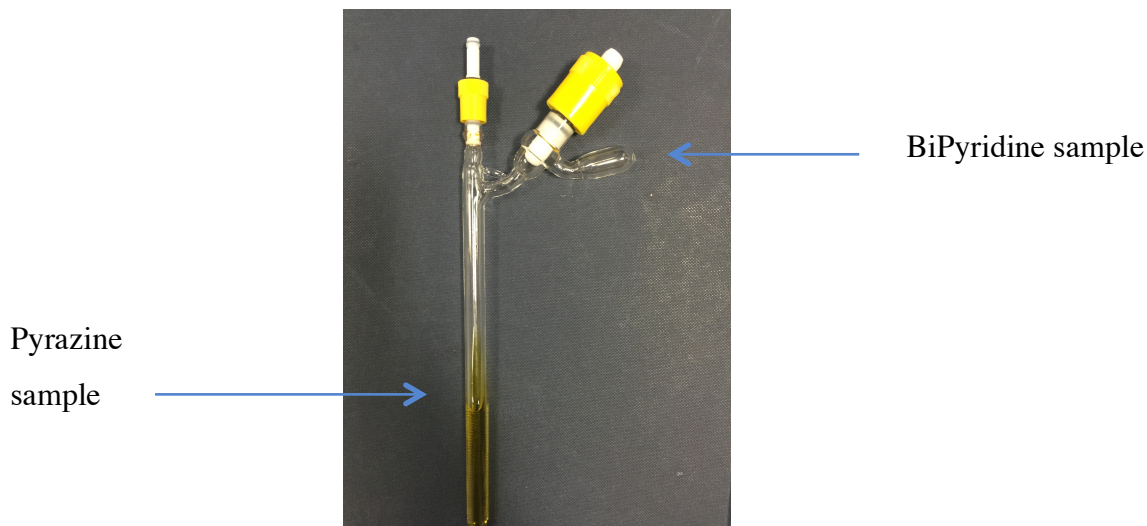
Pyrazine sample

Figure 37: This tube contains two samples: Pyrazine, Catalyst and Methanol-d4 at the bottom of the big tube and biPyridine, which is inserted into a small tube at the top of the main tube. This side tube has a smaller diameter than the main tube

Bipyridine was used as it binds to the catalyst irreversibly and stops any further Pyrazine substrate interacting with the catalyst.

3.2.1.6 Sixth sample: Pyrazine with *ex vivo* tissue

The aim of this experiment is to see if a sample with tissue present has a faster decay (short T1) compared with a control. Quantities in the sample were 25 mg Pyrazine, 10 mg Catalyst and 3 ml of Methanol-d4. In this sample a small amount of rat heart tissue was inserted into the tube.

3.2.1.7 Seventh sample:

The aim of this experiment is to see the effect of turbulence inside the small NMR tube. A smaller 5mm tube was prepared with 5mg Pyrazine, 2mg of catalyst and 0.6 ml Methanol-d4.

After I prepared all the samples above, a high vacuum line was used to remove the air and Parahydrogen was used to activate the samples.

3.2.2 Specific MRI methods in this chapter

3.2.2.1   Field dependence

The main aim of this experiment is to investigate different samples in different fringe field of the MR scanner to observe the decay in the different fields. Pyrazine, Nicotinamide and Pyridine were investigated with different polarisation magnetic fields. The fields ranged from earth's magnetic field of 50 microTesla to 30 mT. The 5mT field was the most commonly used field for imaging the samples. A water reference sample was always compared with the Pyrazine, Nicotinamide and Pyridine. This was done as we could calculate the signal per mole of Hydrogen in the reference sample as well as the signal per mole of Hydrogen in the test sample, the polarisation enhancement could then be calculated for each experiment.

3.3 Results

3.3.1 Hyperpolarisation in single and multiple scans.
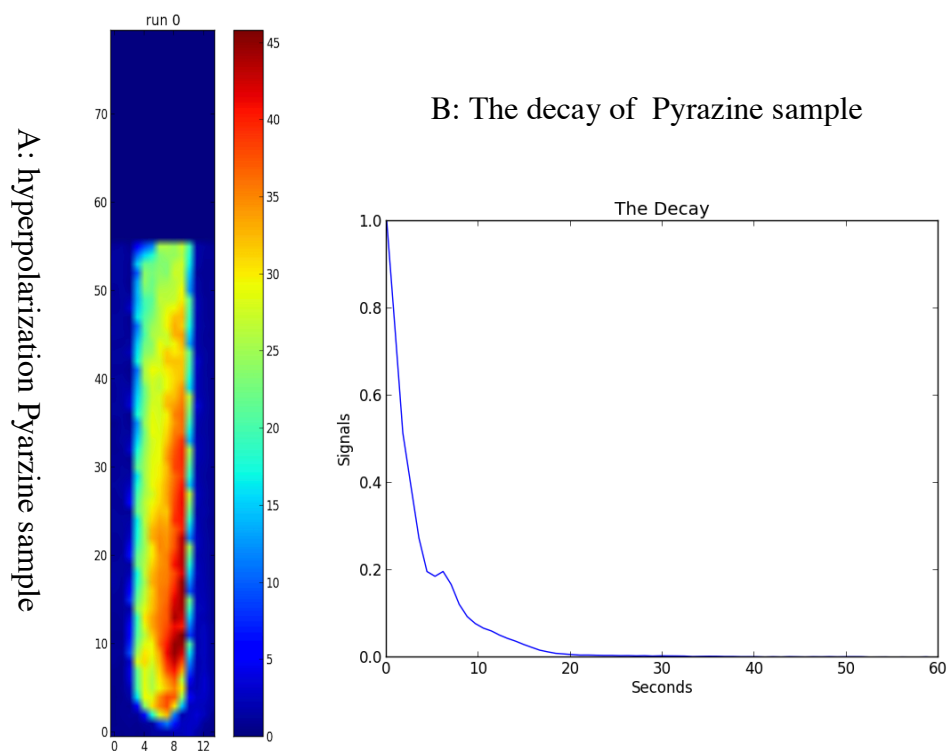
Figure 38: Image Image A shows a colour bar of the hyperpolarisation of the sample after adding the Parahydrogen, scanning following being in a polarisation field of 5 mT. The axes of the image are in mm. Image B shows the decay of image A at the middle of the tube

3.3.1.1 The single hyperpolarised tube at a polarisation field of 5 mT

The first experiment was a simple one and was aimed at investigating whether an image of a hyperpolarised sample could be obtained in a 3T Human MRI scanner. Sample 1, of Pyrazine, was prepared and Parahydrogen was introduced into the headspace in the tube. The sample was shaken in the fringe field of the scanner. The fringe field was calibrated using a fluxgate magnetometer and the 5mT contour line was chosen as previous published work had shown (Highton, 2013) that this field was optimal for spin transfer from Parahydrogen to a sample such as Pyridine. Figure 39A shows a pseudocolour image of sample 1 (Pyrazine) immediately after it has been placed in the scanner. The scale is arbitrary but demonstrates that hyperpolarisation is larger towards the lower surface of the tube (it is angled in the

holder). Image B shows the decay of the signal in the middle of the tube with respect to the initial maximum signal. Repeat images were made every 0.8 seconds of a single slice. The surprising observation is that a non-exponential decay is occurring with growth in the signal at about 8 seconds. The initial hyperpolarisation in the tube is very high compared to the water reference that was scanned in the same environment. A method of calculating the degree of signal enhancement was developed that used the water reference as a way of calculating the enhancement without a quantification of how many nuclei contribute to the signal. This was performed by calculating the signal per mole of molecule present.

The amount of Hydrogen in the water in the reference tube was 0.3334 moles. The amount of Hydrogen in the Pyrazine in the sample tube was 0.001246 moles. The signal in a single voxel in the sample tube, due to Hydrogen in Pyrazine was 1636 whereas that due to water in an equivalent voxel was 252. Thus, it is clear that hyperpolarised Pyrazine is producing a much larger signal even though there are much fewer contributing Hydrogens. Therefore, the signal per mole for Pyrazine Hydrogens is 1313001 whereas that for the Water Hydrogens is 695. A polarisation enhancement of 1886.9 was seen. If we wish to increase a MRI signal from that grow by the Boltzmann distribution for a sample in a field of 3T by that amount using the brute force method we would have to increase the B0 magnetic filed to 3660 Tesla.

The question here is why these results were obtained. A single exponential decay is expected because the NMR spectrum of Pyrazine has just one peak as all the Hydrogen in that molecule contributes equally with the same chemical shift to the signal. Distribution of the hyperpolarisation signal at the edge of the tube may be due to the effect of the tube glass, partial voluming or of gravity and therefore of how the fluids flow after shaking. Abnormal decay may occur because the timing of relaxation is different in different parts of the tube. Another possible cause is the turbulence that brings fresh spin from different parts or diffusion of spins that brings fresh signals to the measurement point.
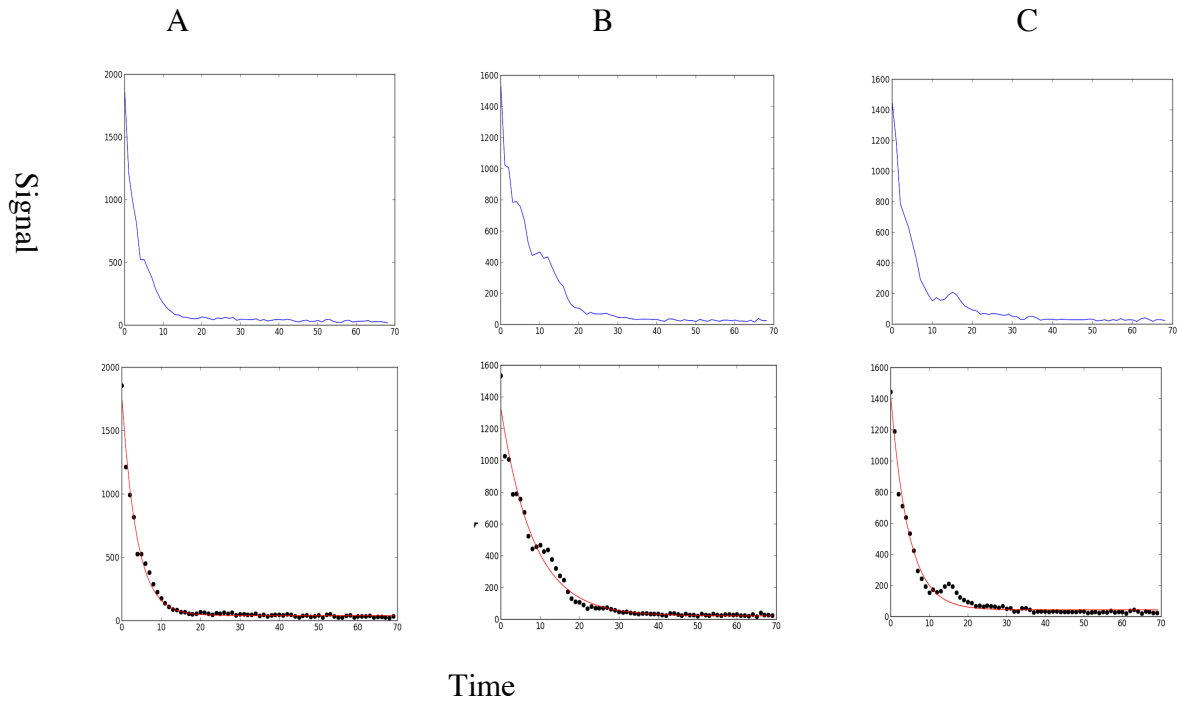
Figure 39: These images show the decay in different areas of the tube

To start to investigate the initial observation of a hyperpolarised image in a Human 3T scanner, three points were selected in different parts of the tube. The first point was at the bottom centre of the tube A; the second point at the middle of the tube B and the last point at top centre of the tube C near the fluid/gas interface. As seen in Figure 39, the three different areas of the tube illustrate different patterns of decay. For each decay curve, a single exponential decay curve is fitted to the data and this fit is shown in the lower row.

The images show the decay at the bottom, middle and top of the tube respectively. At the bottom of the tube the decay is apparently better fitted by a single exponential than other parts of the tube. In addition, a higher signal can be produced at the bottom of the tube than in other positions at the middle or top of the tube. It also appears to be the case that the non-exponential decay occurs later at the top of the tube. These observations would suggest that maybe fluid flows throughout the tube may be responsible but the later small increase in

signal would not be compatible with fresh signal arising from Parahydrogen diffusing into the top of the tube creating fresh signal. This is because the concentration of Parahydrogen is decreased during the scan and the sample needs a fresh Parahydrogen. It might be suggested that less flow occurs at the bottom of the tube and that is why the signal is higher and has an exponential decay.

If the reason for the delayed increase in signal were related to fluid flow, then it might be expected that this would be a random event if due to turbulence. Therefore, a statistical approach was used by observing what happened if repeat measures were used.

3.3.2 Scanning in one or several batches

3.3.2.1 The hyperpolarisation tubes (30 scans) at 5mT.

One sample of Pyrazine was scanned 30 times using the same environment, parameters. As with the original observation, the hyperpolarisation in the tube is high and appeared on one side. There is variance in the hyperpolarisation in the tubes from one scan to another. However, the hyperpolarisation as seen in the original observation is repeatable, high, and provides signals as shown in Figure 40. This means the colour of hyperpolarisation tubes is different but they provide similar signals.
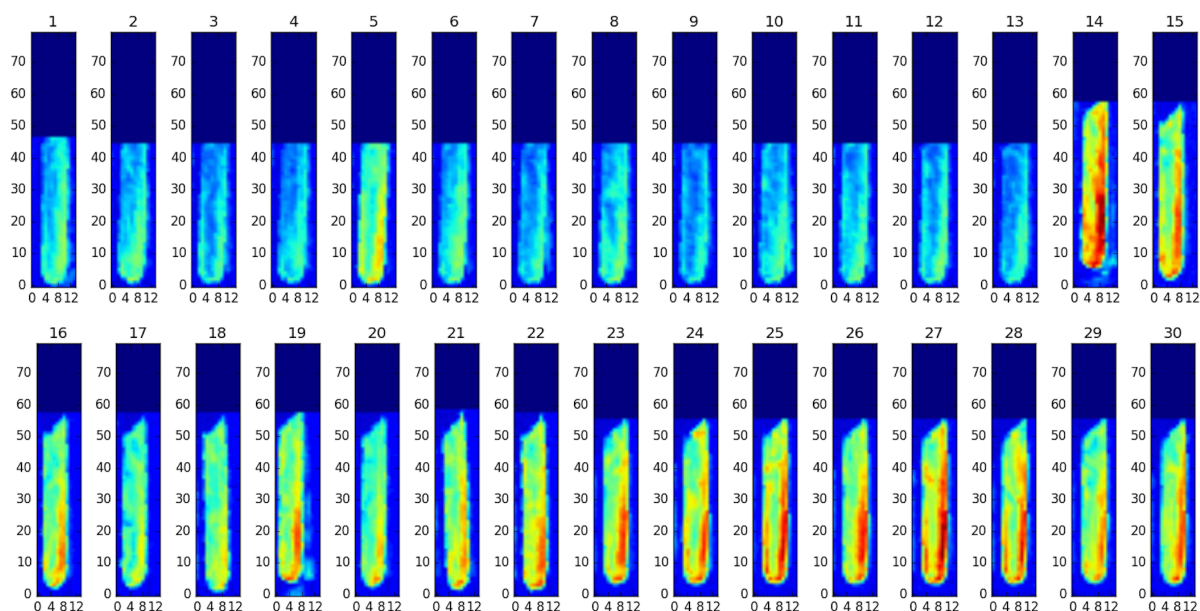
Figure 40: Pyrazine sample was scanned 30 times at the same environment and at 5mT on the same day

3.3.2.2 Different Pyrazine samples, 10 mg of Catalyst shaken for 10s.

Four different Pyrazine samples were scanned with the same parameters. Some batches were scanned a multiple number of times and one batch was only scanned once. The result was 30 different scans on different days of these batches. This was performed to see how much variability there was across randomly chosen scans. In this case the hyperpolarisation is different between batches and scans, but hyperpolarised signals were still obtained from all of them. All the scans in Figure 41 are on the same scale. It can be noticed that the single scan batch (no. 20) has the highest hyperpolarisation compared to the rest of scans. This might have occurred due to differences in the batches or because the amount or purity of Parahydrogen may have been different from one batch to another. It can also be seen that the last few samples appear to have no signal. This could be because of a failure of the Parahydrogen generator or that the catalyst has been destroyed, or that Oxygen has entered the tube.
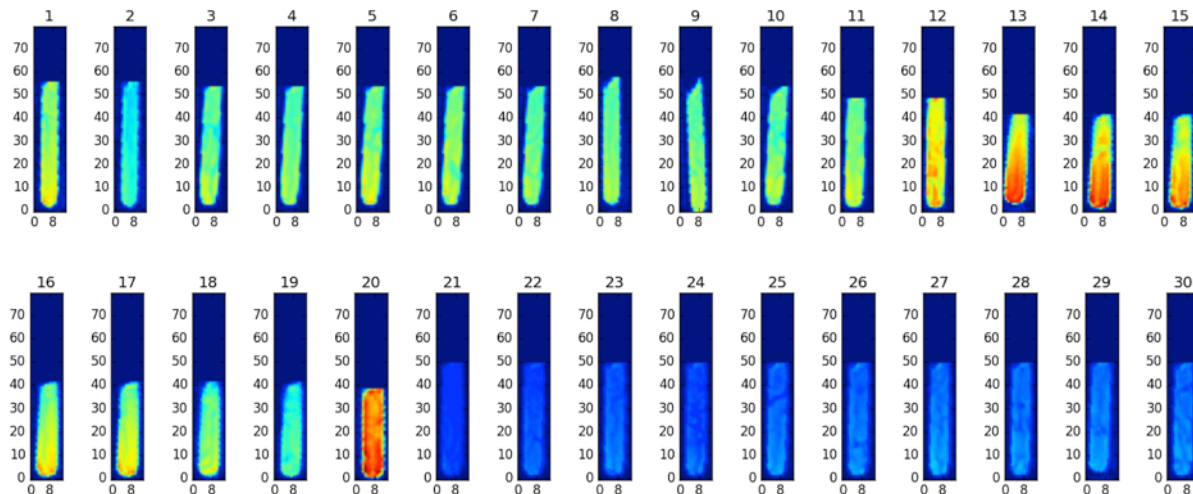
Figure 41: The The Pyrazine sample was scanned four times (four days) using the same parameters but on different days. From 1 to 10 were scanned in the first day and from 11 to 19 scanned in the second day. Numbers 20 was scanned alone in the third day and lastly from 21 to 30 were scanned in the fourth day. When these were added together the hyperpolarisation shows different colours. Each batch has the same colour scale.

3.3.2.3 The decay of the Pyrazine sample: 10mg of Catalyst, shaken for 10s

The signal in all 30 experiments is different from one batch to another. Some of the decay has less hyperpolarisation and another group has high hyperpolarisation. This may be due to scanning the samples in different batches and variation in sample and catalyst concentration, although all were done using the same magnetic field and parameters. If the images are reanalysed with respect to their own maximal, initial scan, Figure 42, then they all have the almost the same main shape of the decay curve, suggesting that it is the initial magnetisation that varies. This could be due to a variation in Parahydrogen purity, not quite the same polarisation magnetic field or a variation in Parahydrogen concentration after shaking to dissolve the gas into the solvent.

Normalised signal
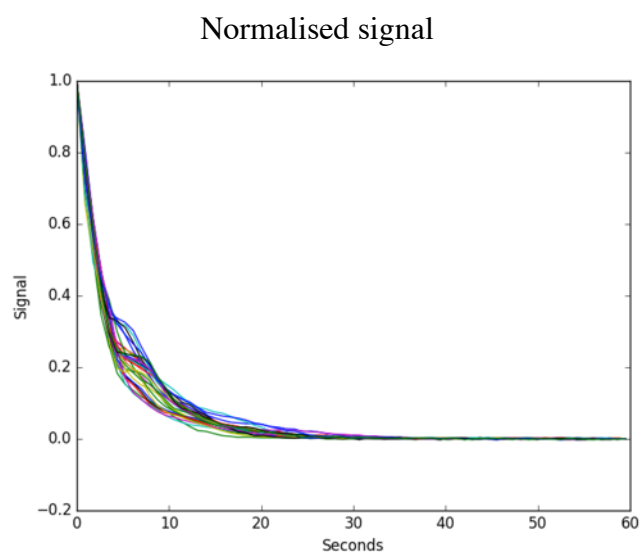
Figure 42: Image shows the 30 experiments of Pyrazine sample shaken for 10 seconds with Iridium at 10 mg. The signals are all referenced to the initial signal strength.

3.3.2.4 The mean of the Pyrazine sample with 10 mg of Catalyst shaken for 10s

All 30 experiments shown in Figures 41 and 42 have been averaged, the mean obtained and that fitted with a single exponential and the mean obtained. The result and the fit (in red) are shown in Figure 43. A small deviation from an exponential decay can be seen.
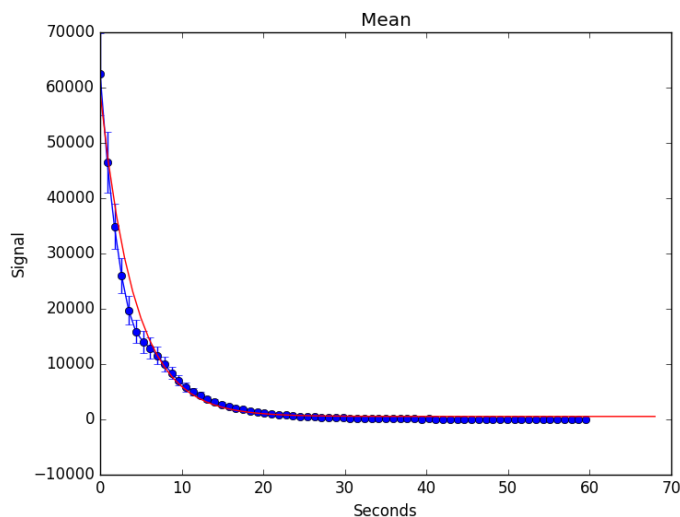
Figure 43: Graph showing the mean of all 30 experiments plotted in figure 43 but now with the actual signal levels

The observation that the deviation from an exponential decay has largely averaged to a much smoother curve and this could mean that the deviations are random within each experiment and that they are due to some variable process such as turbulence. To clarify these results, the decay of each batch has been analysed alone (see Figure 44 below). It was noticed that there is different decay in each group even though they were scanned in the same batch, but possibly with different shaking times; this could be the reason for variations in the decay.
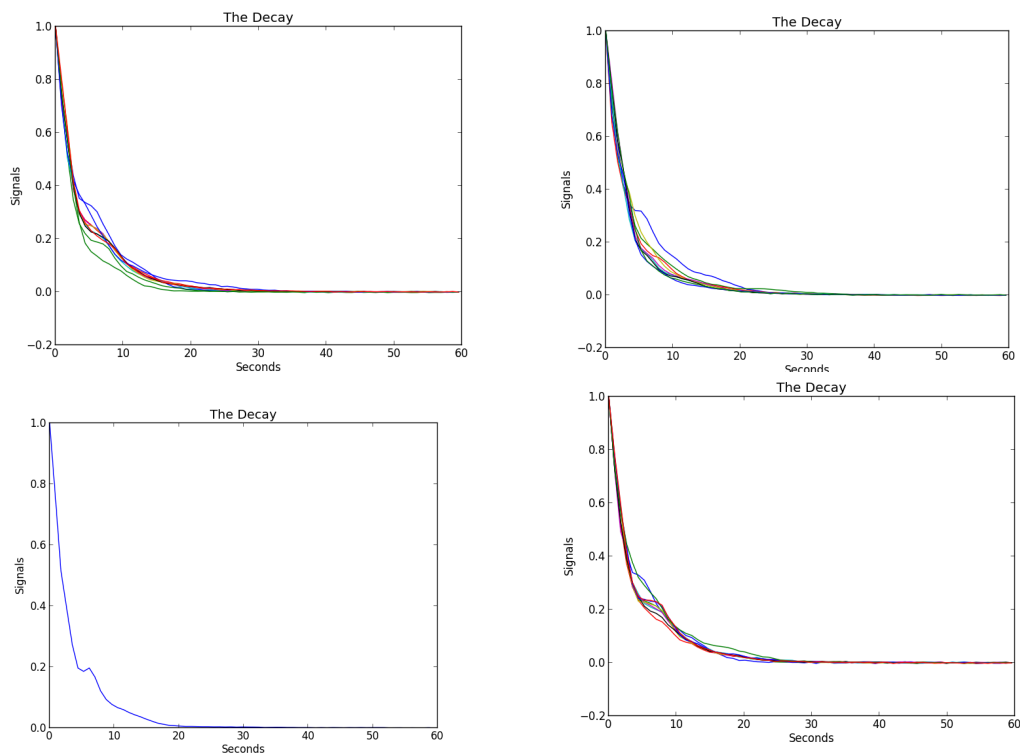
Figure 44: Pyrazine sample with 10s shake and 10 mg of Catalyst. The different rates of decay while using the same parameters and same magnetic field can clearly be seen.

The average of all the figures in 45 was taken as shown below. The non-exponential decay is clear in all graphs but image B is quite different compared to images A, C and D as seen in Figure 43.
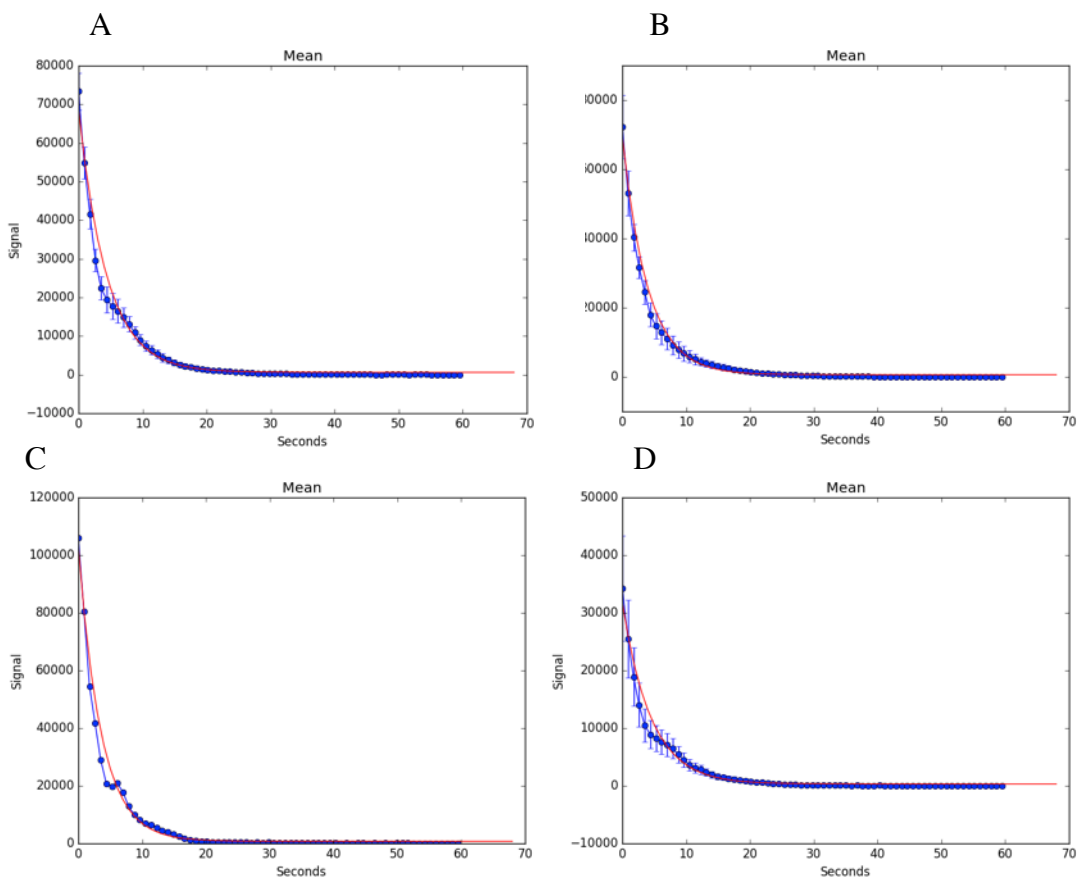
Figure 45: Images A, B, C and D show the average of each batch as in Figure 44

This suggests that there is some difference between batches. If this is due to the length of shaking the tube in the polarisation field, then this is easily tested.

3.3.3 Pyrazine with different shaking times and different catalysts

3.3.3.1 Pyrazine sample shaken for 10s and 45s with 10 mg of catalyst

The Pyrazine samples with 10 mg of catalyst were then investigated at a polarisation field of 5 mT but with different shaking times. Image A in Figure 46 shows the mean of 30 experiments with 10 seconds shaking time, while image B shows the mean of 30 experiments with 46 seconds of shaking time. It is clear that shaking the sample for longer achieves a higher signal. Both samples show non-exponential decay. This is compatible with the variation in the signal strengths in the previous section and shows that a more controlled approach has to be used in exposing the sample to a polarisation field. The small deviation

from an exponential decay is still present and therefore is not due to a change in polarisation time.

A: Sample shaken for 10s   **B: Sample shaken for 45s**
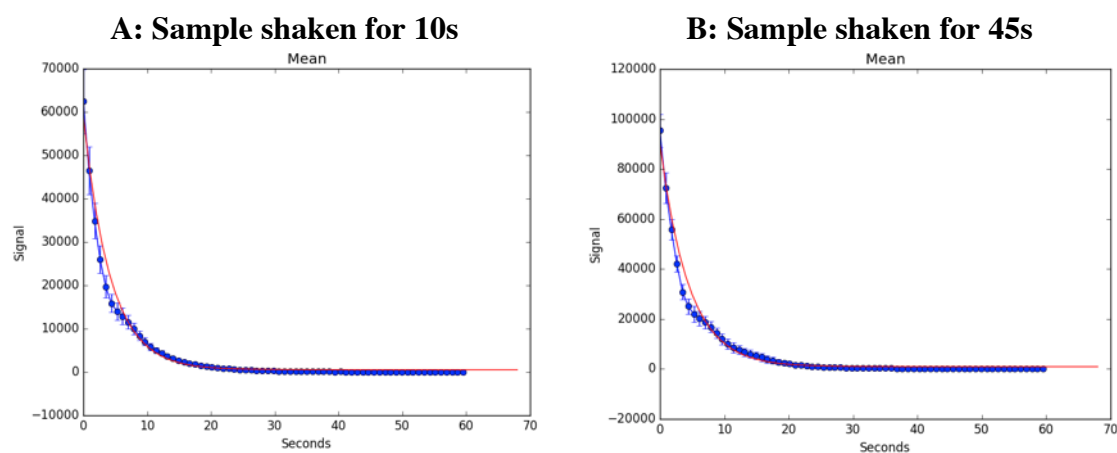
Figure 46: Image A shows the mean of Pyrazine sample shaken for 10 seconds while B shows the mean with 10 mg of Catalyst, shaken for 10s and 45s.

3.3.3.2   Pyrazine sample shaken for 10s and 45s with 1 mg of catalyst

The Pyrazine samples with 1 mg of catalyst were investigated using 10 and 45 seconds of shaking time also in a polarisation field of 5 mT. The reason for changing the level of the catalyst was that it is possible that the non-exponential decay is due to signal originating not from free substrate but also from substrate bound to the catalyst. It could be that polarised free substrate binds to the catalyst and the symmetry of the Pyrazine is broken and releases magnetisation from higher order magnetic states such as long-lived states as predicted in (Green et al., 2012). Therefore, varying the catalyst concentration would be predicted to alter the level of magnetisation and also, potentially affect the size of the deviation from an exponential decay.

It was noticed that this sample gave small signals compared to the Pyrazine sample with 10 mg of catalyst as predicted as less interaction could occur between Parahydrogen, catalyst and substrate. In addition, this sample shows different results when the shaking time and therefore the polarisation time is changed. As before, the sample shaken for 45 seconds produced higher signals than the sample shaken for 10 seconds.

Both samples show non-exponential decay (Figure 47). This suggests that the catalyst concentration is not responsible for the size of the deviation from an exponential decay. This topic is explored later in the thesis after other samples are investigated as possible explanations for these observations.
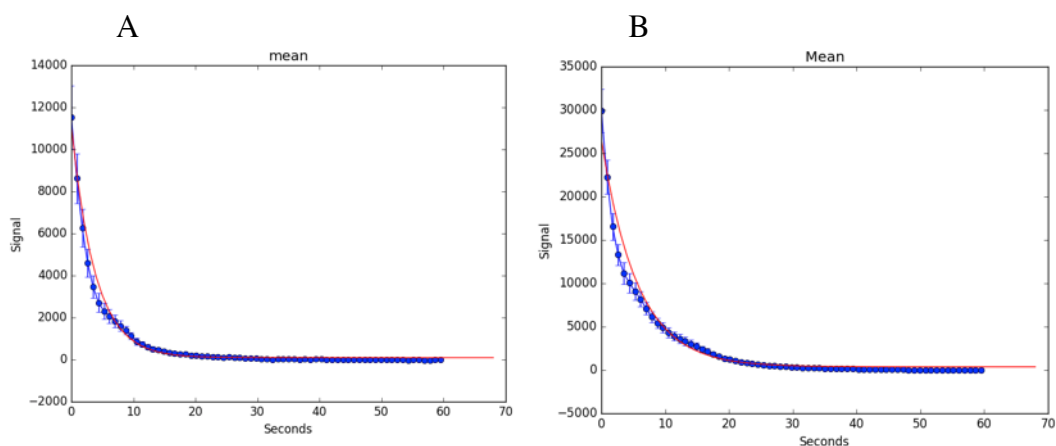
Figure 47: image A shows the mean of the Pyrazine sample (both sample 1 mg) decay curve with 10 seconds shaking time whereas image B shows the same sample but with 45 seconds shaking time.

3.4 Other substrates investigated with a polarisation field of 5 mT

3.4.1 Nicotinamide sample shaken for 10s and 45s

The Nicotinamide sample, sample 2, was investigated at 5 mT with different shaking times. The samples are shown in Figure 46 as the mean of 30 experiments for each condition. Both graphs show a small amount of non-exponential decay, less than that observed for Pyrazine. The sample shaken for 10 seconds shows a higher signal than that shaken for 45 seconds. This case is different to the Pyrazine sample, however, (see Figure 48) where the signal was larger for a longer exposure to the polarisation field.

A: Sample shaken for 10s.   **B: Sample shaken for 45s**
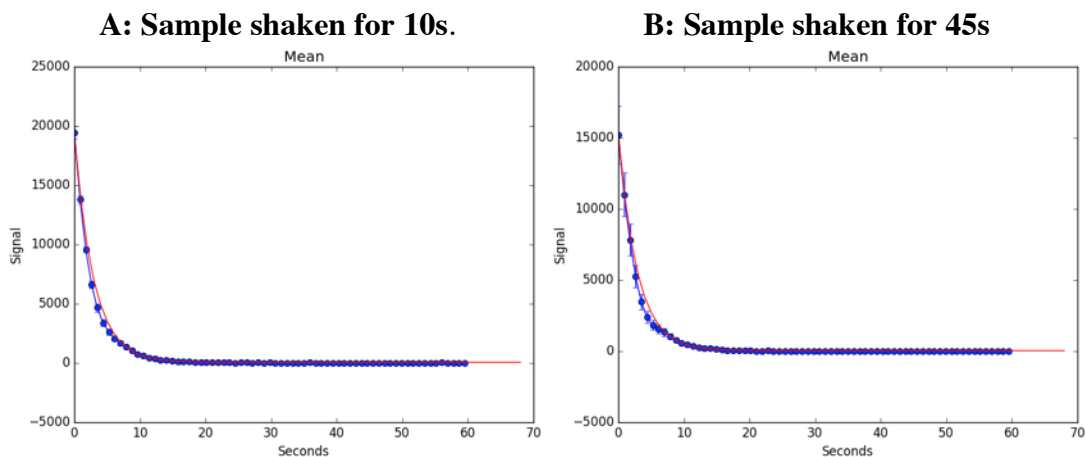
Figure 48: Both images A and B show a small deviation from an exponential decay.

3.4.1.1   Pyridine sample shaken for 10s and 45s

The Pyridine sample, sample 3, was also investigated at 5 mT in 30 experiments with two different shaking times. In figure 49 below, the mean of all 30 experiments also shows a near exponential decay. The sample with 45 seconds shake gave a high signal compared to the sample with 10 seconds shake as with Pyrazine.

A: Sample shaken for 10s   **B: Sample shaken for 45s**
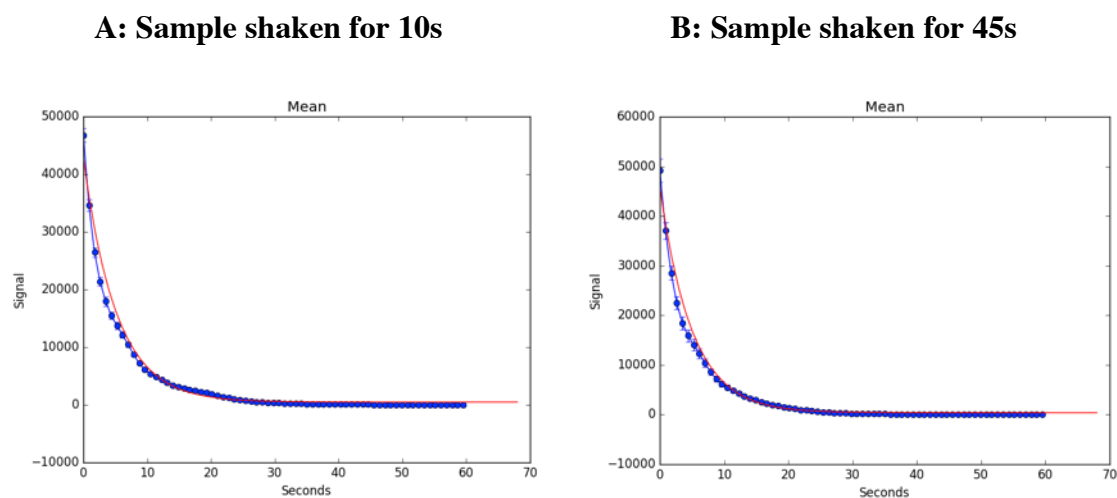
Figure 49: Image A shows the mean of the Pyridine sample with 10 seconds shake and image B shows the same sample but with 45 seconds shake

3.4.1.2   Deuterated MethylNicontinate

The deuterated methylnicotinate sample, sample 4, was scanned 6 times after dissolving Parahydrogen in a 5mT polarisation field for 10 seconds and images were recorded for 1 min. Figure 48 below shows the mean and the deviation of all 6 scans. The non-exponential and long decay time can be clearly seen. The decay curve has a longer time course than that of Nicotinamide (see Figure 50). This is compatible with there being fewer routes for relaxation
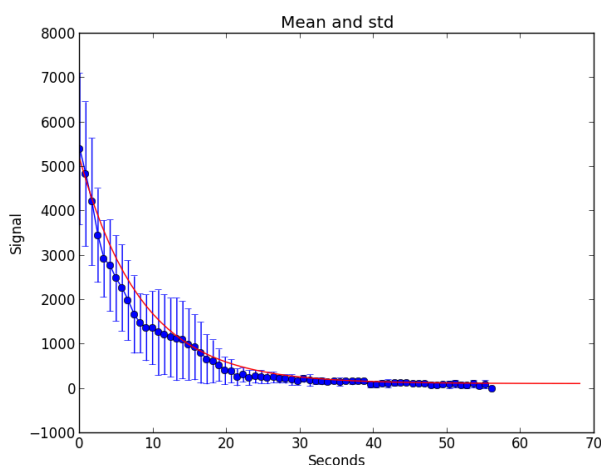
Figure 50: Image shows the non-exponential decay of 6 scans with a longer decay time compared to ordinary Nicotinamide

as there are fewer Hydrogens in the molecule. However, when compared with Nicotinamide under the same conditions, the signal is very much lower. This suggests that the concept that spin transfer into a smaller number of Hydrogens may not be correct. The longer T1 time constant though is of considerable interest at it suggests that changing the relaxation mechanisms within a molecule might have important consequences for biological and in-vivo imaging.

3.4.2 Field dependence results

Three samples (Pyrazine, Nicotinamide and Pyridine) have been scanned in several polarisation fields. (Green et al., 2012) suggests that the relationship between J-coupling within the molecule and the chemical shifts of individual nuclei within that molecule determine how spin transfer occurs. The theory and experiments have demonstrated that the ideal field for spin transfer is likely to be molecule dependent and that, in general, spin transfer will be in low, milliTesla fields. As a large number of molecules have a similar range of J-couplings, then the general range of spin transfer is likely to be similar for many molecules. The details though would be different for each molecule.

It is also the case that if the results in previous sections are just due to turbulence and fluid flow after shaking, then the non-exponential decay should not be field dependent except for its overall magnitude as that would be proportional to the initial magnetisation produced initially by a specific polarisation field.

It can be seen that hyperpolarisation and a non-exponential decay occur maximally at 5, 5.5, 6 and 8 mT, as seen in Figure 51 and is similar for these molecules. The initial magnetisation does depend on field as suggested by theory. This means that the field dependence plays a vital rule of producing the non-exponential decay not due to the turbulence.

To the fit an exponential, this can be done by following equations:

$$Signal = a \times \exp(-b \times time) + c$$
$$= ae^{-bt} + c$$
$$at \ t = \phi \quad signal = a + c$$
$$at \quad t = \phi \quad signal = c$$

Fitted curve from data can be done by equation below

$$\frac{Deviation}{Fit} = \frac{signal - fit\,(a,b,c)}{fit(abc)}$$

Express as a percentage and the plot can be done as a percent deviation
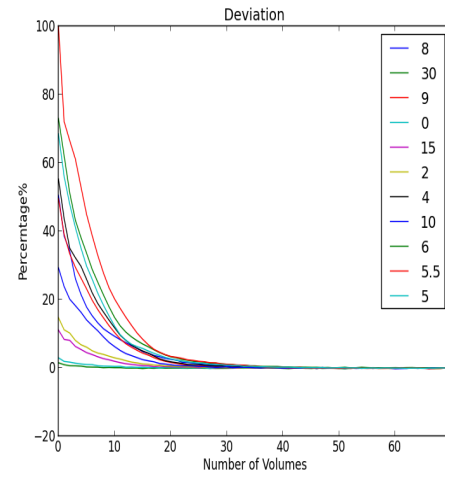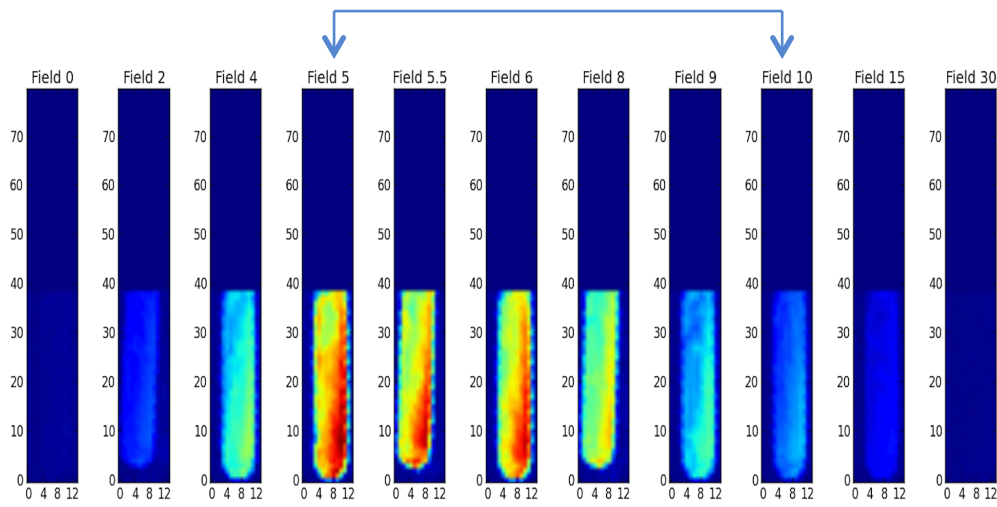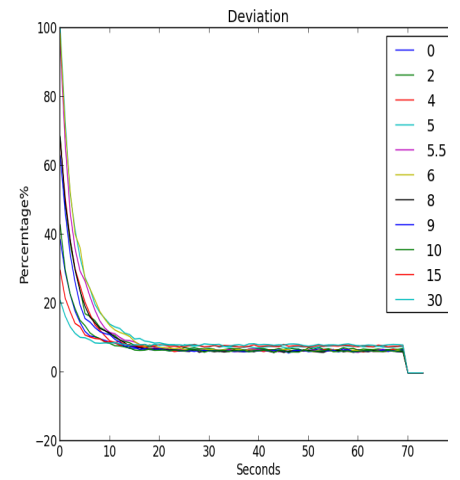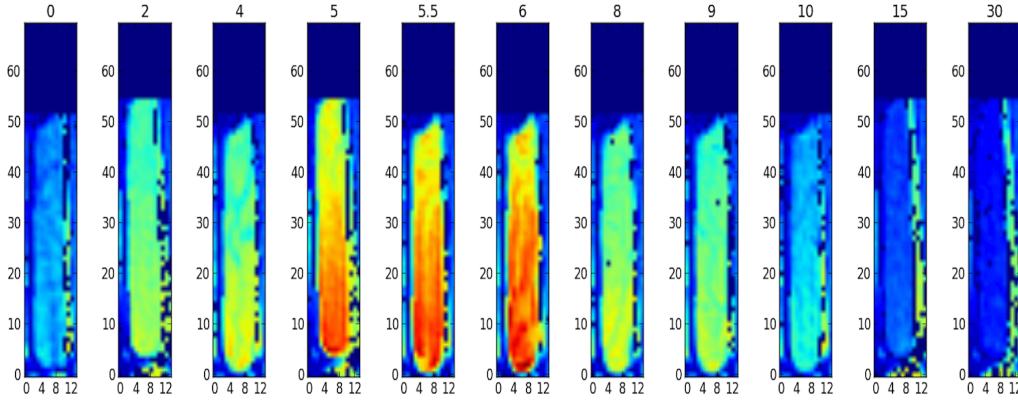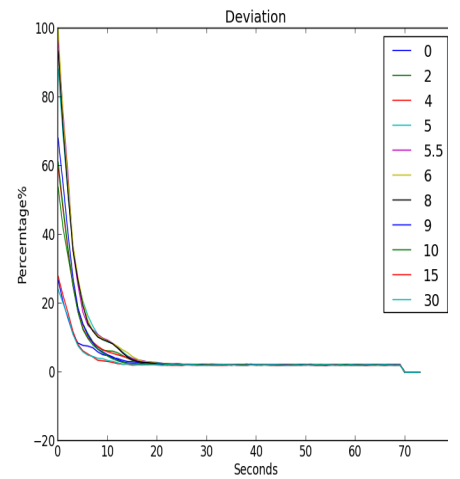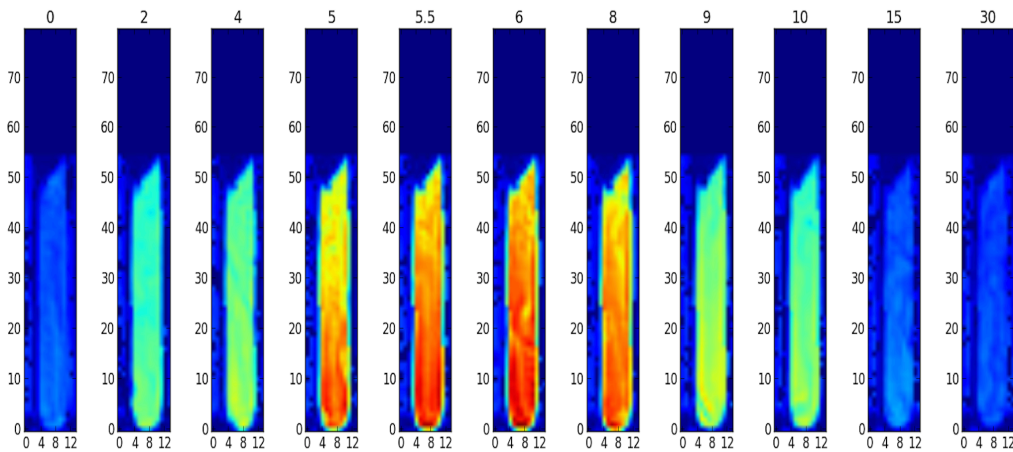
Figure 51: Image A shows the Pyrazine sample, image B shows the Nicotinamide sample and image C shows the Pyridine sample. The hyperpolarisation occurs at 5, 5.5, 6, and 8 mT and the percentage deviation from an exponential decay curve at different fields can be seen all curves.

3.4.2.1 The hyperpolarisation at different tube angles inside the phantom

The main aim of this experiment is to investigate the pyrazine sample with different angles to see the interaction between catalyst and substrate. By placing the sample at 30° small fluid gas will interface with the pyarzine and might increase the relaxation time. In the initial experiments above, the scanning was always performed at a specific physical angle within the holder, the phantom that contained a reference water sample and mineral oil to decrease susceptibility effects within and between the samples

The sample tubes were placed into the phantom at different angles to examine the difference in non-exponential decay. Both samples were measured at the top of the tubes; the first was Pyrazine at 45° in the phantom as seen in image A. The second sample was Pyrazine at 30° in the phantom as seen in image B. Both gave almost the same signals whereas the decay time is slower in B. However, the non-exponential decay is large at 45° as can be seen in Figure 50 and almost absent in the sample held at 30°. This at first glance suggests that the non-exponential decay is purely physical. The lower angle gives a result that is very similar to those obtained when the signal is measured at the bottom of a tube (see Figure 52). This is paradoxical in that most of the sample in the lower angle sample is nearer the fluid/gas interface and this sample is more like that, physically, in A. This suggests that the reason for the delayed peak in A, the more acute angled tube, may be a more complex relationship between the evolution of signal within the sample and the relationship with the fluid/gas interface. This would suggest that the interaction with the catalyst as a potential source of delayed signal requires more investigation.
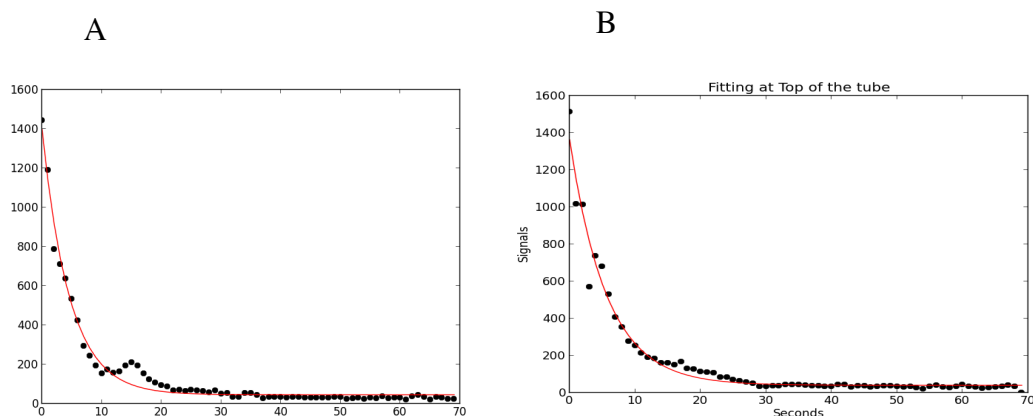
Figure 52: Both Pyrazine samples at the top of tube. Image A with 45° shows large non-exponential decay and faster decay compared to image B with a 30° angle.

3.4.3 Pyrazine with biPyridine samples

The aim of this experiment is to investigate the pyrazine sample with bipyridine to remove the effect of catalyst. It was shown that this did increase the lifetime of the signal and therefore the removal of the catalyst is important to preserve the signal. In this experiment, the tube was changed to one with a smaller diameter (5mm) than in the previous experiment. This was a purely practical, glassblowing, consideration of how to construct a tube with a side arm. The sample tube had a side arm that contained a molecule that irreversibly binds to the catalyst and therefore any further interaction between the catalyst and the polarisation substrate is inhibited. In this experiment the sample, sample 5, was shaken at 5 mT as in many of the original observations made above. biPyridine was added without further shaking. Thus, the idea is that the hyperpolarised signal has been created and then biPyridine stops the catalyst interaction. The hyperpolarisation of these two samples is different as can be seen below. Image A, the control where biPyridine is not added shows high hyperpolarisation at the bottom of the tube as in previous experiments, whereas image B shows the hyperpolarisation at the top of the tube. In graph C the decay of Pyrazine with biPyridine (green) occurs faster than in the Pyrazine sample (blue). The important point here is that there was an exponential decay is observed in *both* samples. This may explain why non-

exponential decay was obtained in the previous Pyrazine samples. The smaller diameter would lead to less turbulence than previously obtained in the 5 mm tube. See Figure 53.
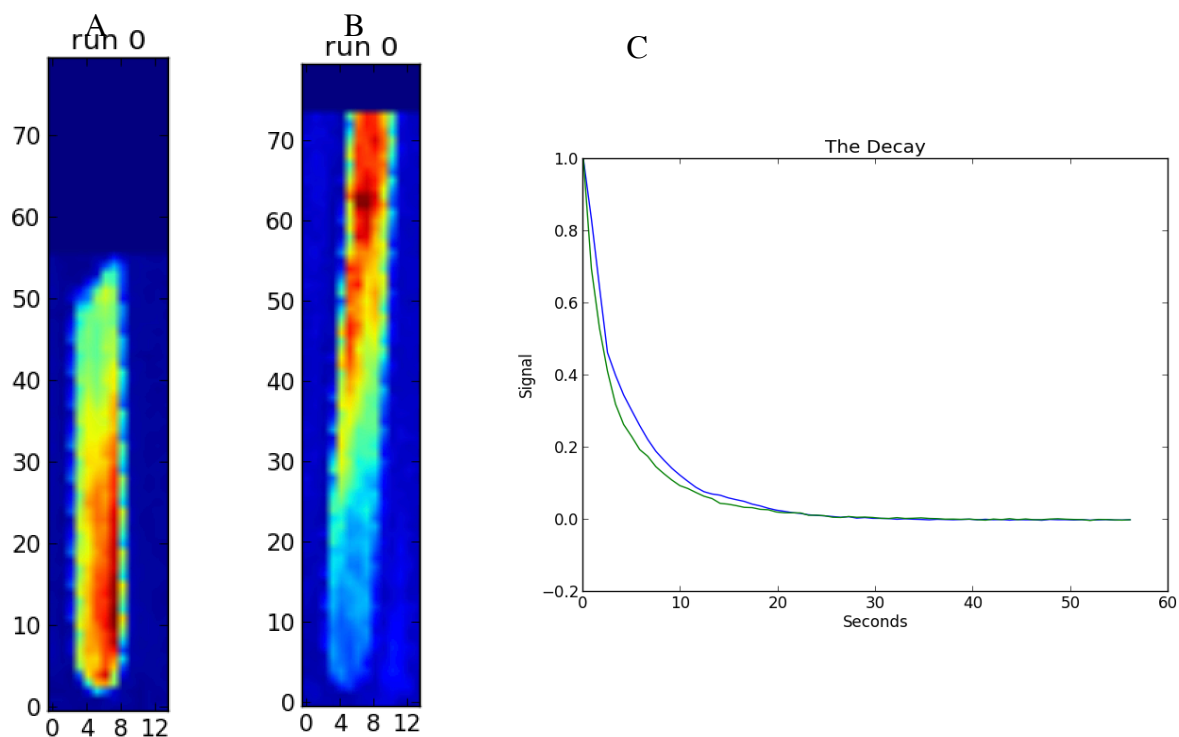
Figure 53: Image A shows the hyperpolarisation tube of the Pyrazine sample. Image B shows the hyperpolarisation tube of Pyrazine with the biPyridine sample. Image C shows the different decay of both samples, Pyrazine sample (blue) and Pyrazine with biPyridine (green).

To compare between the Pyrazine sample and that containing Pyrazine and biPyridine, graphs were plotted using the data recorded from three different areas of the tube, at the bottom, middle and top. See figure 54.

A

B

C
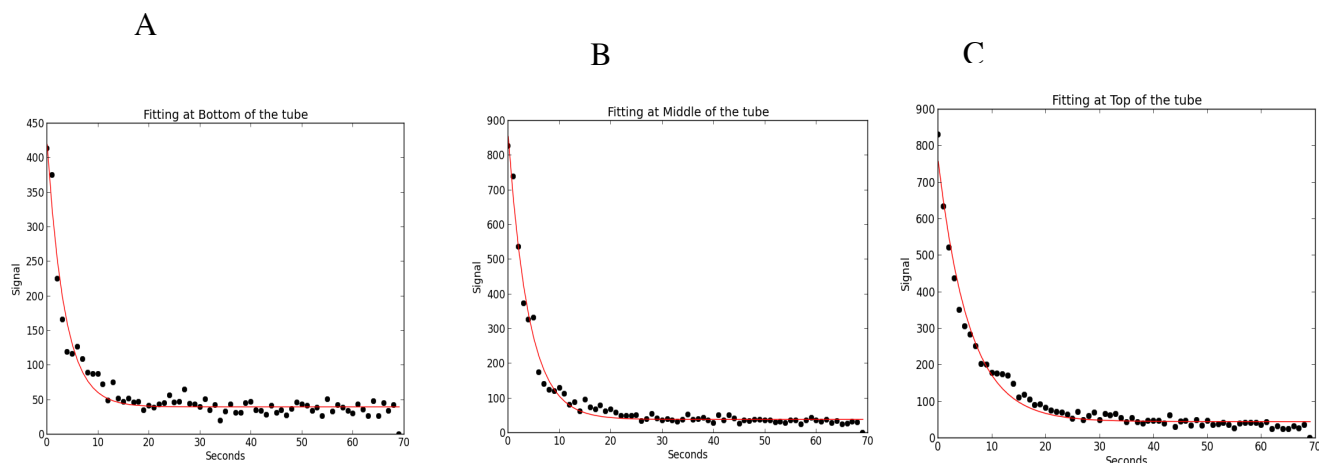
Figure 54: Images A, B and C show the single and fitting of bottom, middle and top of the tube respectively. The exponential decay is clear in A &B but non-exponential decay clear in C.

The decay in these three areas can be seen in Figure 54. Interestingly, as just stated the signal is larger in the presence of biPyridine at the top of the tube and it lasts longer. This suggests that the catalyst is being inhibited at the top of the tube and this slows down relaxation such that a larger signal and slower relaxation is observed. It also suggests biPyridine has more effect at the top of the tube, maybe due to differences in density.

3.4.3.1   Pyrazine with biPyridine sample (total mixture shaken before scanning)

In this experiment, a sample of Pyrazine, sample 5, was prepared and then Parahydrogen was added and the mixture shaken in a polarisation field of 5 mT. The biPyridine was mixed in and the sample shaken, again, in the same field of 5mT. This sample was then dropped into the phantom and scanned. As seen in Figure 55, the hyperpolarisation occurred at the bottom of the tube and not on one side of the tube. An average non-exponential decay, across the tube, is clear in image B below.
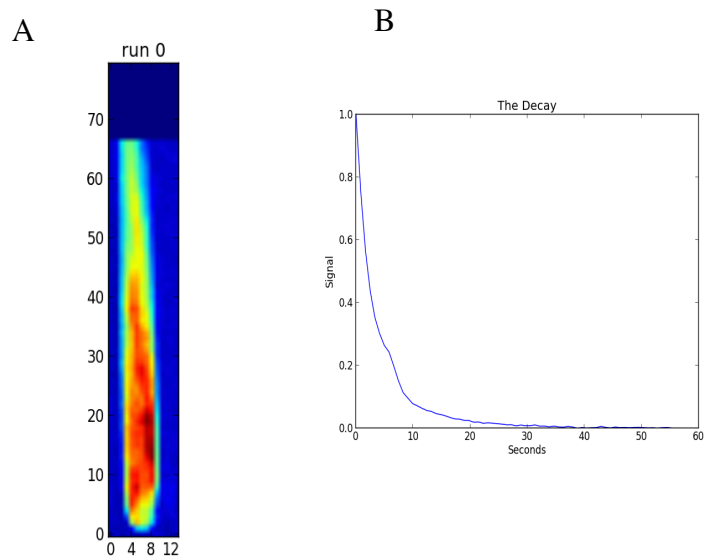
Figure 55: Image A shows the hyperpolarisation tube and image B shows the decay of image A

Three points from the bottom, middle and top of the tube were selected in order to view differences in the decay. The non-exponential decay can be seen at the middle and top of the tube after the biPyridine was mixed with Pyrazine and with Parahydrogen being present, as shown in Figure 56. The decay at the bottom of the tube is slow(er) and is exponential as seen with other samples.
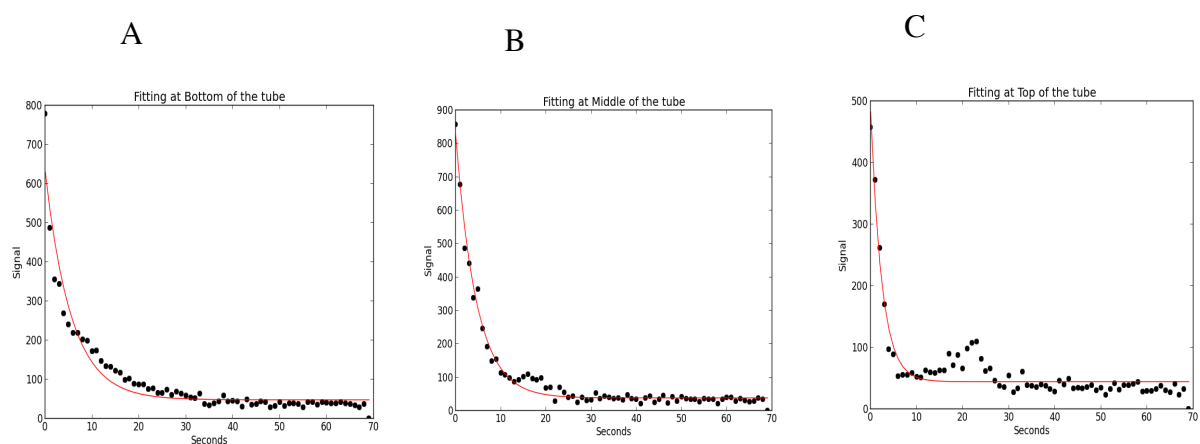
Figure 56 Figure 56: Image A shows the fitting at bottom of the tube, image B shows the fitting at middle of the tube. Image C shows the fitting at top of the tube.

This result suggests that when biPyridine is present, then an exponential decay is seen and that after shaking the effects of biPyridine are greater at the bottom and middle of the tube. At the top of the tube, biPyridine was either not present, or ineffective, as the signal was lower, the relaxation faster and a non-exponential decay was seen. This suggests that the secondary peak is not purely to do with turbulence of fluid flows and requires the presence of the catalyst.

3.4.4 Pyrazine in a 5 mm tube
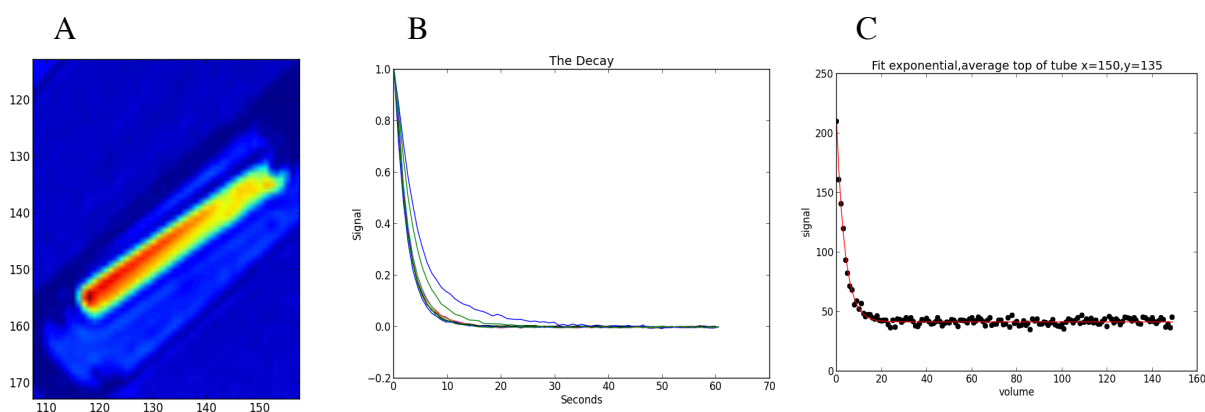
Figure 57: Image A shows the hyperpolarisation tube. Image B shows the decay of 9 scans after polarisation at 5 mT, and image C shows the mean of all 9 scans

In view of these observations, a repeat of one of the earlier experiments was undertaken. In this case the very first experiment was repeated but with a 5mm tube. In this experiment, 5mg Pyrazine, 2mg catalyst, 0.6 mg Methanol-d4 solvent were used, the sample 7, was scanned, after polarisation in a 5mT field, 9 times and the average calculated. It is clear that there is an exponential decay compared to the 10 mm tube, as seen from the figure 57. Exponential decay, smaller signal, as well as fast decay occurs when using a smaller diameter tube.

This again suggests that in a small tube, there might be less fluid motion after shaking and that the result is a simpler decay curve. However, this does not explain the effect of biPyridine, which suggests that the presence of the catalyst has an effect. The implication is that the non-exponential decay, which is in part due to what happens in a larger tube, might be due to Pyrazine interacting with the catalyst. As Pyrazine is known to bind to Pyrazine

binding protein and also to ASIC receptors in the heart, an experiment was designed to see if the presence of heart tissue would affect the decay of the hyperpolarised signal.

3.4.5   Pyrazine with an *ex vivo* tissue.

In this experiment two samples of Pyrazine with and without tissue, sample 6, have been scanned after polarisation in either the earth's magnetic field (0.05mT) or at 5 mT. The maximal deviation from an exponential decay can be seen at 5 mT. The sample with tissue had a shorter T1 and thus decayed faster than the sample without tissue (see Figure 58).
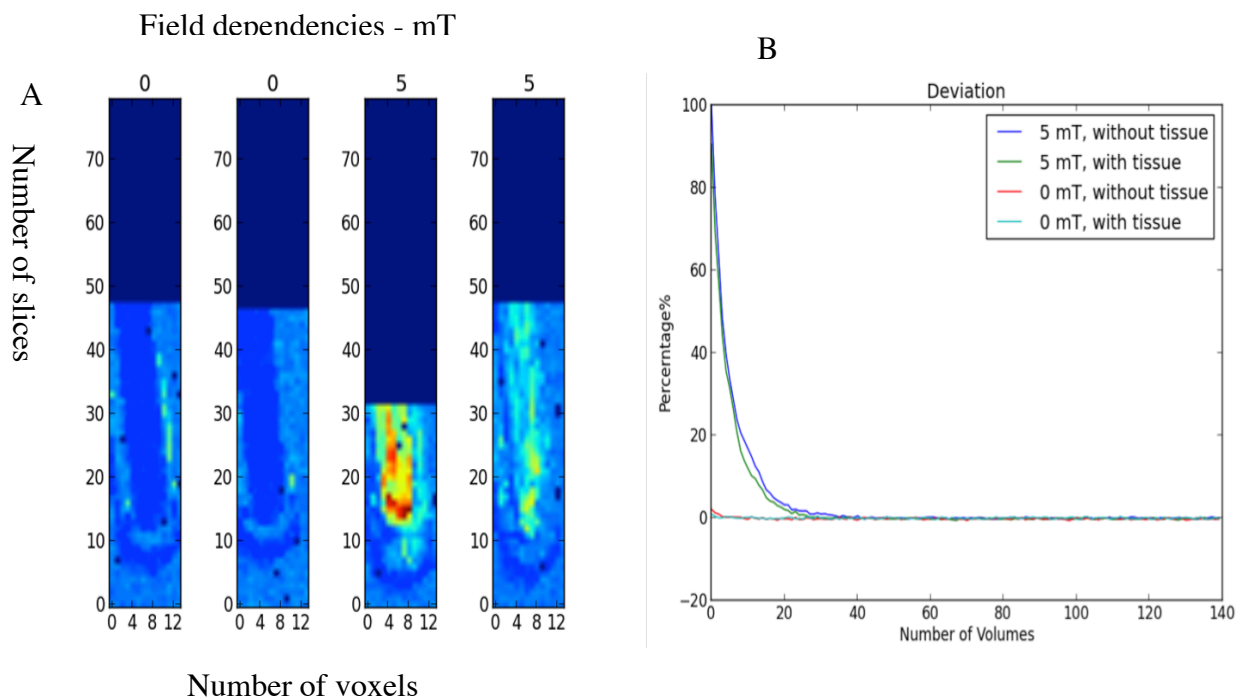
Figure 58: The left image (A) shows that there was no hyperpolarisation in the earth's magnetic field while there was clear hyperpolarisation at 5mT for both samples. The right image (B) shows both samples have a similar deviation but one with tissue (green) decayed faster than the sample without tissue (blue).

3.4.6 Discussion

The SABRE method was used to measure the signals and investigate tubes containing different chemical samples of Pyrazine, Nicotinamide and Pyridine. Generally, the results show non-exponential decay of the different samples. In addition, it is clear that the hyperpolarisation appears on one side of the tube. Several explanations have been proposed for these results and it is thought that turbulence or gravity inside the tube may be part of the reason for this occurrence.

3.4.6.1   Pyrazine sample

Larger non-exponential decay can be seen in the Pyrazine samples compared to the samples with Nicotinamide and Pyridine. The highest signals can be noticed in the Pyrazine sample with 10mg of Catalyst, followed by those in the Pyridine sample and lastly the Nicotinamide sample. The fact that it is molecule dependent can only be consistent with turbulence or fluid flow would only be correct if there was a variation in viscosity and/or density.

For Pyrazine, when a sample using 10 mg of catalyst is shaken for 45s, the signal is increased and the decay is slow, whereas the non-exponential decay is similar to the sample that uses 1mg of Catalyst. Faster decay can be noticed in the Nicotinamide samples and this is followed by Pyridine and Pyrazine.

3.4.6.2   Pyridine and Nicotinamide

In the Pyridine and Nicotinamide samples, the exponential decay is clear compared to the samples of Pyrazine. Although the Nicotinamide sample was investigated in different batches and for different lengths of time, it is clear that the sample shaken for 45s shows more deviation that than the sample shaken for 10s. In the Pyridine sample, the 30 scans were done at the same time using the same batch. It can be seen that the sample shaken for 45s shows more deviation than the sample shaken for 10s. This is of course compatible with longer shaking possibly causing more fluid flow through momentum but this is unlikely.

Ordinary Nicotinamide has a fast and exponential decay, whereas the deuterated Nicotinamide has a long decay and the non-exponential decay is clear.

3.4.6.3 Field dependence

As we have noticed from the field dependence results, the three samples of Pyrazine, Nicotinamide and Pyridine were investigated in different magnetic fields. All of the experiments show hyperpolarisation to be clear from 5 to 8 mT. This tells us that the magnetic field plays a vital role. However, the main signal is dependent upon the polarisation field and therefore it is likely that the deviation from an exponential might also be simply proportional to the main signal size.

The Pyrazine sample was investigated at different phantom angles to see whether there was any effect on the exponential decay or not. The first experiment used a 45° angle in the phantom whereas the second was at a 30° angle. Non-exponential decay occurred in both cases, but was greater and faster at 45° than the sample at 30°. Thus, when there is a larger surface area between the fluid and the pressurised gas in the headspace, the non-exponential decay is smaller. This is further evidence for the deviation being related to fluid flow.

3.4.6.4 Pyraznie and biPyridine

The type of tube was changed because we needed to add the biPyridine to the Pyrazine sample to kill the catalyst in the substrate. Two experiments were performed; in the first the biPyridine was not mixed with the Pyrazine sample before polarisation whereas in the second experiment the biPyridine was mixed in and the sample was shaken at 5 mt. These experiments gave different results as described above. The sample that was not mixed prior to biPyridine addition shows that hyperpolarisation occurred at the top of the tube but not at the bottom. In addition, the exponential decay can be seen. This could either be because the samples were not mixed or because of the change in the tube type. In the second experiment, the biPyridine was mixed with the Pyrazine sample prior to polarisation. In this case hyperpolarisation can be seen at the bottom of the tube and the non-exponential decay can be seen even though that different tube was used. In both samples, the part of the tube showing hyperpolarisation has a long decay (long T1). This suggests that some removal of the catalyst has occurred and it does mean that the catalyst is normally a route for relaxation if the polarised substrate rebinds to the catalyst.

During the experiments, we have used different tubes. In those tubes with a small diameter, e.g. 5 mm, exponential decay is observed. This leads us to try to understand why the change in diameter causes exponential decay.

3.4.6.5   Pyrazine with *ex vivo* tissue

The addition of *ex vivo* tissue has been investigated with polarisation in the earth's magnetic field and at 5 mT. Firstly, an ordinary Pyrazine sample was investigated and secondly another sample with a small amount of rat heart tissue was scanned. The results show that the sample containing the *ex vivo* tissue has a faster decay. In addition, there is no hyperpolarisation signal at earth magnetic field. This important result suggests that the change in T1 could be the basis of a novel contrast mechanism for examining whether a substrate has interacted with biological tissue.

3.4.7 Conclusion

The main aims of this chapter were to establish the background to polarisation and produce polarised images. In addition, to investigate the parameters that optimise the spin hyperpolarisation signal and to investigate different samples in different fringe fields of the MRI scanner.

Using the SABRE technique to investigate diverse chemical samples in the same field has led to different results. The non-exponential decay and deviation are clear in all samples with a tiny difference in decay depending on the amount of catalyst and the length of shaking/polarisation time. It has been found that the different magnetic fields have a significant effect on the substrates that have been investigated. The different phantom degree positions do not have much effect on the decay time course. The Pyrazine with biPyridine gave us different results. The non-mixed sample shows exponential decay whereas the mixed sample (Pyrazine with biPyridine) gave a tiny amount of non-exponential decay but this was not similar to the Pyrazine in the 10 mm tube. In addition, the Pyrazine sample in the 5 mm tube shows exponential decay. These results lead us to conclude that if a small tube is used then exponential decay will occur. Lastly, a small amount of rat heart tissue shows faster decay (short T1). In later chapters, further analysis will be presented to understand why these results were obtained.

Chapter 4   Image Optimization Using SABRE

4.1   Introduction

In the earlier chapters, Signal Amplification By Reversible Exchange (SABRE) has been explored to establish if it can be used as an imaging technique in a standard human MRI scanner. That was established and an exploration of key parameters was started. In this chapter, the imaging parameters are explored further. Three substrates have been investigated at 3 T scanner by using SABRE method.   The same substrates are used, Pyrazine, Nicotinamide and Deuterated MethylNicotinate. Investigation of the imaging of Pyrazine and Nicotinamide are investigated using different flip angles and different delays between volume acquisition. The aim of these experiments is to examine if images can be obtained for a long time. There are many factors which play a vital role to be able to increase the image time such as flip angle, time between volumes, matrix size and relaxation of hyperpolarised signal. In addition, the investigation of Deuterated Methyl Nicotinate has been further opitimised on the 3T scanner using a 6.5 mT polarization field. The aim of this experiment is to get the highest signal compared with water signal in order to obtain the highest enhancement so as to further optimise the imaging parameters.

4.2   Specific Methods for this chapter

4.2.1 Chemical Substrate and Sample preparation

The same samples as used in the previous chapter. The main change was for the Deuterated Methyl Nicotinate sample:
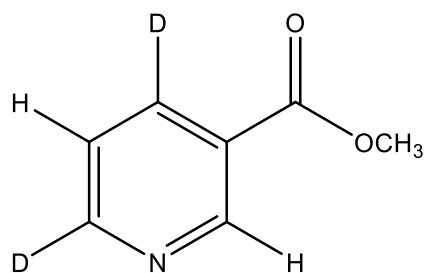
Figure 59: The chemical structure of Deuterated Methyl Nicotinate sample

Two differing quantities used were: 40 and 2 mg , with 10 mg of Catalyst and 3 ml Methanol-d4. The specific form of MethylyNicotinate used had the chemical structure as in figure 59.

4.2.2 Array Spatial Sensitivity Encoding Technique (ASSET)

 This MRI pulse sequence has been used in these experiments. ASSET is dependent on the Sensitivity Encoding (SENSE) method and uses many receive coils to make scanning faster by combining information across the coils to improve the signal to noise ratio in particular. Although it has a longer reconstruction time compared to normal image reconstruction times a major advantage is that one can reduce the number of lines in k-space and this leads to a reduction in RF deposited and thus, with hyperpolarisation, less destruction of the signal. It requires an extra scan that the system uses to calibrate where the signal come from by using a coil sensitivity scan. This calibration scan was performed using non-polarised samples in the phantom. In our ASSET scans 48 lines in k-space were used while normal FLASH scans uses all lines in K-space (King, 2004).

4.2.3 Phantoms and Tubes

Two phantoms were used. The first one, the standard phantom for the work in this thesis, had two inserts; one for the 10 mm reference tube with pure water and other for the sample tube after shaking in a polarization fringe field. This was used for the Pyrazine and Nicotinamide samples in this chapter see figure 60.
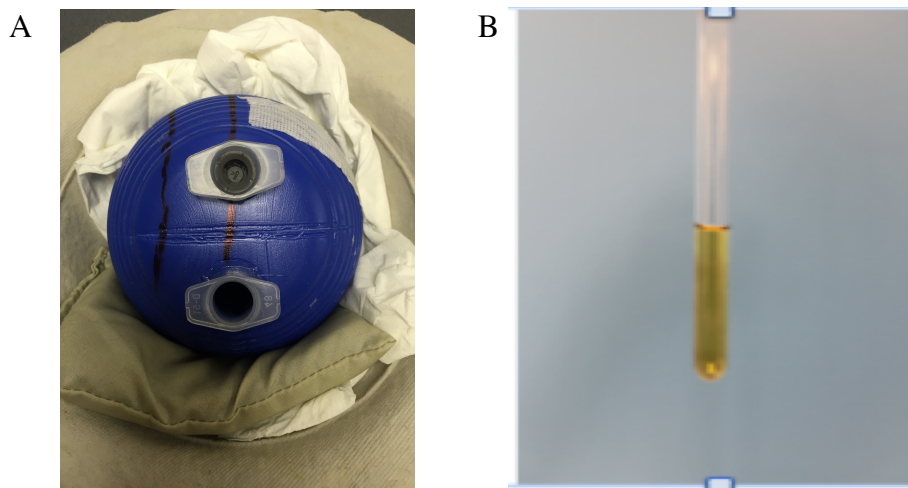
Figure 60: Image A show the stansard phantom and Image B shows a sample tube

The second phantom was used for the Deuterated MethylNicotinate sample and plastic sample tubes were used, see figure 61. The plastic tube is used because of the high pressure of Parahydrogen that was used to increase the solubility of parahydrogen inside the substrate. This leads to get high signal. If glass tube were used with high pressure, they would break (as was found!).
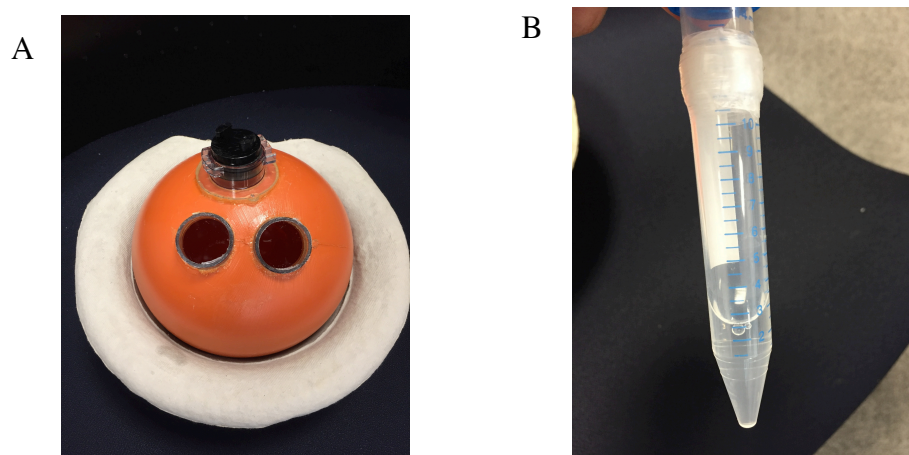
Figure 61: Image A shows the new phantom and image B shows the plastic tube.

4.3　Results

4.3.1　Pyrazine Sample, 10mm tube, 5 flip angle at 5mT

In figure 62, the relationship between signal decay and time can be seen for the Pyrazine sample (sample 1). Every time we excite the volume (a single slice with many excitation pulses – one per line of K-space) the signal gets smaller. There are many factors which must be considered in terms of interpreting this. The ideal is to image for as long a time as possible so that, in due course, in vivo imaging can capture the dynamics of biological processes. In this chapter I explore parameters

　Parameters such as flip angle, time between volumes, matrix size and the inherent relaxation of a hyperpolarised signal.
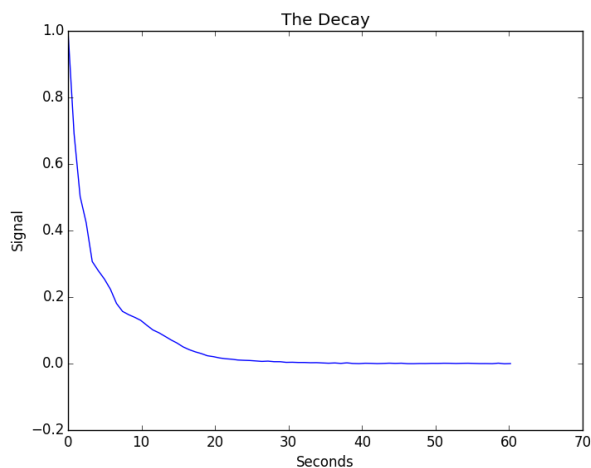
Figure 62: Image shows the decay and the relationship between signal and time.

4.3.2　Theory – signal after repeated single excitations

As I mentioned above the signal get smaller for each of the single RF excitations. Any hyperpolarised signal flipped into the horizontal plane by an excitation pulse is assumed to always return to a thermal equilibrium distribution of spins. If a small flip angle is used, only a small amount of the hyperpolarised signal is used for each line in k space. However, with the 90-degree flip angle all the signal would be used with that single excitation, see figure 63.

At the same time, with and without any RF excitations, the z magnetisation signal, the hyperpolarised signal, is decaying due to quite normal relaxation.
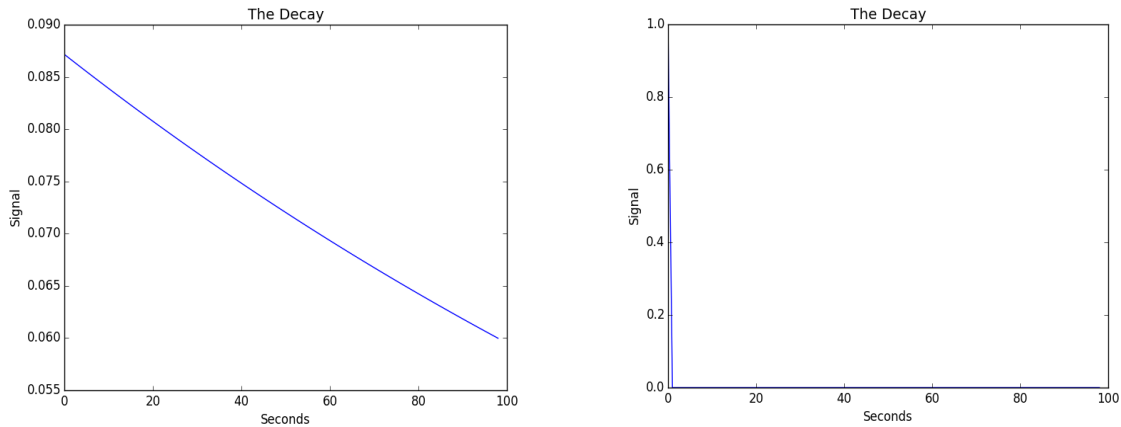
Figure 63: shows results of using different flip angle in theory. Image A shows what happens if a small amount of signal is used for each RF excitation pulse if we use a 5 degree flip angle, whereas image B shows how all of the signal is used, within a single slice acquisition, when a 90 degree flip angle is used

In the case of no relaxation, we start with a signal of size unity ie $1.\emptyset$. We then rotate signal towards the horizontal plane by a specified flip angle. The signal measured is the projection of that vector to the horizontal axis. The measurements destroys that signal, the magnetisation left is the projection back to the z plane. We then repeated the excitation using the same flip angle after a specified delay and obtained a new signal in the horizontal plane. This of course is smaller than the preceding measurement as if is a rotation of a smaller signal from the z direction. The calculations are simply that of using the relationship of the sine and cosine rules.

$$New\ signal = \sin(flip\ (\alpha)angle) \times previous\ z\ componant$$

$$New\ z\ componant = \cos(\alpha) \times previous\ z\ componant$$

$$signal = \sin(\alpha) \times z\ componant\ (t)$$

$$Z\ componant\ (t + delay) = \cos(\alpha) \times z\ componant\ (t)$$

With relaxation, we simply modified these equations to allow for the exponential decay of the z component.

$$Z(t)componant = z \; componant \; (t - delay) \; e^{- \; delay \; \times \; b}$$

Where b = T1 time and delay is time between excitation

4.3.3 The Effect of the Delay – Theory with no T1 relaxation

The apparent decay is predicted to be slow if a small flip angle is used, for multiple volume acquisitions, compared with a large angle if we neglect relaxation. When delays are used between volumes the apparent decay would appear to be slower. To predict what will happen we can start with what will happen if we assume no relaxation and that we start with a signal and just use that up by RF excitation within each volume. The effect, by theory, for both a 5 and 2° degree flip angle, without delay between volumes, is shown in figure 64. The calculation is based on assuming an initial magnetisation in the z direction, the longitudinal magnetisation, of unity. Then a specific flip angle is applied and this tips the vector away from the z direction by that angle towards the horizontal plane. From this, the amount of signal that can be observed is the projection of that vector into the horizontal and the signal left for the next excitation is the projection back to the z axis. Then the whole process is repeated again for every excitation within a volume and for every volume. Graph 64 shows the observed signal in the horizontal plane after all the excitations for each volume. In this case the signal decreases with each excitation and the apparent decay is simply determined by the delay between excitations. The different coloured dots represent different delays.

A: 5-degree flip angle   B: 2-degree flip angle
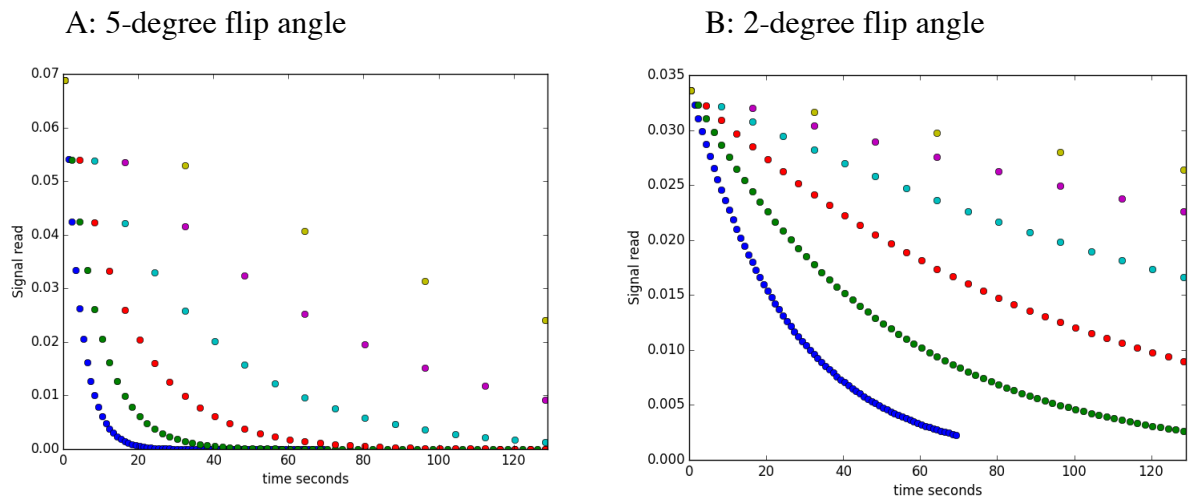
Figure 64: Both figures are theoretical predictions and show the apparent decay without delay in 5 and 2-degree flip angles. Image A with 5-degree flip angle while image B has a 2-degree flip angle

4.3.4 The Effect of Flip Angle with Short T1- Theory

The apparent decay is affected by flip angle – it is simply predicted by theory as in the previous section. If we now add an exponential decay due to relaxation there are two processes at work – the decay due to that relaxation and that due to readout which is proportional to flip angle. It is clear from the graphs below that the apparent decay is faster when using a big flip angle, when there is an assumed short T1, as seen in figure (65). Thus, the readout dominates the decay curve with a large flip angle.

A: 5-dgree flip angle   B: 2-dgree flip angle
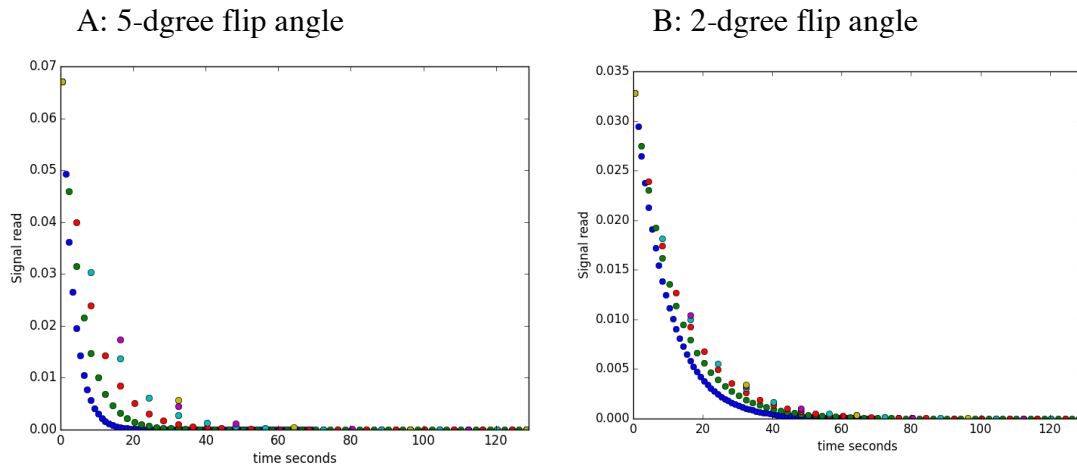
Figure 65: Both figures are theoretical predications and show the apparent decay with 5 and 2-degree flip angles and with short T1. Image A shows the apparent decay with 5-degree flip angle whereas image B show the 2-degree flip angle.

These curves with 2 and 5-degree flip angles have been fitted to compare between using these different angles. In figure 66 Image A below indicates the apparent decay (with no delay) is faster than if we have a long delay between volumes. When the times between volumes are increased, (the different coloured lines), the lines approach the decay values of the true T1. For a small flip angle, the T1 decay dominates and the slopes for any delay between volumes are very similar.

A: 5-dgree flip angle   B: 2-dgree flip angle
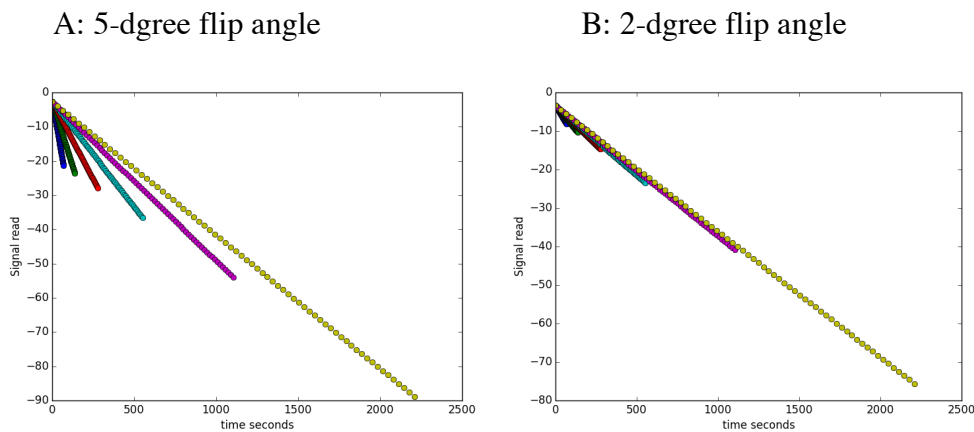
Figure 66: Both figures are theoretical predications and show different apparent decays with different times between volumes. Image A shows the signal decay with a 5-degree flip angle whereas Image B shows the predicted decay with a 2 degree flip angle. The signal magnitude is on a logarithmic scale referenced to the initial signal

4.3.5 Predicted half-life – Theory

As the inter volume delay is increased the predicted half-life increases and clearly becomes slower with a large degree flip angle. When a long delay is used, the true, relaxation, half-life is approached, see figure 67.

A: 2-degree flip angle   B: 5-degree flip angle
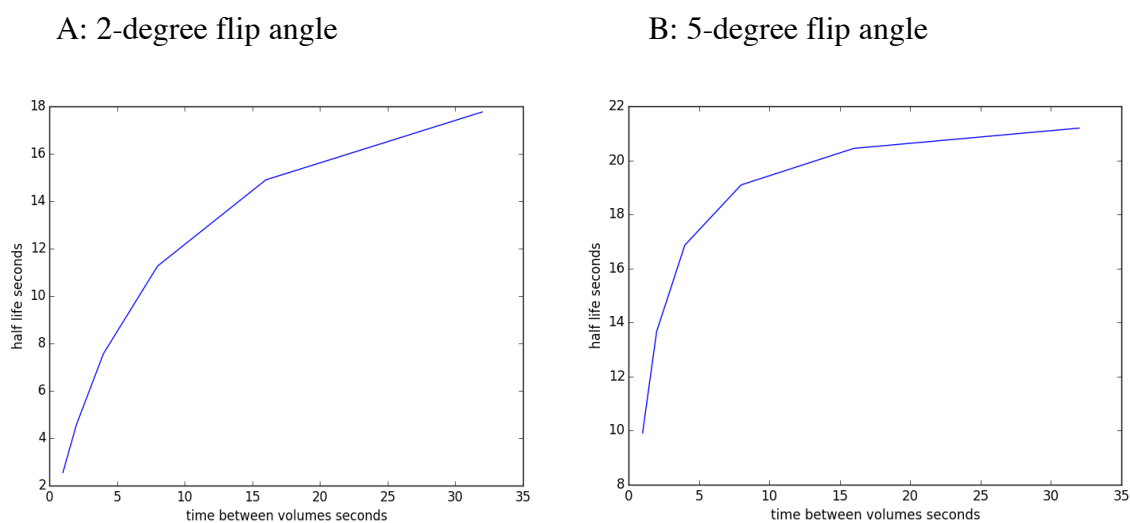
Figure 67: Image A show the predicted half-life with a 2 degree flip angle. Image B shows the predicted half-life with a 5-degree flip angle for the same theoretical T1 relaxation. The true half-life can be seen when a long inter-volume delay is used.

4.3.6 Practical Results – inter volume delay

The decay curve for a Pyrazine sample, sample one, with a 5-degree flip excitation angle can be seen in figure 68. When the time increases between volumes, the apparent decay can be seen to be extended. In image A the decay of signal without inter volume delay demonstrated an apparent shorter T1 as predicted. Image B shows the decay of the very same signal with 4 seconds between volumes. This means the decay in image B is (apparently) longer than the

109

decay in image A. Inter-volume delay is important. One does not want to destroy a signal before its value for interpreting a biological process has been extracted.

A   B
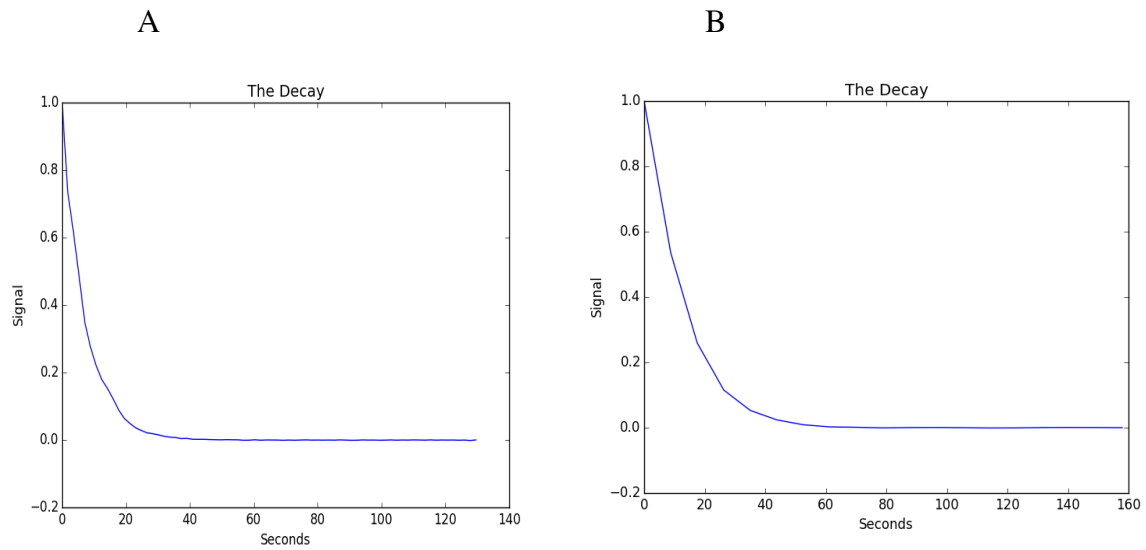
Figure 68: Image A shows the decay without delay between volumes whilst image B shows the decay with 4s between volumes

4.3.6.1   Pyrazine with different inter volume delay (5 flip angle)

The results of hyperpolarised Pyrazine sample interrogated with a 5 degree flip angle. Form the graphs, below image (A) shows us the decay with different delays and the slowest decay was 8s between volumes. The fitted decays with different delays can be seen in image (B). In addition, the different slopes and apparent T1s between a 1s delay and a 8s delay is clear. This means when the time increase between volumes the decay will decrease as seen in figure (69).
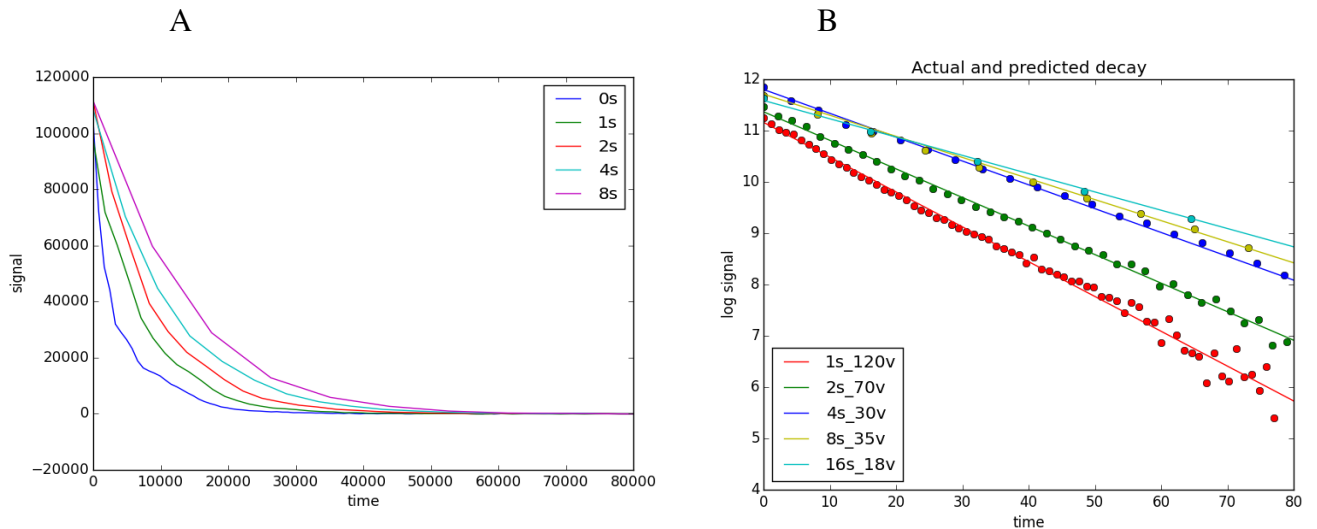
Figure 69: Image A shows the decay with different delay and Image B show the fitted decays with different delays.

The graphs below show the decay at different times between volumes for hyperpolarised Pyrazine, for both a 5 & 2 degree flip angles. Images (A) show the decay when a 5degree flip angle is used and graph (B) shows the decay curves when a 2-degree flip angle is used. The decay of 5-degree flip angle indicates different slopes whereas the decay of 2-degree flip angle shows the slopes are almost the same. The different between 5 and 2 degree flip angles can be seen in figure (70) This is as predicted.
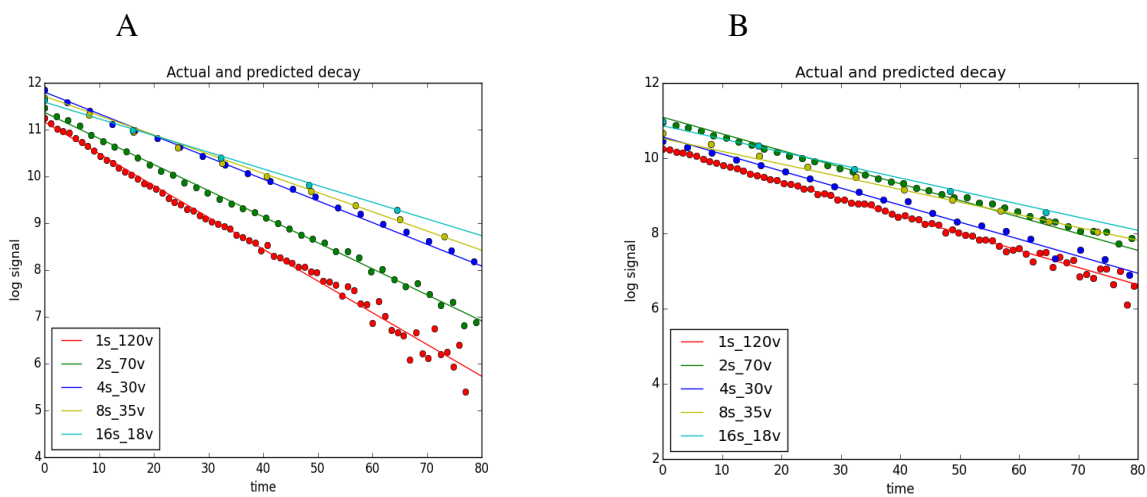
Figure 70: Image (A) shows the fitted slopes with 5 degree angle whereas Image (B) shows the fitted slopes with 2 degree flip angle
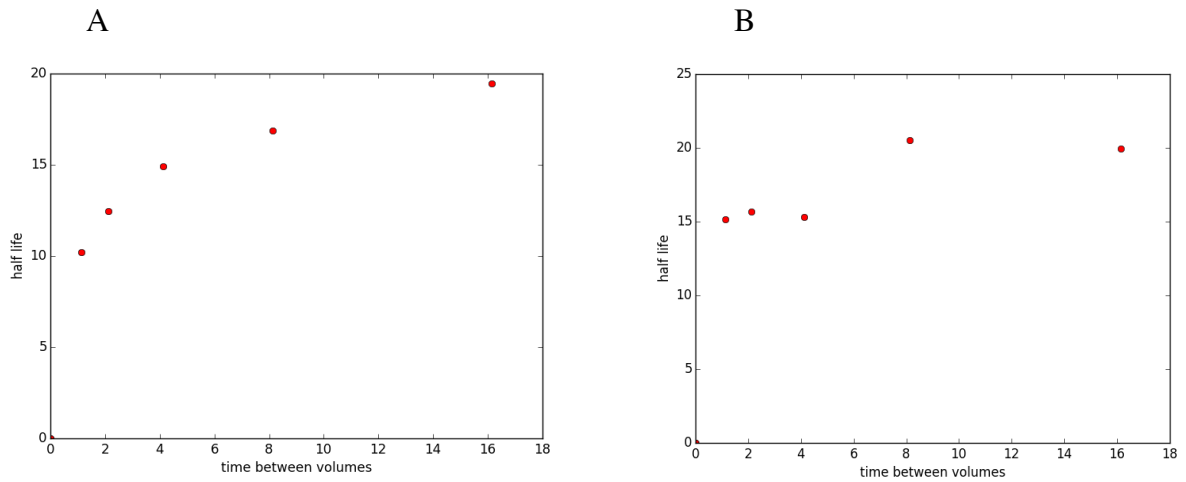
Figure 71: Graph A shows the half-life with 5 degree flip angle whereas graph B shows the half-life with 2 degree flip angle excitation.

The practical results of half-life of 2 and 5-degree flip angles can be seen in figure (71). The longer delay the more likely we are to get the true half-life and this can be obtained by using a low degree flip angle.

4.3.7 Theory & Practical - 5 & 2 flip angles:

Although the change in slopes from using differing delays between volumes and flip angles is predicted from theory, the initial magnetisation is not, see figure (72). This is an artefact in that the scanner did not immediately take a result in these experiments and the initial signal is affected by the volume delay.
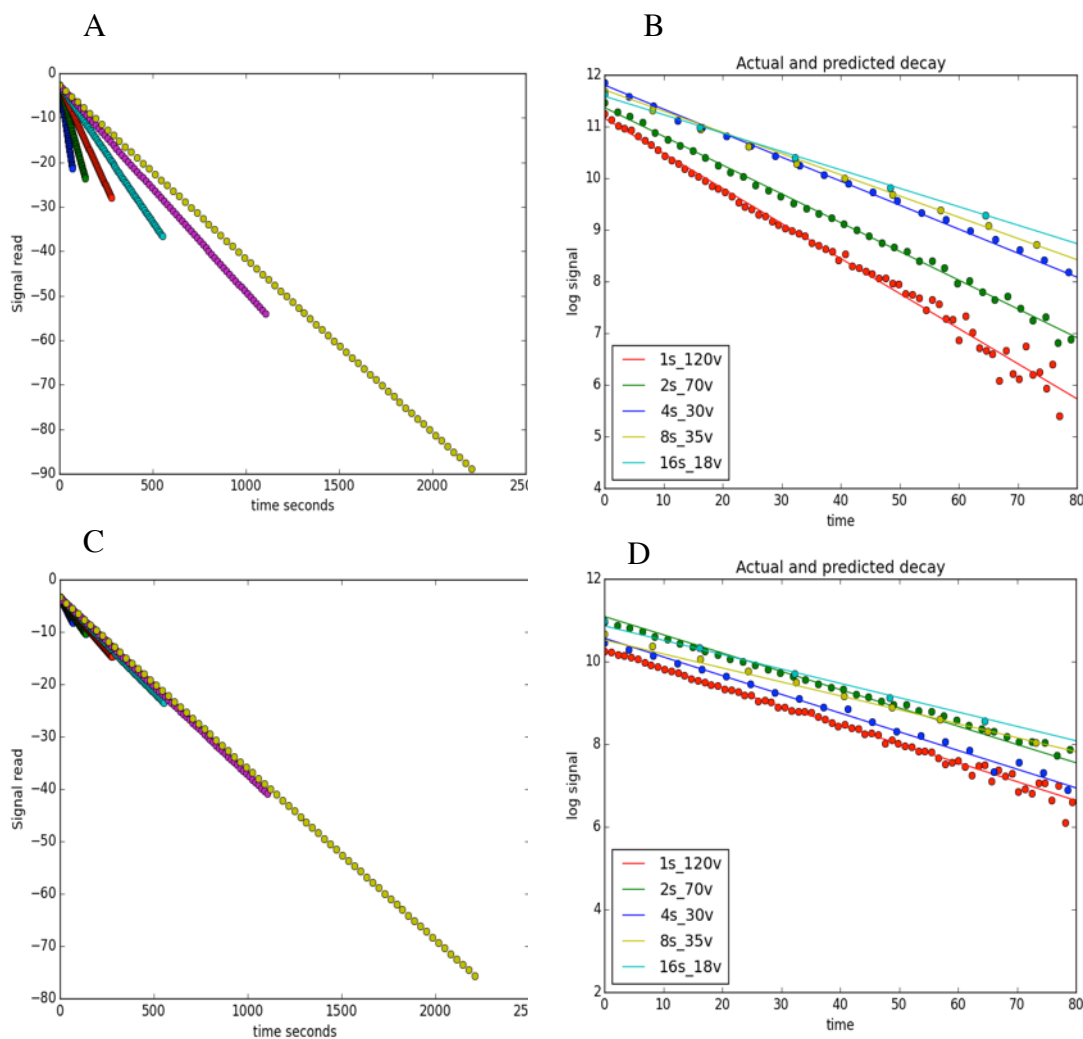
Figure 72: Graphs A & B show the theory and practical results of 5 flip angle while image C & D show the 2 degree flip angle

4.3.8 Nicotinamide Results

The same experiments have been done with Nicotinamide to see the difference between Pyrazine and Nicotinamide. The prediction would be that the true T1 for each molecule could be determined. The images below show the decay at different times between volumes. The longest decay in 5-degree flip angle is 8s between volumes. The slopes for 2 degree flip angle are not significantly different as predicted by theory, see figure 73.

A: 5-dgree flip angle   B: 2-dgree flip angle
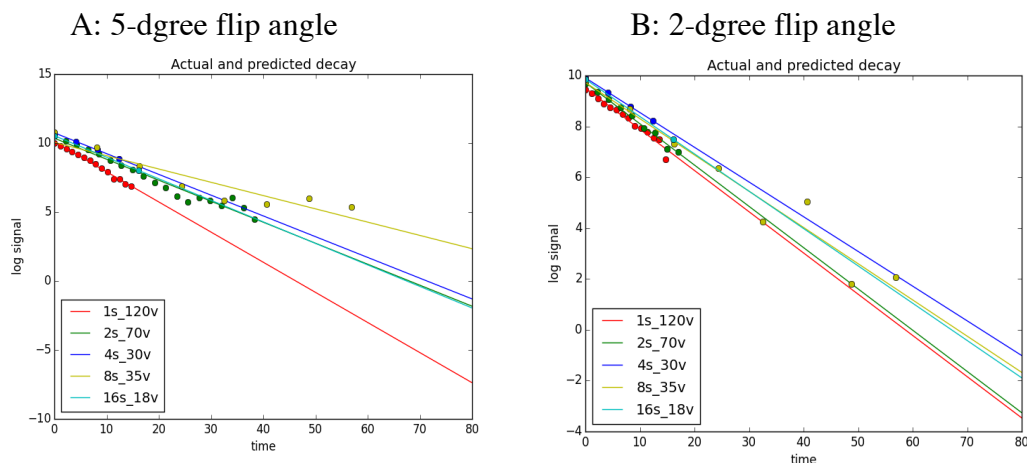
Figure 73 shows the results of pyrazine sample. Graph A shows the decay when using a 5-degree flip angle with different delays between volumes. The 8s seconds between volumes shows the long decay (yellow). Graph B shows the decay using a 2-degree flip angle and the long decay is 4 seconds between volumes (blue). Both graphs are for hyperpolarised Nicotinamide practical results

4.3.9 Results for Deuterated Methyl Nicotinate:

The same study was applied to hyperpolarised Deuterated Methyl Nicotinate. It has already been noted that this compound exhibits a long T1. In this section, the effect of using different substrate concentration is also investigated, The effect of changing the ratio of catalyst to substrate can be predicted to change the apparent T1 in terms of the route to relaxation via binding of the hyperpolarized substrate back onto the catalyst.

A high signal from the hyperpolarized substrate, for both 40 and 2 mg of substrate was observed compared with water.

The sample with 40 mg of substrate was investigated with both a 5 and 2-degree flip angle. The results show that the signal disappeared after 60 seconds with a 5 degree flip angle whereas the signal when a 2 degree flip angle was used was still present after 60 seconds as seen in figure (74). These images were taken without delay and the sample was shaken 20 seconds in the polarization field before insertion in the phantom.

A: 5-degree flip angle

B: 5-degree flip angle

Hyperpolarised tube of
Deuterated Methyl
Nicotinate at first
second of scan.

Hyperpolarised
tube of
Deuterated
Methyl
Nicotinate after
60 seconds

C: 2-degree flip angle

D: 2-degree flip angle

Hyperpolarised tube of
Deuterated Methyl
Nicotinate at first
second of scan.

Hyperpolarised
tube of
Deuterated
Methyl
Nicotinate after
60 seconds

Figure 74 shows shows the results of Deuterated Methyl Nicotinate sample. Image A&B with 5 degree flip angle and Image C&D with 2 flip angle. Image (A&C) shows the image at first second of scan. Image B&D show the signal was taken after 60 seconds of scan.

The enhancement of the 2 mg sample is larger than that of the 40 mg sample, whereas the signal is smaller (2mg =10508 and 40mg = 6423 relative to water). In figure (75) the images show that the signal has disappeared after 30 seconds of scanning.
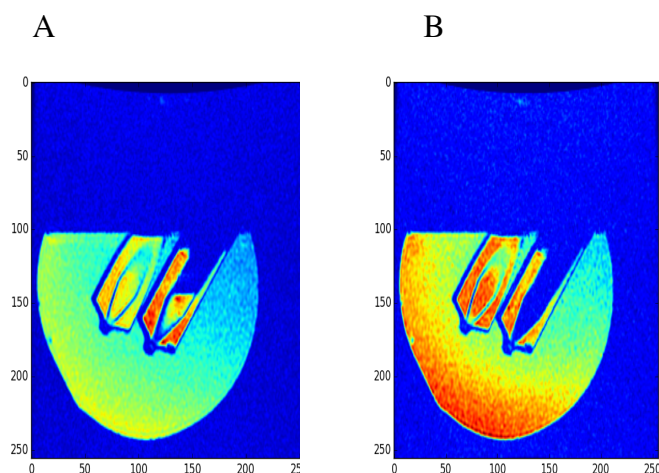
Figure 75: Image A&B with 5 degree flip angle excitation and 2 mg of substrate. Image A shows the signal at the first second of scannning whereas image B shows signal has disappeared after 30 seconds. 2mg of Methyl Nicontinate

4.3.10 Actual and Predicated Decay of Deuterated Methyl Nicotinate

Deuterated Methyl Nicotinate has been scanned with different degree flip angles, different times between volumes and different amounts of the substrates. The slowest decay is observed when a 4 second delay between volumes is used with a low flip angle. The sample with a 5 degree excitation flip angle and 2 mg of substrate has the faster decay but high enhancement as seen in figure (76). For the same flip angle (5 degrees) and for the same time between volumes (no delay), a sample with a lower concentration of substrate has a much faster apparent T1.
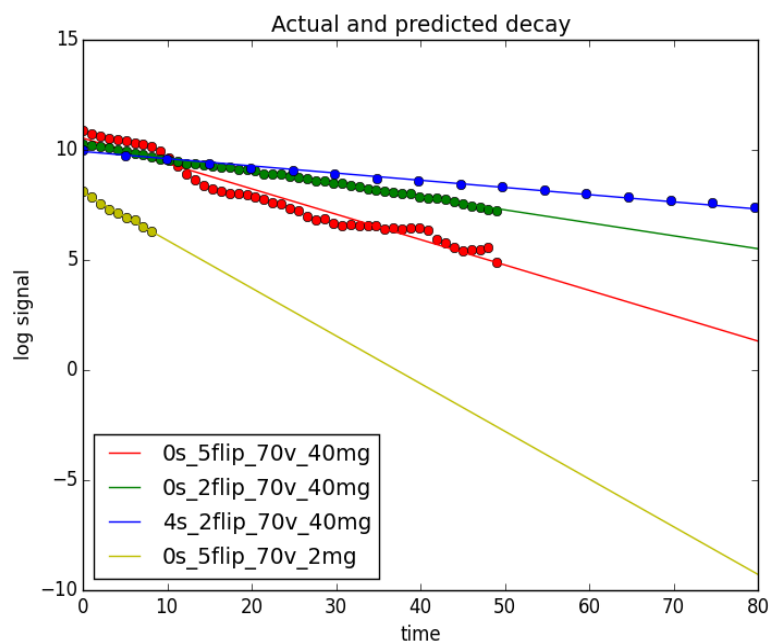
Figure 76 shows the actual and predicated decay of 4 experiments. The longest decay is blue slope (4s between volumes) and the fastest decay is the yellow slope (no delay, 2mg and 5 degree flip angle).

4.4   Discussion

In this chapter three substrates, Pyrazine, Nicotinaimde and Deutrated Methyl Nicotinate were investigated. Firstly, the results of Pyrazine can be discussed and followed by Nicotinamide and Deuterated Methyl Nicotinate. As I mentioned above the aim was to image for longer time by using SABRE with different MRI settings and with these chemical substrates.

4.4.1 Pyrazine sample

For the Pyrazine results, there is an evidence of a slower apparent decay in the hyperpolarised Pyrazine signal when the time is increased between volumes and this is compatible with theory. In addition, when the lower 2 degree flip angle is used a longer decay is also observed compared with using a 5 degree flip angle. This means using small flip angles with time between volumes (delay) will give us a longer apparent decay. Five experiments were carried out for the Pyrazine sample and each one had a different time between volumes. As predicted using a small degree flip angle will use a smaller amount of signal at each excitation. However, when a larger degree flip angle is used such us 90 degrees, all the signal will be used within one volume. The fitted results of Pyrazine with 2 and 5 degree flip angles were as predicted.

4.4.2 Nicotinamide sample

A second sample, Nicotinamide was investigated to see if T1 times for molecules could be estimated. The overall results of using a 5-degree flip angle are similar to that for the Pyrazine sample. The lower flip angle experiment reveals a very large difference in the T1 between Pyrazine and Nicotinamide. The highly symmetrical Pyrazine molecule has a much longer true T1 than Nicotinamide.

4.4.3 Deuterated Methyl Nicotinate sample

Deuterated Methyl Nicotinate was the third sample. It has been investigated after polarization at 6.5 mT also with different degree flip angles. The phantom and tube were changed to be suitable for our experiments. The tube was plastic instead of glass because 7 bar Parahydrogen was placed in the headspace rather than 3 bar as it was used in the previous experiments. Using 7 bar was increased the solubility of parahydrogen inside the substrate and led to increased the relaxation time. If a glass tube is used with 7 bar there is a serious risk that it will explode. Two different amounts of substrates were used 40 mg and 2 mg. By using a 5-degree flip angle with 40mg of substrate and no delay, the signal disappeared within 60 seconds. However, when the 2-degree flip angle is used the signal can still be seen

after 60 seconds. The 2mg sample has a similar amount of substrate and catalyst. Although the enhancement was higher, the signal as expected was smaller. However, the apparent decay is much faster than when a high concentration of substrate is used. This has important implications for the preparation of hyperpolarized samples for imaging. It would be desirable to use high substrate to catalyst concentrations.

4.5   Conclusion

To summarize this chapter, the choice of MRI scanning parameters has a major effect on the ability to view hyperpolarised images for a long time. Although small flip angles inevitably give rise to lower signal to noise and thus lower contrast images, they can be observed for a longer period of time and the delay between volumes is not so important. It was also observed that the apparent half-life of a hyperpolarised signal is also substrate concentration dependent. In the next chapter, ex vivo tissue will be investigated with same samples at 3T scanner.

Chapter 5   Imaging using SABRE with ex-vivo tissue

5.1   Introduction

In this chapter, several measurements were used to investigate whether imaging of ex vivo tissue could be achieved with SABRE and a human MRI scanner. The hypothesis was that an interaction substrate with biological tissue could be observed either as a change in contrast due to relaxation changes or that unobservable magnetic states might evolve into observable magnetisation after an insteraction between a hyperpolarised substrate and the tissue. The substrate used was Pyrazine. Rat heart was used as the ex-vivo tissue. During the work for this chapter the main scanner that could be used for investigations changed from a GE scanner to a Siemens 3T scanner Magnetom Prisma. The head coils was head coil with 12 channels

The hypotheses of this chapter are:

- To test that the imaging of Pyrazine samples in different scanners (GE and Siemens) was the same.
- That Pyrazine binds to specific ion channels and that would result in a change in signal observed as this would increase relaxation and signal decay.
- That within hyperpolarized Pyrazine there would be higher order magnetic states, singlet states, that would evolve into observable magnetisation in the presence of tissue.

5.2 Amiloride Receptor:

Amiloride is a potassium sparing diuretic and was approved for clinical use in 1967. It was used to manage hypertension, congestive heart failure and cystic fibrosis. However, it is has been superseded by other agents because of its short time action (Rodgers & Knox, 2001). Amiloride blocks the epithelial sodium channel (ENaC). Therefore, the sodium reabsorption in the distal convoluted tubules and the ducts is collected in the kidney. This leads to loss of water and sodium but no loss of potassium (Loffing & Kaissling, 2003). Another action of amiloride, that it can also block Acid Sensing Ion Channels (ASICs) in the heart and other tissues. This channels also contain the ENaC proteins that characterise this class of Sodium channel. Blockage of these channels reduces reperfusion injury in ischemic attacks (Cogan, 1990). In ischemia when oxygen levels drop in the tissues, the tissues switch to anaerobic metabolism and the local pH drops. When the ischaemic block is released, blood flowing back is associated with reperfusion injury as a host of inflammatory factors lead to oxidative stress and free radicals that damage cells. In this case, amiloride is a useful drug because it blocks Sodium-Hydrogen exchange and stops the influx of Calcium when the potential of hydrogen (pH) is low. This helps prevent cell death. The Amiloride structure contains the Pyrazine motif at its core. See the figure 77.
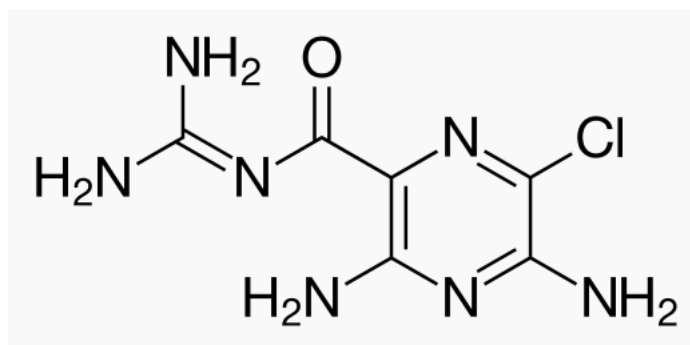
Figure 77: Amiloride

The amiloride is known to bind to the ENaC ion channel. One mechanism is via the Pyrazine moiety binding to the Pyrazine binding protein component of the ENaC (de la Rosa, Canessa, Fyfe, & Zhang, 2000). In the last few years, the function of ASICs channels have been found to be involved in the normal mechanisms of memory, learning and pain. The ASICs are

neuronal voltage insensitive channels that are stimulated by extracellular protons. There are many ENaC proteins which result from four genes, Amiloride-sensitive cation channel 1 (ASIC1), Amiloride-sensitive cation channel 2 (ASIC2), Amiloride-sensitive cation channel 3 (ASIC3) and Amiloride-sensitive cation channel 4 (ASIC4) (Hanukoglu & Hanukoglu, 2016).

5.3   Pyrazine and heart tissue

When hyperpolarised Pyrazine is added to tissue with ASICs then it can be predicted, from the results of chapter 4, that the signal decay will be faster. Another expectation, if the Pyrazine interacts with this heart receptor would be that the symmetry of Pyrazine will be broken as results of changing the chemical shift in the protons on the heterocyclic ring.

5.4   Specific methods for this chapter

5.4.1 Phantom

A new phantom was constructed with many internal references. These were 4 tubes containing normal saline, two small tubes of pure water and two medium tubes of mineral oil as can be seen in figure (78). The sample tube insert was made with a larger bore to facilitate the insertion of a sample when the Siemens scanner was used as this has a much longer magnet bore.
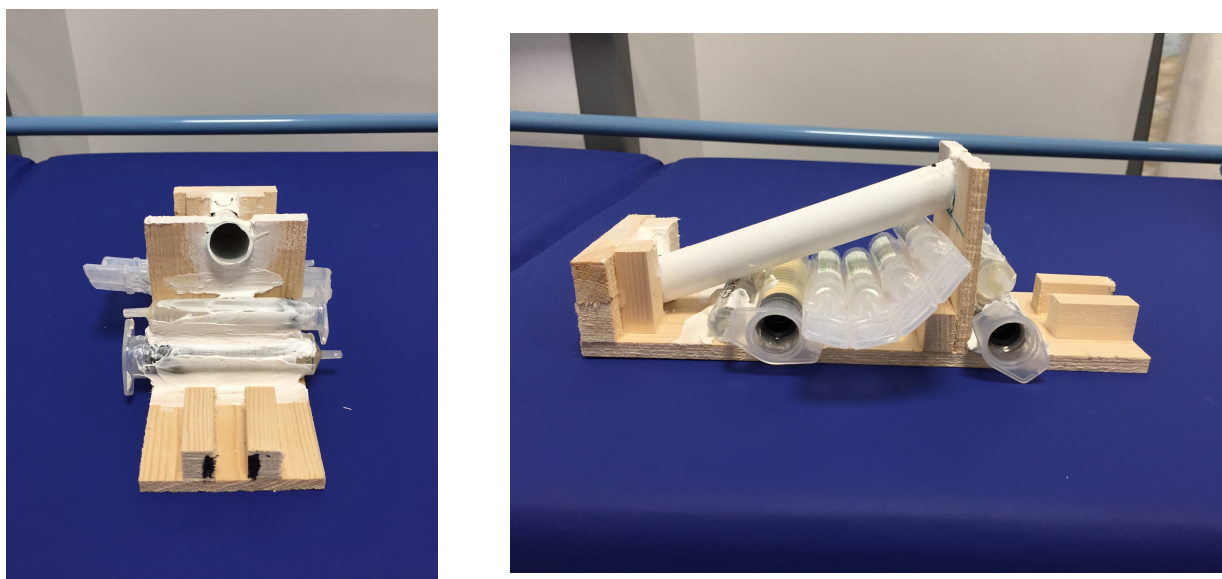
Figure 78: Images shows the phantom that was used in this chapter

5.4.2 Animal Ethics

Animal experiments were approved by the University of York Ethical Review Panel and under a UK Home Office licence.

5.4.3 Heart Preparation (ex-vivo)

The animal (Rat) was humanly killed using a schedule 1 procedure after ethical approval. The hearts were quickly excised and saved in low room environment (low temperature). The Rat heart was then cut into small pieces and mixed with the test chemicals inside a glass NMR tube. In figure (79) below we can see a rat heart and an NMR tube that contains the substrate and heart tissue.
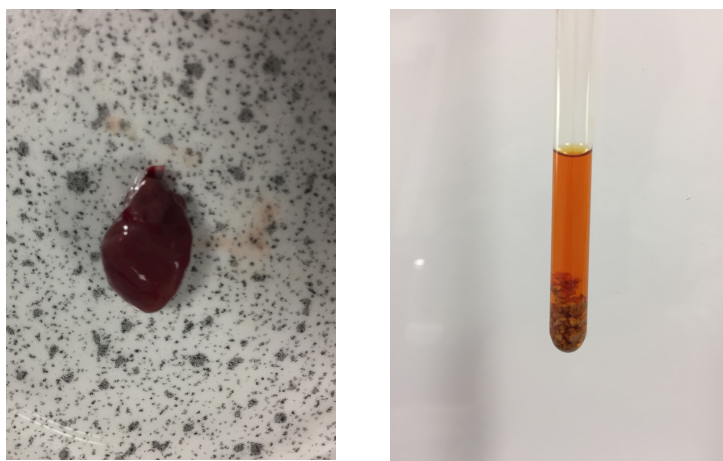
Figure 79: Image A shows the whole Rat heart whereas image B shows the NMR tube with small pieces of heart in the tube.

5.5 Results

Figure 80 shows an image of a hyperpolarised sample of Pyrazine along with the reference signals of the new phantom. Also shown is the position of four mask locations (circles) that were used to calculate the average signal strength in each region of interest within the sample tube.
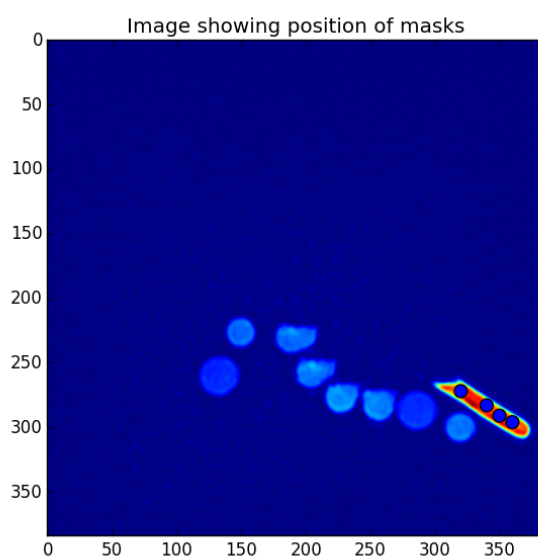
Figure 80: Position of masks on the hyperpolarised Pyrazine sample

5.5.1 Control images and time course

Figure 79 shows the sample and reference tubes immediately after hyperpolarisation when just Parahydrogen is added to the sample and dissolved in a polarisation field of 5mT for 10 seconds.
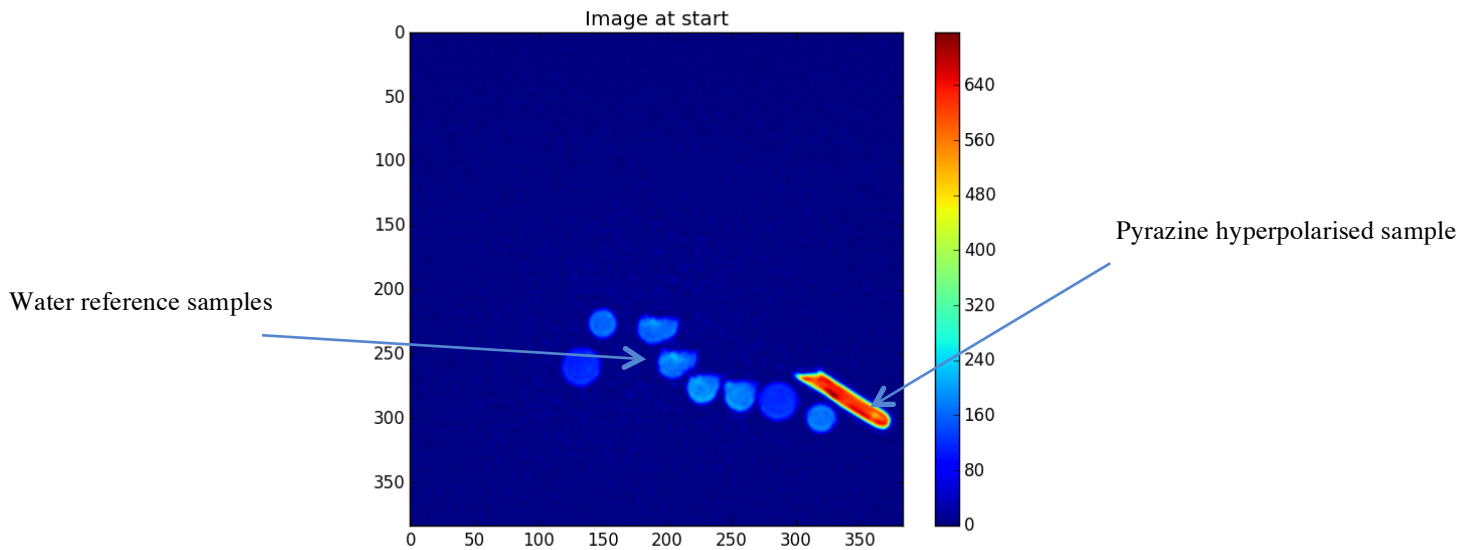
Figure 81: Pyrazine sample and this image at start

The same image just 6.4 seconds later demonstrates that the signal from Pyrazine has decreased. See figure 82.
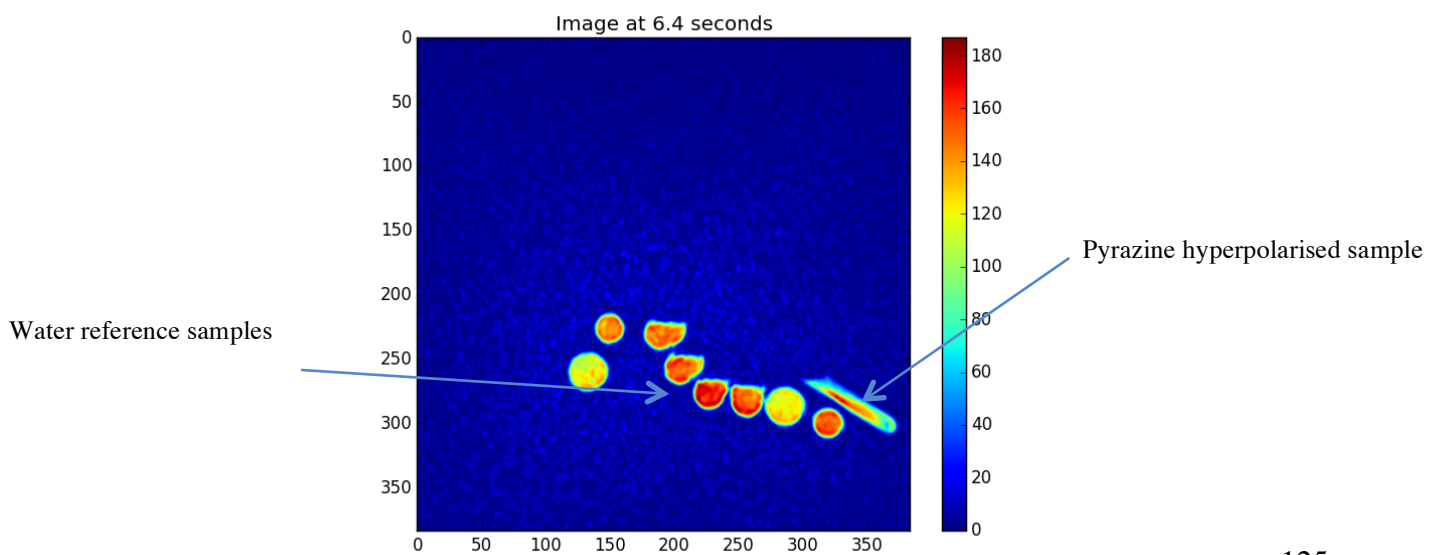
Figure 82: Pyrazine sample and this image at 6.4 seconds

At 24.8 seconds and at 50.4 seconds it can be seen that the hyperpolarised signal has decreased to the background noise level as seen in figure 83.
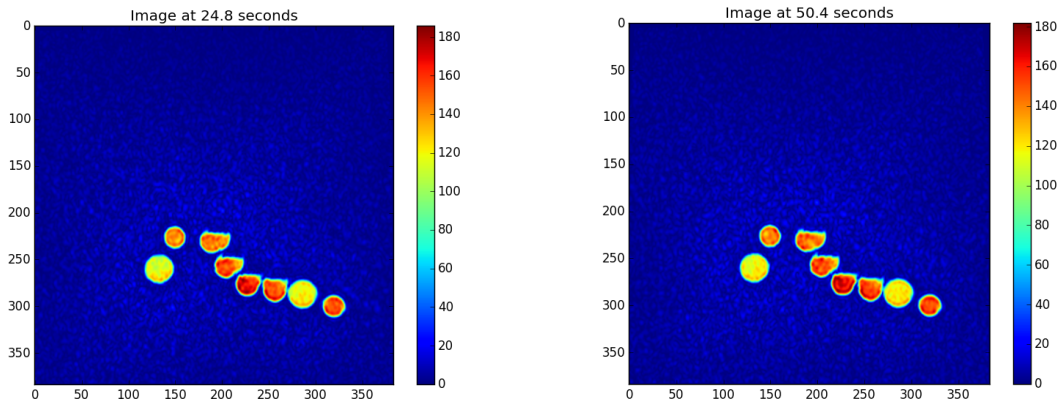
Figure 83: Signal in both images has decreased to the background noise level

Figure 84 shows the time course of the hyperpolarised signals. Each region of interest within the tube shows strong hyperpolarisation that decays with time until only a noise level signal is observed. The same slight deviation from a non-exponential decay is observed as in earlier chapters.
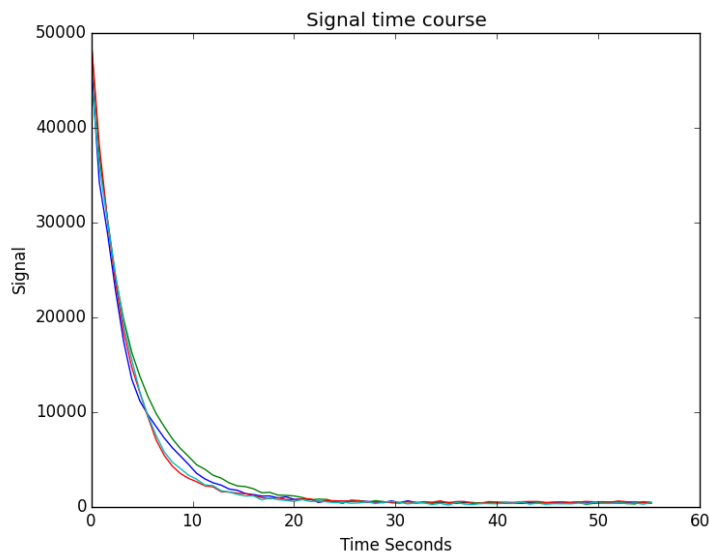
Figure 84 shows the time course of the hyperpolarised signals

5.5.2 The effects of heart tissue

The same images and time courses were captured from the same regions of the Pyrazine tube as in the previous section. The difference is that in this case Rat heart tissue was added before polarisation.

The initial image, immediately after polarisation, figure 85, can be directly compared to figure 81. The most obvious features are that one can see the location of the heart tissue in the

Pyarzine hyperpolarised sample with heart tissue
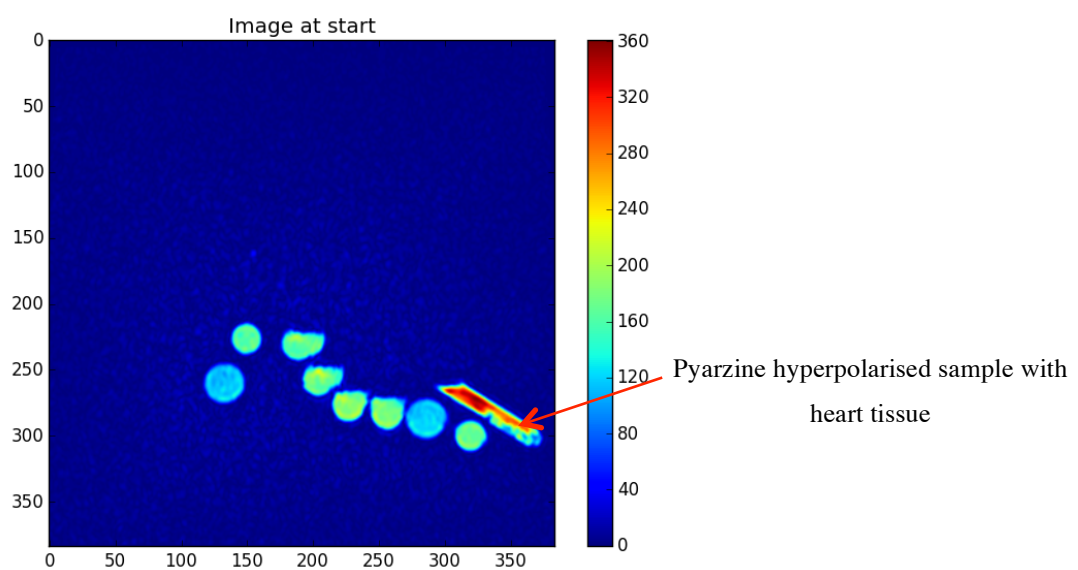
Figure 85: Image at start shows the hyperpolarised tube included heart tissue

bottom of the tube and that the maximum signal from the Pyrazine is much lower than in the control sample. As shown in chapter 4 section 4.4.5, the presence of tissue leads to faster relaxation and this could account for the small signal.

Again, the effect of heart tissue can be observed at 6.4 seconds and compared with the control, see figure 86.
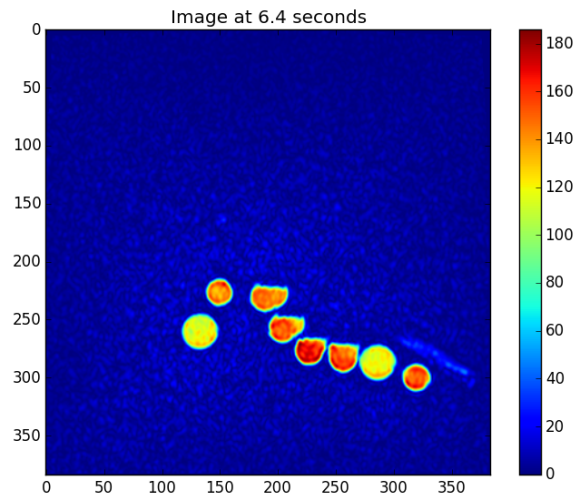
Figure 86: Image at 4.6 seconds with tissue

Again, the signal is much lower at 6.4 seconds in the presence of tissue but still higher than the background noise. This is again compatible with the tissue having an effect through increased relaxation. As discussed in chapter 4 this form of negative contrast could still be of use in clinical imaging.

To compare between figure 82 and figure 86, it can bee seen that the figure 86 with tissue has low signal whereas the figure 80 without tissue has signal similar to the water.

The surprising difference though is what can be observed at 20.8 and 50. 4 seconds see figures 87 & 88. To compare between figure 83 (Pyrazine without tissue) and figure 87 and 88, it can be seen the signal disappeared after 24.8 seconds in figure 83 whereas still appear in figure 87 and 88 at 24.8 seconds and at 50.4 seconds.

It can be clearly seen that the signal in the sample tube is still above that of the background at both time points throughout the sample tube. It would appear that a persistent signal is present.
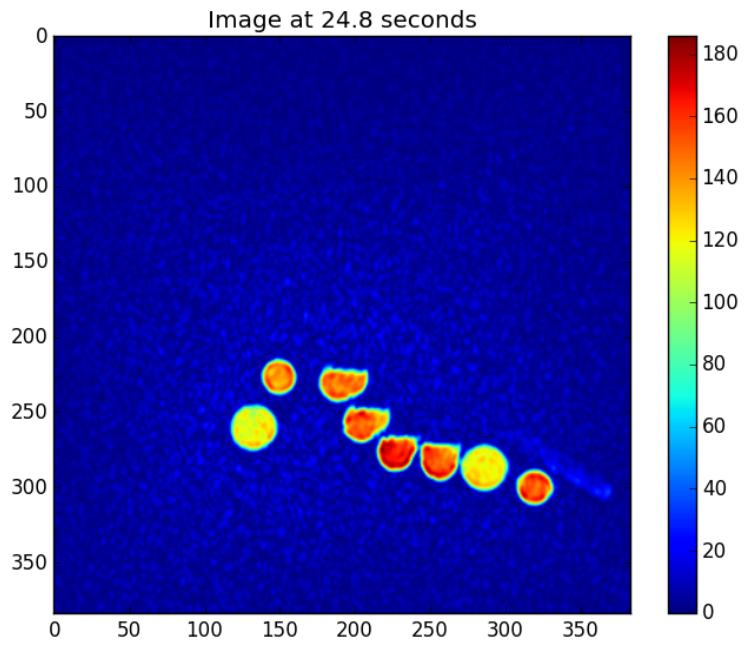
Figure 87: Image at 24.8 seconds with tissue

Water reference samples

Pyrazine hyperpolarised sample with tissue
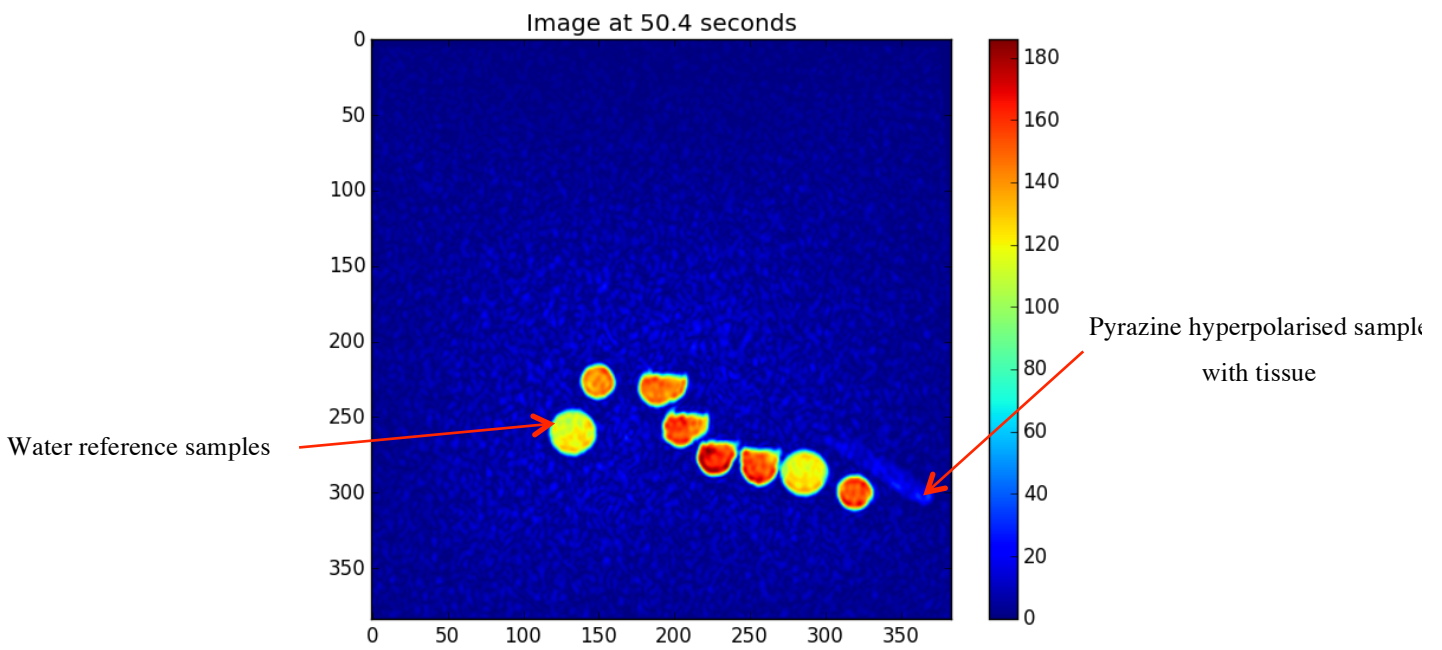
Figure 88: Pyrazine sample and this image at 50.4 seconds with tissue

If the time course of the signal is examined at the same regions of interest as in the control sample, figure 89A, then one can observe that the signal decays faster in the presence of tissue, the signal reaches a minimum at about 10 seconds and then returns and is slowly growing over a long period. However, in figure 89 B (Pyrazine without tissue), the signal has longer decay and reaches a minimum at about 20 seconds with no returns.

This experiment was repeated six times and the same observations were made. A long persistent signal is seen if rat heart tissue is present.

A: Pyrazine with tissue   B: Pyrazine without tissue
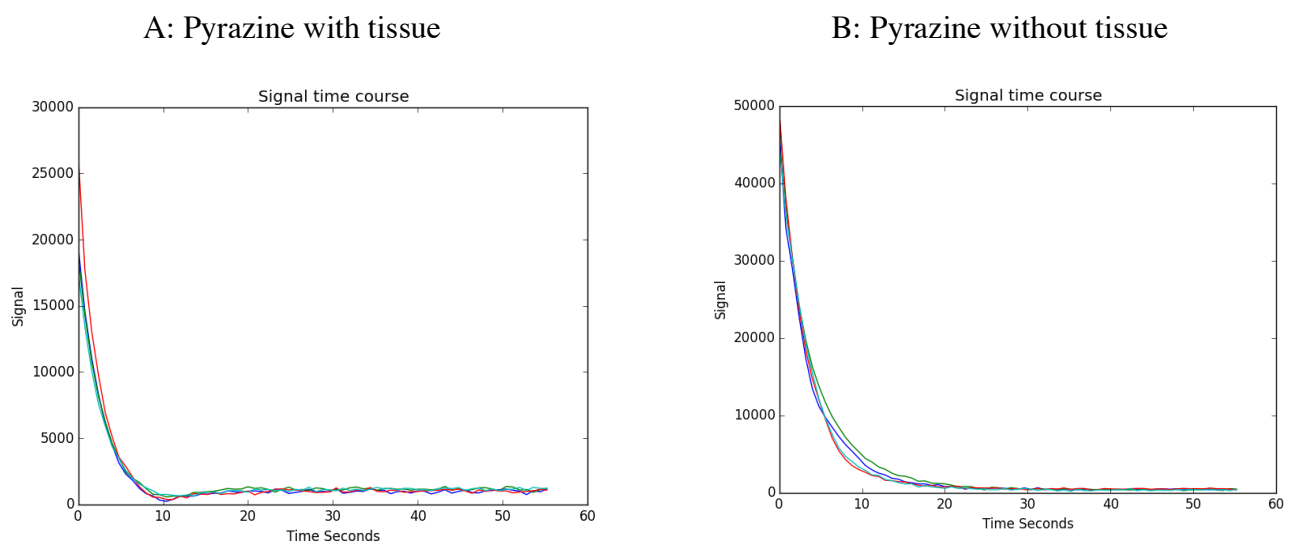
Figure 89: image A shows the signal time course with tissue. Image B shows the time course of the hyperpolarised signals without tissue. Decay in image A is faster decay than image B.

5.6 Discussion

The results in chapter 4 has already demonstrated that the presence of tissue could affect the time course of a hyperpolarised signal. The tissue increased the relaxation of the signal and this showed as a faster half-life and a decreased initial hyperpolarisation. This observation has been repeated here.

The major finding in this chapter though is that when heart tissue is present, after the signal has returned to the baseline noise level, it recovers and persists throughout the tube not just where the heart tissue is found.

This could be due to the presence of singlet states that are not observable and only become so if the symmetry of Pyrazine is broken. This could occur if there were ASIC channels present and if the Pyrazine were to bind to the channel proteins. This is the first evidence of a source of magnetisation beyond the normal T1 decay of a signal. If it is correct and could be optimised, then this is a novel source of contrast for in vivo imaging.

5.7 Conclusion

The major conclusion reached in this chapter is that a new persistent magnetic signal has been observed when hyperpolarised Pyrazine and a biological tissue interact. The next chapter explores whether singlet states can be imposed on a molecule in an attempt to extend MRI observation times even beyond the minute that the signal was shown to last here.

Chapter 6   Long Lived State with an ex vivo tissue

6.1   Introduction

The earlier chapters of this thesis have demonstrated that it is possible to create MRI images after using SABRE to greatly enhance the signal from molecules. The parameters for optimised imaging were explored and it was shown that manipulation of simple parameters such as the flip angle and the delay between volumes could be used to produce images that, with the correct molecule be observed for up to 60 seconds. However, if the technique is to be used in-vivo then it would be desirable to increase the imaging time to much longer times. This would allow an injected molecule to be transported around the body, to reach sites after passing through barriers by diffusion or active transport and then to be modified or take part in metabolic processes.   Having the molecules hyperpolarised would allow these physiological and biochemical processes to be monitored using MRI.

Therefore, the ideal enhancement of the SABRE should be provided for so as to last as long as possible and be transferred it to the area of interest. But, a result of the short T1 lifetime of proton magnetisation, there are still obstacles to be overcome if this is to be achieved. Proton signals are useful because they can be read on any standard clinical scanner. DNP uses 13C signals normally and this implies that the clinical scanner must have a 13C transmit and receive capability. 13C and 15N have the advantage of being associated with longer T1s and can be also used with SABRE, but again scanners have to have multinuclear capabilities which is expensive. Therefore, if the T1 lifetime is increased, for protons, the better the advantages of standard MRI will be realised (Vasos et al., 2009).

Low field nuclear spin states (Carravetta, Johannessen, & Levitt, 2004) or long-lived states (LLS)(Vasos et al., 2009) might be utilized to preserve the nuclear spin order as their lifetimes are longer than the spin lattice relaxation mechanism of T1. These methods have been used to increase imaging times by 10 times compared with that normally observed and

limited by spin lattice relaxation. The intermolecular dipole-dipole relaxation does not affect the low field nuclear spin singlet (Carravetta et al., 2004). In recent studies, long lifetimes of magnetic spin have been created to address the short decay. This can be done by creating a nuclear spin singlet state that might create extremely long lifetimes (Carravetta et al., 2004; Levitt, 2010). For instance, it has been demonstrated that amazingly long lifetimes for a magnetisation encoded in a 15N pair for about 26 min in solution (Pileio, Carravetta, Hughes, & Levitt, 2008). Therefore, the long-lived singlet state (LLS) is very important for developing NMR spectroscopy (Marco-Rius et al., 2013; Warren, Jenista, Branca, & Chen, 2009) and potentially MRI. Long live states are an attractive possibility for *in-vivo* MRI researches using hyperpolarisation methods (Tayler & Levitt, 2011).

Using SABRE as a method to make hyperpolarised LLS in a weak of 1H spin pairs coupled has been recorded but the magnetization continued for about 27s. If this could be further developed then such signal enhancement has major implications for further developing the power of MRI diagnostic imaging in biological tissue (Olaru et al., 2016; Roy, Rayner, Norcott, Green, & Duckett, 2016). In addition, the long lifetimes have many advantages in the area of NMR spectroscopy by allowing the study of diffusion; slow chemical ex-change and the evolution of hyperpolarised spin states (Ahuja, Sarkar, Vasos, & Bodenhausen, 2009; Bodenhausen, Vasos, & Sarkar, 2009; Sarkar, Vasos, & Bodenhausen, 2007; Vasos et al., 2009). There is evidence that singlets can be exploited to transfer information to neighbouring magnetic nuclei (Tayler, Marie, Ganesan, & Levitt, 2010) hence extending the utility of NMR. But, the singlet state is not observable in itself, it is a non-magnetic state. This state is not changed by excitation, magnetic field, rotation or other normal NMR or MRI manipulations. Magnetic field and excitation bring about spin rotation such that the final state has the same components with identical amplitude and relationships within the state (Levitt, 2010); (Tayler & Levitt, 2011).

There are three different stages in an experiment required to exploit nuclear singlets. Firstly, the standard longitudinal magnetistion of nuclei has to be converted into a nuclear singlet. Secondly, the singlet has to be protected by suppression of the effects of any differences in the chemical shifts within the molecule. Thirdly, again by exploiting the chemical shift differences, the singlet is converted back to observable nuclear magnetization. In the second stage, the long lifetime is preserved and can be demonstrated. This has been achieved by

suppressing any singlet to triplet conversion by transferring the sample to the area of low magnetic field (Carravetta et al., 2004; Carravetta & Levitt, 2005), or by using a chemical reaction to switch the molecule symmetry (Warren et al., 2009).

These methods just described, offer new exciting ways to access the long-lived state. But it would be more desirable to achieve the same without having to require a low magnetic field or a chemical reaction. However, in recent studies, there is a new method that shows that it one access the singlet state even if the nuclei are nearly magnetically equivalent. When the chemical shift of two nuclei sites are the same, the spin systems are called nearly equivalent or extremely coupled. This means the spin-spin coupling is more than the chemical shift frequency differences. Consequently, as result of suppression of any small chemical shift by spin-spin coupling, the NMR spectrum of spin pairs show a single peak. This is the situation at high magnetic field when the chemical shifts of protons are close, and is a common case for NMR in low magnetic field.

There is a special technique to obtain, preserve and detect the singlet state. This method depends on a series of 180-degree pulses that are matched with the spin-spin coupling among nuclei. In addition, long-lived states can be created by SABRE in high magnetic field without chemical change and can be detectable as observable signals after long delays (Olaru et al., 2016). This can be done by moving Zeeman derived polarization that is 1500 times bigger than that associated with conventional thermal equilibrium at 400 MHz. This is the longitudinal signal created by hyperpolarisation. This is normally associated with a short $T1$ lifetime, In the Olaru et al. study, 2-aminothiazole was used as a substrate and mixed with a catalyst that was used to improve the SABRE level and to control the substrate relaxation by deuteration similar to that used in this thesis in chapter 4. By applying a series of 180degree pulses Olaru et al. created very long live states that survived much longer than the normal $T1$ lifetime.

Another study was published in 2016 showing a new way of obtained long $T1$ times by using the SABRE technique in high magnetic field. This study used Pyrazine and Nicotinamide and they showed larger than 4% net H-polarization which remained measurable for 90 seconds (Roy, Rayner, et al., 2016). As this large hyperpolarization offers the opportunity to also be stored as a long lived state it would interesting to explore if the Olaru et al methods could be applied.

In this chapter, I will discuss the hyperpolarization of Pyridazine with and without heart tissue in a vertical NMR magnet. In particular we use the Olaru et al. methods to store magnetisation in a singlet state and then wait for a long delay before making the singlet state observable. The aim of this study is to see if there is an interaction between substrate and heart tissue or not as well as to see if magnetisation can be stored

6.2 Specific methods for this chapter

6.2.1 Chemical substrate

In the experiment, deuterated Pyridazine (figure 90) was used as a substrate. The sample was prepared by dissolving the 0.5 of [Ir (IMes)(COD) Cl] catalyst and 1.5 mg of Pyridazine in 0.6 ml of Methanol-d4 utilizing a 5 mm NMR tube as seen in figure (91). This tube has been investigated with and without heart tissue in the vertical NMR magnet as seen in figure (93). After I prepared the sample, a high vacuum line was used to remove air and a Parahydrogen generation was used to add Parahydrogen to activate the sample.
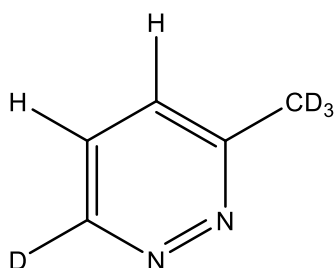
Figure 90: Pyridazine derivative 2-CD3, 4-D chemical structure
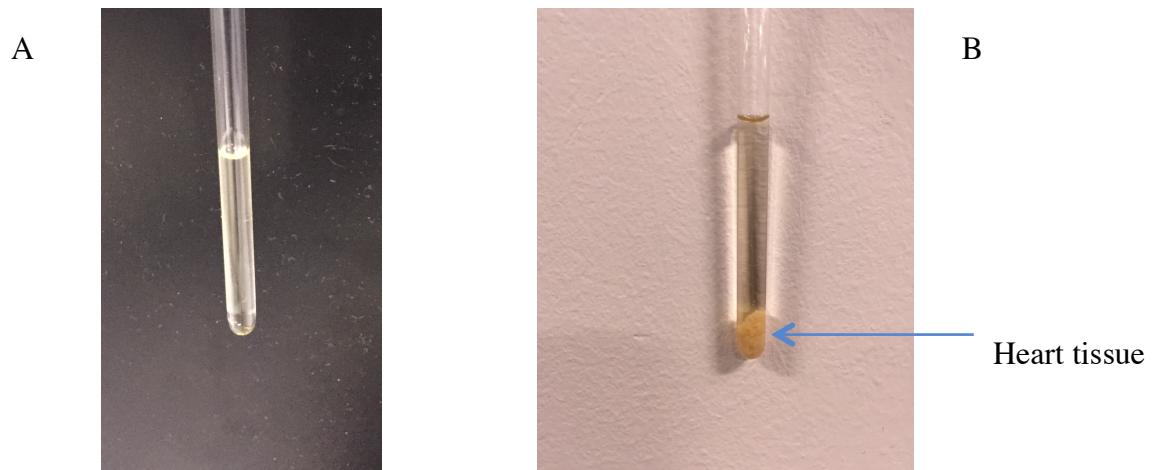
Heart tissue

Figure 91: Pyridazine sample, image A shows the control 5 mm tube whereas image B shows the 5 mm tube with heart tissue.

6.2.2 IKA Homogenizers

A IKA Homogenizers ULTRA-TURRAX disposable workstation with disperser tube, as seen in figure (92), has been used to mix and chop the heart tissue with Methanol-d4. This instrument can be used for sterile tissue homogenization, as it is a closed homogenizing system.

Figure 92: IKA IKA Homogenizers ULTRA-TURRAX disposable workstation with disperser tube

6.2.3 NMR spectrometer

This experiment has been done in a 400 MHz Bruker Avance III spectrometer as seen in figure 93. Figure 94 shows the transfer scheme for automatically polarising the sample and delivering it into the scanner. The Pyridazine, catalyst and Parahydrogen are mixed in a polarisation field magnetic field under computer control. Then, the solution is moved to the NMR spectrometer where the pulse sequence is applied to produce the SABRE-LLS.

Figure 93: the vertical NMR magnet or NMR spectrometer
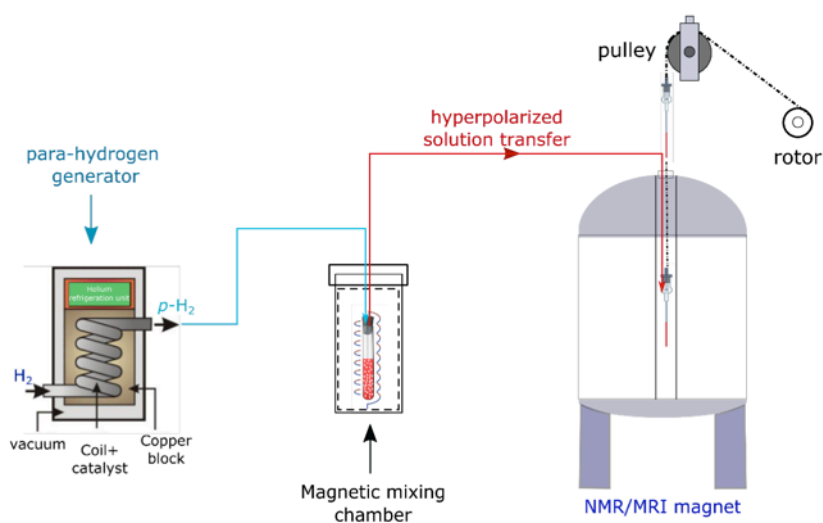
Figure 94: SABRE - long lived state scheme, taken from (Roy, Norcott, et al., 2016)

137

6.2.4 M2S-S2M pulse sequence

The M2S-S2M sequence is the sequence which can be used to transfer the original
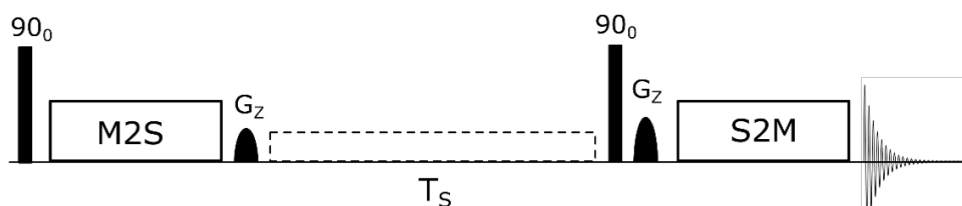
Figure 95: the M2S-S2M pulse sequence, taken form (Roy, Norcott, et al., 2016)

polarisation into a singlet state, store it for a period of time and then turn the state back into observable magnetisation, see figure (95). I used the sequence that was developed by (Roy, Norcott, et al., 2016). The M2S –S2M pulse sequence can be used to measure the singlet state lifetime (T_{LLS}). By varying the delay between the magnetisation-to-singlet step to the singlet-to-magnetisation step. After the M2S step a gradient is applied to maintain the signal coherence that achieved by the M2S pulse, see figure 96. Then a waiting time is followed by 90^0 pulse to suppress the magnetization that recovered during that interval and after that, the reversed time M2S (S2M) converts the singlet state to magnetization. A final 90^0 RF pulse is applied to detect the magnetization.
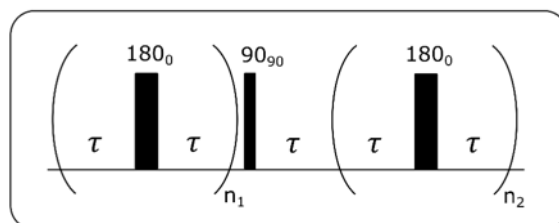
Figure 96: M2S block pulse sequence, taken form(Roy, Norcott, Rayner, Green, & Duckett, 2016)

6.2.5 Sample Preparation

A sample of [Ir (IMes)(COD)Cl] was prepared in Methanol-d4 solution with the deuterated Pyridazine derivative 2-CD3, 4-D, and placed under Parahydrogen (p-H_2). This resulted in the observation of a hydride signal at δ-21.70 for [Ir (H_2) (IMes) (pyridazine)$_3$]Cl, the active SABRE catalyst.

6.3 Results

Here we discuss the results achieved from M2S-S2M measurements. Figure 97 summarizes the outcome. The enhancement by standard SABRE experiment is shown in Fig. 97B which was enhanced by >1000 fold compared to the thermal signal shown in Fig. 97A. For comparison purpose thermal signal was vertically expanded by 1000 times compared to all other spectra presented in Fig. 97. After the initial SABRE screening, we added a rat heart tissue into the solution to observe the behaviour of the NMR signal. In Fig. 97C, we recorded a spectra that was first SABRE hyperpolarized then the heart tissue was inserted and corresponding NMR measurement was done after 10 sec. Signal losses due to relaxation can be visible from the resulted spectra. Before adding the heart tissue, we also performed a SABRE-LLS (by M2S-S2M pulse sequence as presented earlier) experiment to show that hyperpolarized magnetization can be stored in a Long-lived States (LLS) for a much longer duration than standard magnetization. Figure 97D shows the SABRE-LLS spectra acquired immediately after transfer. Now we use this SABRE-LLS to see heart tissue's role and significance. Figure 97E showing the SABRE-LLS spectra when heart tissue is present in the solution and the measurement was done after 10 sec. When compared the spectra (E) with spectra C, we get much larger (more than double) signal even in the presence of the heart tissue. All the spectra presented in Figure 97 are in the same scale except in A which was vertically multiplied by 1000 fold for comparison purpose.
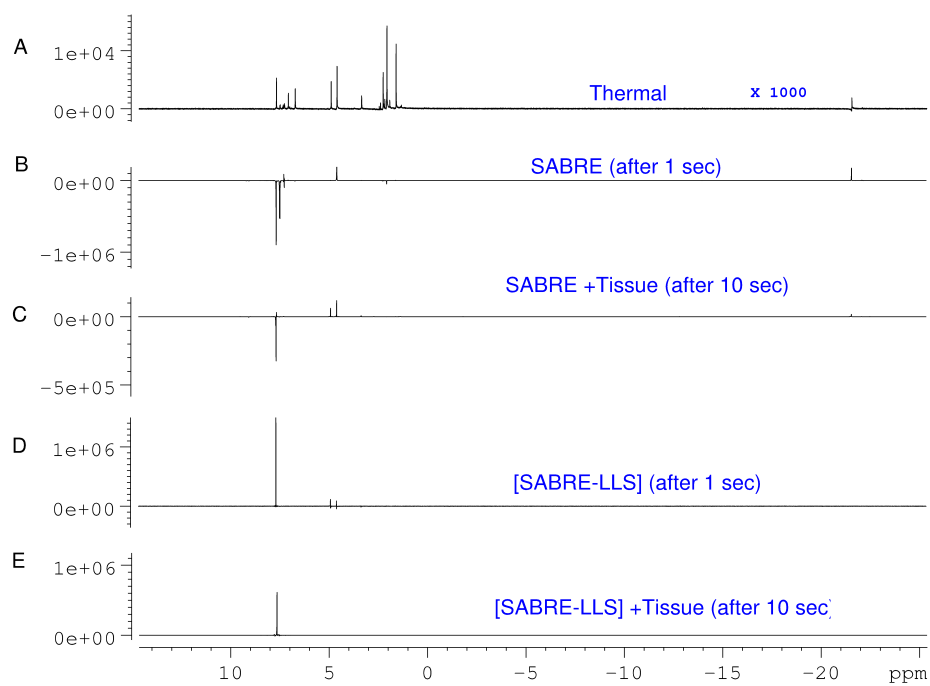
Figure 97: Image (A) shows the thermal spectra. Image (B) shows the SABRE after one second. Image (C) indicates the SABRE with heart tissue after 10 seconds. Image (D) shows the SABRE-LLS after 1 second. Image (E) SABRE –LLS with tissue after 10 seconds. All the spectra are in same scale.

6.4   Discussion and future work

This experiment has been done in the NMR spectrometer because there was a M2S-S2M pulse sequence. The sequence has yet to be written for a 3T human scanner. The Pyridazine was investigated with and without tissue in the NMR spectrometer by exploiting the sequence in conjunction with SABRE to form long-lived states. This has been termed SABRE-LLS.

There were two major findings; First that a singlet state could be produced in Pyridizine and that the single could be maintained for several minutes. This far exceeds the normal T1 lifetime of Pyridizine. The second major finding is that the presence of the heart tissue does not alter SABRE-LLS performance. This suggests, as in the previous chapter, that heart tissue may be favourably supporting the singlet states in maintaining its long lifetime. Both of these observations have implications for in-vivo imaging. It is clear that a new storage mechanism can be exploited to preserve signals and secondly that a new contrast method can be exploited through the interaction of that storage state and tissue.

6.5   Conclusion

Pyridazine has been examined with and without heart tissue in a NMR spectrometer. The main aim of this chapter was to create singlet states using SABRE-LLS of ^{1}H nuclei. This was successful and shows that long-lived signals can be created on protons and therefore used in the future on standard clinical scanners. It is possible to programme the M2S-S2M sequence on 3T MRI scanners and it has been done in Simon's Duckett group but it was out of my scope for my PhD. The experiment would have to be re-investigated in a 3T-MRI after the M2S-S2M sequence is installed and programmed.

Chapter 7   Conclusion and Future work

7.1   Conclusion

NMR and MRI with hyperpolarisation have become important tools for the investigation and diagnosis of diseases in recent years. However that hyperpolarization has been carried out by using Dynamic Nuclear Polarisation which is both expensive and difficult to implement. The main aim of this project was to bring about spin polarisation enhancement by using SABRE in a milliTesla magnetic field and then to use a standard scanner to create images. This is both cheap and easy to implement. Another important aim was to develop and use the SABRE measurements in biological tissue.

In chapter 3, I have investigated substrates such as Pyrazine, Nicotinamide and Pyridine an imaged them in a 3T GE scanner after SABRE polarisation. I focused on a Pyrazine sample at 5mT throughout my thesis. I found that the Pyrazine had the largest signal, had a non-exponential decay when compared to other substrates. I explored the parameters that determined the features of the decay and the optimum for signal enhancement. It was argued that some of the non-exponential decay was due to fluid movements in the tube or to turbulence, but this was not the only explanation and that other source of magnetic signal might be present.

I also investigated the effect on the Pyrazine after adding bipyridine to remove the catalyst. It was shown that this did increase the lifetime of the signal and therefore the removal of the catalyst is important to preserve the signal. But this effect was quite small and therefore another route for signal preservation had to be investigated. This was performed in later chapters.

Then I moved to test the Pyrazine with and without heart tissue. It was found that a sample with tissue present had a faster decay (short T1) compared with a control.

In chapter 4. I continued the exploration of the way by which a hyperpolarised image could be examined over longer periods. This was achieved by varying the flip angle and the delay between image volumes. It was shown that the readout method had a big effect on the apparent T1 of the signal and this could be simply predicted by theory. This has major implications for the imaging of any hyperpolarised signal. At the end of that chapter, Deuterated methyl nicotinate was investigated. It was shown that deuteration can extend the T1 of a signal as well as result in a larger signal.

In chapter 5, the crucial effects of adding a hyperpolarized sample to tissue were investigated. The major result was that a novel, persistent signal was observed over 50 seconds after polarization. This was hypothesized to be the result of a singlet state being made observable because of a specific interaction between the hyperpolarized substrate, Pyrazine, and ASIC ion channels. This novel signal could form the basis of a new contract for imaging in-vivo.

Finally, in chapter 6, a new pulse sequence was exploited, in conjunction with SABRE to store magnetisation for over three minutes. This time course far exceeds that which could be achieved by deuteration or by varying the MRI parameters such as flip angle. Crucially, it was also demonstrated that the presence of tissue increased the final observable magnetization and this, in conjuction with the results of chapter 5 highlight that SABRE can be used to target specific biological mechanisms.

7.2   Future work

Using SABRE hyperpolarisation in a standard clinical 3T scanner has been used in this project. This work involved the investigation of many aspects of the methodology such as SABRE characterisation, different amount of substrates, investigation of the effects of biological tissue and the development of materials and system and, crucially, the study of ways by which the SABRE signal could be preserved over longer lifetimes.

For the future work, further investigations of all the substrates that have been tested in this thesis would need to be carried out, this would include solvent dependency, optimising the amount of catalyst that is required and scaling up the production of hyperpolarised substrate amount. For example, ethanol could be used instead of Methanol-d4 because it has lower

toxicity. Even better would be for a biologically compatible solvent to be developed that worked efficiently with SABRE. This would allow SABRE to be used for in-vivo studies.

In chapter 6, SABRE-LLS was used to investigate the storage of signals for protected periods. However, in this time at York this can only can be done in a NMR spectrometer. This is because this system has an M2S-S2M pulse sequence. Therefore, a crucial next step would be to set up and programming the 3T scanner for the M2S-S2M sequence. Therefore, experiments of *ex vivo* and *in vivo* tissue should be done. This might lead to the development of an the MRI imaging system where the signal lifetimes could become competitive with the lifetimes of signals from radioactive compounds used in PET imaging.

The target of this project was to optimise the SABRE method for imaging and for the imaging of tissue. This was successful but the next crucial step and main point of future work would be to use hyperpolarisation by SABRE for use in living humans.

List of Abbreviations

2D	Two-dimensional
3D	Three-dimensional
ALTADENA	Adiabatic longitudinal after dissociation engender nuclear alignment
CE	Cross effect
COPD	Chronic obstructive pulmonary disease
DNP	Dynamic nuclear polarisation
DWI	Diffusion weighted imaging
FID	Free induction decay
GE	Gradient echo or General Electric
Hz	Hertz
MRI	Magnetic resonance imaging
MRS	Magnetic resonance spectroscopy
NMR	Nuclear magnetic resonance
OE	Overhauser effect
PASADENA	Parahydrogen and Synthesis allow dramatically enhanced nuclear alignment
PHIP	Parahydrogen induced polarisation
ppm	Parts per million
RF	Radiofrequency
SABRE	Signal amplification by reversible exchange
SE	Solid effect or Spin echo
SNR	Signal to noise ratio
TE	Time to echo
TM	Thermal effect
TMS	Tetramethylsilane
TR	Time to repeat
VDV	Ventilation defect volume
LLS	Long lived-state
T_{LLS}	Singlet state lifetime
NMV	Net magnetic moment
M_z	Magnetisation in the longitudinal or Z direction
S	Angular momentum quantum number
FOV	Field of view
T	Tesla or Time
SEOP	Spin exchange optical pumping
RARE	Rapid acquisition with relaxation enhancement
FLASH	Fast Low Angle Shot Magnetic Resonance Imaging
PH	Potential of hydrogen
LD	Lethal dose
SENSE	Sensitivity Encoding

Bibliography

Adams, E., & Goodkind, J. (1963). Cryostat for investigations to temperatures below 0· 02° K. *Cryogenics, 3*(2), 83-85.

Adams, R. W., Aguilar, J. A., Atkinson, K. D., Cowley, M. J., Elliott, P. I., Duckett, S. B., . . . Williamson, D. C. (2009). Reversible interactions with para-hydrogen enhance NMR sensitivity by polarization transfer. *Science, 323*(5922), 1708-1711.

Aguilar, J. A., Elliott, P. I., Lopez-Serrano, J., Adams, R. W., & Duckett, S. B. (2007). Only para-hydrogen spectroscopy (OPSY), a technique for the selective observation of para-hydrogen enhanced NMR signals. *Chemical Communications*(11), 1183-1185.

Ahuja, P., Sarkar, R., Vasos, P. R., & Bodenhausen, G. (2009). Diffusion coefficients of biomolecules using long-lived spin states. *Journal of the American Chemical Society, 131*(22), 7498-7499.

Albert, M., & Balamore, D. (1998). Development of hyperpolarized noble gas MRI. *Nuclear Instruments and Methods in Physics Research Section A: Accelerators, Spectrometers, Detectors and Associated Equipment, 402*(2), 441-453.

Albert, M., Cates, G., Driehuys, B., Happer, W., Saam, B., Springer, C., & Wishnia, A. (1994). Biological magnetic resonance imaging using laser-polarized 129Xe.

Albert, M. S., Balamore, D., Cates Jr, G. D., Driehuys, B., Happer, W., Saam, B., & Wishnia, A. (1996). Magnetic resonance imaging using hyperpolarized noble gases: Google Patents.

Altes, T. A., & Salerno, M. (2004). Hyperpolarized gas MR imaging of the lung. *Journal of thoracic imaging, 19*(4), 250-258.

Ardenkjær-Larsen, J. H., Fridlund, B., Gram, A., Hansson, G., Hansson, L., Lerche, M. H., . . . Golman, K. (2003). Increase in signal-to-noise ratio of> 10,000 times in liquid-state NMR. *Proceedings of the National Academy of Sciences, 100*(18), 10158-10163.

Aue, W., Bartholdi, E., & Ernst, R. R. (1976). Two-dimensional spectroscopy. Application to nuclear magnetic resonance. *The Journal of Chemical Physics, 64*(5), 2229-2246.

Bajaj, V. S., Hornstein, M. K., Kreischer, K. E., Sirigiri, J. R., Woskov, P. P., Mak-Jurkauskas, M. L., . . . Griffin, R. G. (2007). 250GHz CW gyrotron oscillator for dynamic nuclear polarization in biological solid state NMR. *Journal of Magnetic Resonance, 189*(2), 251-279.

Blazina, D., Duckett, S. B., Halstead, T., Kozak, C., Taylor, R., Anwar, M. S., . . . Carteret, H. A. (2005). Generation and interrogation of a pure nuclear spin state by parahydrogen-enhanced NMR spectroscopy: a defined initial state for quantum computation. *Magnetic Resonance in Chemistry, 43*(3), 200-208.

Bloch F., e. a. (1946). Nuclear Induction, Proceedings of the American Physical Society. *Physical Review.*

Bock, K., & Thøgersen, H. (1983). Nuclear magnetic resonance spectroscopy in the study of mono-and oligosaccharides. *Annual reports on NMR spectroscopy, 13*, 1-57.

Bodenhausen, G., Vasos, P., & Sarkar, R. (2009). Singlet-state exchange NMR spectroscopy for the study of very slow dynamic processes: Google Patents.

Bowers, C. R., & Weitekamp, D. P. (1986). Transformation of symmetrization order to nuclear-spin magnetization by chemical reaction and nuclear magnetic resonance. *Physical review letters, 57*(21), 2645.

Bowers, C. R., & Weitekamp, D. P. (1987). Parahydrogen and synthesis allow dramatically enhanced nuclear alignment. *Journal of the American Chemical Society, 109*(18), 5541-5542.

Brown, M. S. (1999). MRI, basic principles and applications.

Carravetta, M., Johannessen, O. G., & Levitt, M. H. (2004). Beyond the T 1 limit: singlet nuclear spin states in low magnetic fields. *Physical review letters, 92*(15), 153003.

Carravetta, M., & Levitt, M. H. (2005). Theory of long-lived nuclear spin states in solution nuclear magnetic resonance. I. Singlet states in low magnetic field. *The Journal of Chemical Physics, 122*(21), 214505.

Carver, T., & Slichter, C. (1953). Polarization of nuclear spins in metals. *Physical Review, 92*(1), 212.

Carver, T. R., & Slichter, C. P. (1956). Experimental verification of the Overhauser nuclear polarization effect. *Physical Review, 102*(4), 975.

Chen, K., & Chen, X. (2010). Design and development of molecular imaging probes. *Current topics in medicinal chemistry, 10*(12), 1227.

Claridge, T. D. (2008). *High-resolution NMR techniques in organic chemistry* (Vol. 27): Newnes.

Clark, C., Hockings, P., Joyce, D., & Mazucco, R. (1997). Application of magnetic resonance imaging to pre-and post-harvest studies of fruits and vegetables. *Postharvest Biology and Technology, 11*(1), 1-21.

Cleveland, Z. I., Cofer, G. P., Metz, G., Beaver, D., Nouls, J., Kaushik, S. S., . . . McAdams, H. P. (2010). Hyperpolarized 129Xe MR imaging of alveolar gas uptake in humans. *PLoS One, 5*(8), e12192.

Cogan, M. G. (1990). Angiotensin II: a powerful controller of sodium transport in the early proximal tubule. *Hypertension, 15*(5), 451-458.

Couch, M. J., Blasiak, B., Tomanek, B., Ouriadov, A. V., Fox, M. S., Dowhos, K. M., & Albert, M. S. (2014). Hyperpolarized and Inert Gas MRI: The Future. *Molecular Imaging and Biology*, 1-14.

Cowley, M. J., Adams, R. W., Atkinson, K. D., Cockett, M. C., Duckett, S. B., Green, G. G., . . . Mewis, R. E. (2011). Iridium N-heterocyclic carbene complexes as efficient catalysts for magnetization transfer from para-hydrogen. *Journal of the American Chemical Society, 133*(16), 6134-6137.

Cowley, M. J., Adams, R. W., Atkinson, K. D., Cockett, M. C. R., Duckett, S. B., Green, G. G. R., . . . Mewis, R. E. (2011). Iridium N-Heterocyclic Carbene Complexes as Efficient Catalysts for Magnetization Transfer from para-Hydrogen. *Journal of the American Chemical Society, 133*(16), 6134-6137. doi: 10.1021/ja200299u

Damadian, R. (1971). Tumor detection by nuclear magnetic resonance. *Science, 171*(3976), 1151-1153.

Daniel Bellus, S. G., Norbert Haider, Wolfgang Holzer, Tsutomu Ishikawa, Shigekazu Ito, Danijel Kikelj, Masakatsu Matsumoto, Magoichi Sako, Nobuhiro Sato, Ryu Sato, Frank Seela, Ichiro Shinkai, Uros Urleb, Yoshinori Yamamoto, Masaaki Yoshifuji, Silvia von Angerer. (2014). Science of Synthesis: Houben-Weyl Methods of Molecular Transformations Vol. 16.

De Graaf, R. A. (2008). *In vivo NMR spectroscopy: principles and techniques*: John Wiley & Sons.

de la Rosa, D. A., Canessa, C. M., Fyfe, G. K., & Zhang, P. (2000). Structure and regulation of amiloride-sensitive sodium channels. *Annual Review of Physiology, 62*(1), 573-594.

Dominik Weishaupt, V. D. K., Borut Marincek. (2013). How does MRI work?: An Introduction to the Physics and Function of Magnetic Resonance Imaging.

Duckett, S. B., & Mewis, R. E. (2012). Application of Para hydrogen Induced Polarization Techniques in NMR Spectroscopy and Imaging. *Accounts of chemical research, 45*(8), 1247-1257.

Duckett, S. B., & Sleigh, C. J. (1999). Applications of the parahydrogen phenomenon: a chemical perspective. *Progress in nuclear magnetic resonance spectroscopy, 34*(1), 71-92.

Duckett, S. B., & Wood, N. J. (2008). Parahydrogen-based NMR methods as a mechanistic probe in inorganic chemistry. *Coordination Chemistry Reviews, 252*(21), 2278-2291.

E. A. Davis, I. F. (1997). J.J. Thompson And The Discovery Of The Electron.

Eisenschmid, T. C., Kirss, R. U., Deutsch, P. P., Hommeltoft, S. I., Eisenberg, R., Bargon, J., . . . Balch, A. L. (1987). Para hydrogen induced polarization in hydrogenation reactions. *Journal of the American Chemical Society, 109*(26), 8089-8091.

Ernst, R., & Anderson, W. (1966). Application of Fourier transform spectroscopy to magnetic resonance. *Review of Scientific Instruments, 37*(1), 93-102.

Ernst, R., R. (1990). Principles of Nuclear Magnetic Resonance in One and Two Dimensions.

Faro, S. H., Mohamed, F. B., Law, M., & Ulmer, J. T. (2011). *Functional Neuroradiology: Principles and Clinical Applications*: Springer Science & Business Media.

Gateway. (2013). MRI Hyperpolarization and Molecular Imaging.

Glöggler, S., Colell, J., & Appelt, S. (2013). Para-hydrogen perspectives in hyperpolarized NMR. *Journal of Magnetic Resonance, 235*, 130-142.

Glöggler, S., Müller, R., Colell, J., Emondts, M., Dabrowski, M., Blümich, B., & Appelt, S. (2011). Para-hydrogen induced polarization of amino acids, peptides and deuterium–hydrogen gas. *Physical Chemistry Chemical Physics, 13*(30), 13759-13764.

Golman, K., Axelsson, O., Jóhannesson, H., Månsson, S., Olofsson, C., & Petersson, J. (2001). Parahydrogen-induced polarization in imaging: Subsecond 13C angiography. *Magnetic Resonance in Medicine, 46*(1), 1-5.

Goodson, B. M. (2002). Nuclear magnetic resonance of laser-polarized noble gases in molecules, materials, and organisms. *Journal of Magnetic Resonance, 155*(2), 157-216.

Green, R. A., Adams, R. W., Duckett, S. B., Mewis, R. E., Williamson, D. C., & Green, G. G. (2012). The theory and practice of hyperpolarization in magnetic resonance using parahydrogen. *Progress in nuclear magnetic resonance spectroscopy, 67*, 1-48.

Hanukoglu, I., & Hanukoglu, A. (2016). Epithelial sodium channel (ENaC) family: Phylogeny, structure-function, tissue distribution, and associated inherited diseases. *Gene*.

Highton, L. (2013). Using SABRE in NMR and MRI.

Jerrold T. Bushberg, J. M. B. (2011). The Essential Physics of Medical Imaging.

Jóhannesson, H., Axelsson, O., & Karlsson, M. (2004). Transfer of para-hydrogen spin order into polarization by diabatic field cycling. *Comptes Rendus Physique, 5*(3), 315-324.

Kauczor, H.-U., Surkau, R., & Roberts, T. (1998). MRI using hyperpolarized noble gases. *European radiology, 8*(5), 820-827.

Keeler, J. (2013). *Understanding NMR spectroscopy*: John Wiley & Sons.

Kelvin, S. (2013). High polarization of nuclear spins mediated by nanoparticles at millikelvin temperatures. *Physical Chemistry Chemical Physics, 15*(25), 10413-10417.

Kemsley, J. (2008). Sensitizing NMR. *Chemical & engineering news, 86*(43), 12-15.

King, K. F. (2004). *ASSET–Parallel Imaging on the GE Scanner*. Paper presented at the 2nd international workshop on parallel MRI; October.

Kirby, M., Svenningsen, S., Owrangi, A., Wheatley, A., Farag, A., Ouriadov, A., . . . McCormack, D. G. (2012). Hyperpolarized 3He and 129Xe MR imaging in healthy volunteers and patients with chronic obstructive pulmonary disease. *Radiology, 265*(2), 600-610.

Kohler, S., Yen, Y., Wolber, J., Chen, A., Albers, M., Bok, R., . . . Vigneron, D. (2007). In vivo 13carbon metabolic imaging at 3T with hyperpolarized 13C-1-pyruvate. *Magnetic Resonance in Medicine, 58*(1), 65-69.

Kurhanewicz, J., Vigneron, D. B., Brindle, K., Chekmenev, E. Y., Comment, A., Cunningham, C. H., . . . Rajan, S. S. (2011a). Analysis of cancer metabolism by imaging hyperpolarized nuclei: prospects for translation to clinical research. *Neoplasia, 13*(2), 81-97.

Kurhanewicz, J., Vigneron, D. B., Brindle, K., Chekmenev, E. Y., Comment, A., Cunningham, C. H., . . . Rajan, S. S. (2011b). Analysis of cancer metabolism by imaging hyperpolarized nuclei: prospects for translation to clinical research. *Neoplasia (New York, NY), 13*(2), 81.

Lauterbur, P. C. (1973). Image formation by induced local interactions: examples employing nuclear magnetic resonance. *Nature, 242*(5394), 190-191.

Leupold, J., Hennig, J., & Scheffler, K. (2008). Moment and direction of the spoiler gradient for effective artifact suppression in RF-spoiled gradient echo imaging. *Magnetic Resonance in Medicine, 60*(1), 119-127.

Levitt, M. H. (2008). *Spin dynamics: basics of nuclear magnetic resonance*: John Wiley & Sons.

Levitt, M. H. (2010). Singlet and other states with extended lifetimes. *eMagRes*.

Lilburn, D. M., Lesbats, C., Six, J. S., Dubuis, E., Yew-Booth, L., Shaw, D. E., . . . Meersmann, T. (2015). Hyperpolarized 83Kr magnetic resonance imaging of alveolar degradation in a rat model of emphysema. *Journal of The Royal Society Interface, 12*(107), 20150192.

Lingwood, M. D., Siaw, T. A., Sailasuta, N., Abulseoud, O. A., Chan, H. R., Ross, B. D., . . . Han, S. (2012). Hyperpolarized water as an MR imaging contrast agent: feasibility of in vivo imaging in a rat model. *Radiology, 265*(2), 418-425.

Loffing, J., & Kaissling, B. (2003). Sodium and calcium transport pathways along the mammalian distal nephron: from rabbit to human. *American Journal of Physiology-Renal Physiology, 284*(4), F628-F643.

Maly, T., Debelouchina, G. T., Bajaj, V. S., Hu, K.-N., Joo, C.-G., Mak–Jurkauskas, M. L., . . . Temkin, R. J. (2008). Dynamic nuclear polarization at high magnetic fields. *The Journal of Chemical Physics, 128*(5), 052211.

Mansfield, P., Pykett, I., Morris, P., & Coupland, R. (1978). Human whole body line-scan imaging by NMR. *The British journal of radiology, 51*(611), 921-922.

Marco-Rius, I., Tayler, M. C., Kettunen, M. I., Larkin, T. J., Timm, K. N., Serrao, E. M., . . . Levitt, M. H. (2013). Hyperpolarized singlet lifetimes of pyruvate in human blood and in the mouse. *NMR in Biomedicine, 26*(12), 1696-1704.

Maximilian F Reiser, W. S., Hedvig Hricak. (2007). Magnetic Resonance Tomography.

Mazzanti, M. L., Walvick, R. P., Zhou, X., Sun, Y., Shah, N., Mansour, J., . . . Albert, M. S. (2011). Distribution of hyperpolarized xenon in the brain following sensory stimulation: preliminary MRI findings. *PLoS One, 6*(7), e21607.

McRobbie, D. W., Moore, E. A., Graves, M. J., & Prince, M. R. (2006). *MRI from Picture to Proton*: Cambridge university press.

Mewis, R. E. (2015). Developments and advances concerning the hyperpolarisation technique SABRE. *Magnetic Resonance in Chemistry, 53*(10), 789-800.

Mewis, R. E., Atkinson, K. D., Cowley, M. J., Duckett, S. B., Green, G. G., Green, R. A., . . . Lohman, J. A. (2014). Probing signal amplification by reversible exchange using an NMR flow system. *Magnetic Resonance in Chemistry, 52*(7), 358-369.

Morris, P. G. (1986). Nuclear magnetic resonance imaging in medicine and biology.

Mugler, J. P., Driehuys, B., Brookeman, J. R., Cates, G. D., Berr, S. S., Bryant, R. G., . . . Erickson, C. J. (1997). MR imaging and spectroscopy using hyperpolarized 129Xe gas: preliminary human results. *Magnetic Resonance in Medicine, 37*(6), 809-815.

Natterer, J., & Bargon, J. (1997). Parahydrogen induced polarization. *Progress in nuclear magnetic resonance spectroscopy, 31*(4), 293-315.

Ogawa, S., Lee, T., Kay, A., & Tank, D. (1990). Brain magnetic resonance imaging with contrast dependent on blood oxygenation. *Proceedings of the National Academy of Sciences, 87*(24), 9868-9872.

Olaru, A. M., Roy, S. S., Lloyd, L. S., Coombes, S., Green, G. G., & Duckett, S. B. (2016). Creating a hyperpolarised pseudo singlet state through polarisation transfer from para hydrogen under SABRE. *Chemical Communications, 52*(50), 7842-7845.

Oschkinat, H., Griesinger, C., Kraulis, P. J., Sørensen, O. W., Ernst, R. R., Gronenborn, A. M., & Clore, G. M. (1988). Three-dimensional NMR spectroscopy of a protein in solution. *Nature, 332*(6162), 374-376.

Pileio, G., Carravetta, M., Hughes, E., & Levitt, M. H. (2008). The long-lived nuclear singlet state of 15N-nitrous oxide in solution. *Journal of the American Chemical Society, 130*(38), 12582-12583.

Purcell, E. M., et al. (1946). Resonance Absorption by Nuclear Magnetic Moments in a Solid. Physical Review,.

Ray Hashman Hashemi, W. G. B., Christopher J. Lisanti. (2012). MRI: The Basics.

Roberts, L. D., & Dabbs, J. (1961). Nuclear orientation. *Annual review of nuclear science, 11*(1), 175-212.

Rodgers, H., & Knox, A. (2001). Pharmacological treatment of the biochemical defect in cystic fibrosis airways. *European Respiratory Journal, 17*(6), 1314-1321.

Rogers, N. J., Hill-Casey, F., Stupic, K. F., Six, J. S., Lesbats, C., Rigby, S. P., . . . Meersmann, T. (2016). Molecular hydrogen and catalytic combustion in the production of hyperpolarized 83Kr and 129Xe MRI contrast agents. *Proceedings of the National Academy of Sciences, 113*(12), 3164-3168.

Roy, S. S., Norcott, P., Rayner, P. J., Green, G. G., & Duckett, S. B. (2016). A Hyperpolarizable 1H Magnetic Resonance Probe for Signal Detection 15 Minutes after Spin Polarization Storage. *Angewandte Chemie International Edition, 55*(50), 15642-15645.

Roy, S. S., Rayner, P. J., Norcott, P., Green, G. G., & Duckett, S. B. (2016). Long-lived states to sustain SABRE hyperpolarised magnetisation. *Physical Chemistry Chemical Physics, 18*(36), 24905-24911.

Rule, G. S., & Hitchens, T. K. (2006). *Fundamentals of protein NMR spectroscopy* (Vol. 5): Springer Science & Business Media.

Sarkar, R., Vasos, P. R., & Bodenhausen, G. (2007). Singlet-state exchange NMR spectroscopy for the study of very slow dynamic processes. *Journal of the American Chemical Society, 129*(2), 328-334.

Swanson, S. D., Rosen, M. S., Agranoff, B. W., Coulter, K. P., Welsh, R. C., & Chupp, T. E. (1997). Brain MRI with laser-polarized 129xe. *Magnetic Resonance in Medicine, 38*(5), 695-698.

Tayler, M. C., & Levitt, M. H. (2011). Singlet nuclear magnetic resonance of nearly-equivalent spins. *Physical Chemistry Chemical Physics, 13*(13), 5556-5560.

Tayler, M. C., Marie, S., Ganesan, A., & Levitt, M. H. (2010). Determination of molecular torsion angles using nuclear singlet relaxation. *Journal of the American Chemical Society, 132*(24), 8225-8227.

Theis, T., Ledbetter, M. P., Kervern, G., Blanchard, J. W., Ganssle, P. J., Butler, M. C., . . . Pines, A. (2012). Zero-field NMR enhanced by parahydrogen in reversible exchange. *Journal of the American Chemical Society, 134*(9), 3987-3990.

Theis, T., Truong, M., Coffey, A. M., Chekmenev, E. Y., & Warren, W. S. (2014). LIGHT-SABRE enables efficient in-magnet catalytic hyperpolarization. *Journal of Magnetic Resonance, 248*, 23-26.

Uecker, M., Zhang, S., Voit, D., Karaus, A., Merboldt, K. D., & Frahm, J. (2010). Real-time MRI at a resolution of 20 ms. *NMR in Biomedicine, 23*(8), 986-994.

Vasos, P., Comment, A., Sarkar, R., Ahuja, P., Jannin, S., Ansermet, J.-P., . . . Bodenhausen, G. (2009). Long-lived states to sustain hyperpolarized magnetization. *Proceedings of the National Academy of Sciences, 106*(44), 18469-18473.

Warren, W. S., Jenista, E., Branca, R. T., & Chen, X. (2009). Increasing hyperpolarized spin lifetimes through true singlet eigenstates. *Science, 323*(5922), 1711-1714.

Weishaupt, D., Froehlich, J., Nanz, D., Köchli, V. D., Pruessmann, K., & Marincek, B. (2008). *How does MRI work?: an introduction to the physics and function of magnetic resonance imaging*: Springer Science & Business Media.

Weisman, I. D., Bennett, L. H., Maxwell, L. R., Woods, M. W., & Burk, D. (1972). Recognition of cancer in vivo by nuclear magnetic resonance. *Science, 178*(4067), 1288-1290.

Westbrook, C., & Roth, C. K. (2011). *MRI in Practice*: John Wiley & Sons.

Westbrook, C., & Roth, C. K. (2013). *MRI in Practice*: John Wiley & Sons.

Wood, M. L., Silver, M., & Runge, V. M. (1987). Optimization of spoiler gradients in FLASH MRI. *Magnetic resonance imaging, 5*(6), 455-463.

Zhou, X., Sun, Y., Mazzanti, M., Henninger, N., Mansour, J., Fisher, M., & Albert, M. (2011). MRI of stroke using hyperpolarized 129Xe. *NMR in Biomedicine, 24*(2), 170-175.